Response to the comments from the editor on the manuscript entitled

Application of a two-step approach for mapping ice thickness to various glacier types on Svalbard

presented on 01.03.2017

by

Fürst et al.

First of all we want to thank again the editor for his constructive comments. Pending comments from the initial submission have been taken into account and a list of answers and undertaken actions is given below. Answers are indented and in italic type while a ***short summarising reply*** *is provided in italic, bold-face type. Before addressing the pending comments, a short summary of the major undertaken action is given in response to all reviewers.*

Summary of major changes *in the revised manuscript*

Main changes were mostly necessary in response to the detailed and very constructive comments from reviewer #1. Here we want to briefly give an overview of our actions in response to the major concerns.

First-step flux direction
We consider the redefinition of flux directions in the first step as the key improvement to the revised manuscript. Initially, the ad-hoc choice was that the flux should follow a crudely smoothed version of the steepest surface slopes. Now, we rely on the ideas presented in Brinkerhoff and Johnson (2015) and determine the flux direction by a well-constrained smoothing of the driving stress field, used for directing the balance flux . We experienced a significant improvement in the smoothness of the flux solution.

Document structure
The article was re-structured according to the suggestions of reviewer #1. Methods are now presented prior to the case study.

Input uncertainties
As requested by reviewer #1, we now motivate uncertainties associated with each input field in Sect. 3. We also differentiate between measurement errors from various GPR and airborne RES surveys.

Internal boundary conditions
Though not directly requested by reviewer #1, we removed the internal bound-

ary conditions on ice thickness during the second step to improve the conditioning of the problem and avoid fictitious source/sink terms in the final apparent mass-balance field.

Formal error estimate
Reviewer #1 had also strong concerns on the motivation of the upstream propagation of input uncertainties. As the ice thickness is expected to be constrained just upstream of a measurement, we now give more details on the inherent assumption of this error propagation. Yet, for this article we refrain from exchanging the present error assessment, originating from two internationally peer-reviewed publications, with a more strict Bayesian approach. Such a step requires a significant amount of future development work.

Spatial skill of error-estimate map
Despite the aggregate assessment of median values of the error estimate and the actual mismatch, we also present the how reliable the map is in a spatial sense. For this purpose a table was added that indicates the 'frequency by which the actual mismatch falls below the predicted error'.

Editor Initial Decision: Publish subject to technical corrections (14 Mar 2017) by Andreas Vieli
Comments to the Author:

Dear Johannes Fuerst and co-authors,
Thank you for your submission to TC/TCD. As you may know, papers fully accepted for TCD appear immediately on the web for comment and review. [...].

1. Originality (Novelty): 2
The topic of this manuscript is within the scope of TC [...].

2. Scientific Quality (Rigour): 2
The overall methodology is explained well and seems sound and the uncertainties/errors are quantitatively assessed and potential sensitivities are investigated and well discussed.

[...]

1) One point that in my view would have been interesting is how step two (ve-

locity constraints) would have improved the estimates that had only minimal (1%) thickness constraints (radar measurements). This, although not crucial, may be considered in a future revision.

> *We now added a figure similar to the previous Fig. 8 for the second step in the reconstruction. It shows that mismatch values between inferred and observed thickness values are in fact a bit larger after the second step. Potential reasons are that the velocity observations introduce another source for uncertainty and that thickness measurements are not imposed on the solution during the second step, which allows a larger discrepancy.*
> ***Added aggregate error analysis***

2) [...]

3) different periods are used for dh/dt and SMB in order to calculate the flux divergence, does this affect the results?

> *Difference in the averaging periods add an additional uncertainty to the reconstruction. This additional term is not accounted for in the error estimate map but clearly presented in the discussion. Both averaging periods exceed 20 years, so an adjustment would not exceed the SMB sensitivity of the results as described in the appendix.*
> ***Expanded discussion*** *on this point.*

4) [...]

3. Significance (Impact): 2
Estimating glacier thickness is important for predictions of glacier change and relevant in context of global warming. This study potentially makes a valuable contribution to the development of methods for ice thickness and glacier bed topography estimations and in particular provides a better understanding of the related uncertainties and errors. It further investigates the role of thickness constraints from radar on the inferred ice thickness estimates.

4. Presentation Quality: 3
The paper is well written and structured and mostly well supported with evidence and useful figures [...].

The editor, Andreas Vieli 12/3/2017

List of issues to be adressed:
[...]

> ***All points raised here have been addressed*** *prior to the review phase.*

Response to the
Interactive comment on "Application of a two-step approach for mapping ice thickness to various glacier types on Svalbard" by Johannes Jakob Furst et al.

O. Eisen
olaf.eisen@awi.de
Received and published: 24 March 2017

First of all we want to thank the reviewer for constructive comments on our manuscript. All comments have been taken into account and a list of answers and undertaken actions is given below. Answers are indented and in italic type while a ***short summarising reply*** *is provided in italic, bold-face type.*

The authors spend some effort on providing formal estimates on the overall accuracy of the method, which is greatly appreciated. I suggest that they also look into the detailed comparison of various radar processing schemes provided by Moran et al. (2000). Those authors compare raw 1D vs. 2D vs 3D array radar data processing and come up with estimates of ice thickness errors which are larger than those often used in other studies. Lapazaran, as the most recent and comprehensive study on this issue, cite it, too, but the original paper might be worth looking into, as your study also includes very mountainous valleys.

> *We certainly appreciate this comment and checked how the error estimate in Moran et al. (2000) compares to the study from Lapazaran et al. (2016), which we considered. Moran et al. (2000) describe differences between inferred thickness values from treating the GPR data as single measurements, line measurements or as a 3D measurement array during the processing. They only give relative differences for their specific setup, which are difficult to transfer to our geometries. Lapazaran et al. (2016) recognise that this uncertainty term can become important. Yet they are unable to estimate it for Werenskioldbreen and were forced to discard it from their analysis. However, they gave an advise for how this term should be included if known.*
>
> *As our results are based on the same GPR measurements as used in Lapazaran et al. (2016), we follow their analysis and thus ignore this extra source term in the measurement error.*
>
> ***Added reference*** *to Moran et al. (2000) stating that the analysis of Lapazaran et al. (2016) discards an important but not well quantifiable source term in the error analysis.*

Delineation of a complexly dipping temperate glacier bed using short-pulse radar arrays Moran, M. L.; Greenfield, R. J.; Arcone, S. A.; Delaney, A. J. Journal of Glaciology, Volume 46, Number 153, March 2000, pp. 274-286(13)

Response to the
Interactive comment on "Application of a two-step approach for mapping ice thickness to various glacier types on Svalbard" by Johannes Jakob Furst et al.

D. Brinkerhoff (Referee #1)
douglas.brinkerhoff@gmail.com
Received and published: 28 March 2017

First of all we want to thank the reviewer for constructive comments on our manuscript. All comments have been taken into account and a list of answers and undertaken actions is given below. Answers are indented and in italic type while a ***short summarising reply*** *is provided in italic, bold-face type.*

Summary
In this study, Fürst and others present an updated method for solving the problem of inferring ice thickness from sparse observations coupled with surface data. They then apply this method to three glacial systems on the Svalbard Archipelago. The validity of the resulting estimations of ice thickness are established with a detailed error analysis.

The paper is clearly relevant and within the appropriate scope for the journal. Contemporary interest in methods for inferring ice thickness are of great interest to the community, as evinced by numerous recent publications on the subject, including a comprehensive intercomparison (Farinotti et al., 2016). This paper's contribution to the field stems primarily from its presentation of a way to circumvent some of the arduous data requirements required by the method on which it is based (Morlighem et al., 2010). I am concerned that this paper inherits some of the potential shortcomings from that work, namely an error analysis which is not, in my view, completely justified, as well as a misunderstanding of the definition of error for PDE-constrained optimization. Nonetheless, the manuscript does a commendable job with respect to discussing its own limitations and in firmly placing the issue in the context of error analysis. I am not sure that the paper will provoke a sea-change in thinking about Svalbard's glaciological processes, but I imagine that the results will be useful for modellers and others needing ice thickness estimates.

Stylistically, I think that the paper could benefit from significant distillation. The elimination of superfluous words, sentences, and perhaps even sections would help the reader to focus on essential points. As it stands, the manuscript feels like a methods paper mixed up with a case study. A stronger partitioning between these two parts would help. The paper also contains a fair amount of questionable English. I have tried to make corrections where I can, but a more detailed reading by the authors themselves is in order.

The manuscript was re-structured and copy-edited by native speakers during

the revision. In addition, an effort was made to further distill the presentation of the results.

Ultimately, under the assumption that the authors can address the criticisms that I have presented below, I would encourage resubmission.

1 Major Points

1.1 On the use of "apparent flux divergence"

The phrase "apparent mass balance" is well ensconced in the literature at this point, and the reasoning for its use is fairly clear: when $\partial_t h$ is used as an observation, it acts identically to $\dot{b}$, which is a source term. Combining them leads to a simplified equation involving the flux divergence and this unified source term. The term 'apparent flux divergence' makes no sense at all. In fact, a more correct statement would be to just call the apparent mass balance the flux divergence (rather than apparent flux divergence), because that is what the equal sign implies. However, this would be confusing and tautological to say that the flux divergence equals the flux divergence. It is equally confusing, but perhaps less correct to say that the apparent flux divergence equals the flux divergence. If it's not clear already, I suggest using the term 'apparent mass balance' instead.

As the reviewer rightly points out, the 'apparent mass balance' is a difference between all mass balance terms (internal, surface and basal accumulation and ablation) and the surface elevation changes $\partial_t h$. Relying on the 'Glossary for glacier mass balance', this difference is certainly not referred to as a mass balance, except if $\partial_t h$ is zero, which is most evident. That's why we initially refrained from invoking the term 'mass balance'. Yet we understand the concern of the reviewer on our choice for the term 'apparent flux divergence'. In lack of a better alternative and since the term 'apparent mass balance' is somehow already established in the literature, we adjusted the manuscript appropriately.

Corrected *as suggested.*

1.2 General characteristics section, and the extensive use of proper nouns

This paper walks a difficult line between a methods paper and a case study. I don't have a problem with that, as it's generally useful to see methods applied to real cases to evaluate their worth. However, I think that the organization of this paper is such that it can be quite confusing. I would suggest reorganizing the paper such that the methods are completely stated (including the theory behind the error analysis; more on that in a minute), then switch gears and begin discussing the nuances of Svalbard's geometry and data availability. Thus I would not have to remember what and where Austre Torrellbreen is after reading many pages about hyperbolic PDEs.

Agreed. We rearranged the manuscript accordingly and present the methodology prior to the presentation of the study site.

Corrected *as suggested.*

Additionally, all figures need to be labelled with salient features discussed in the text. The reader should not have to cross-reference Figure 2, while at the same time reading the paper text and analyzing the figure content. Additionally, some basic annotations describing some particular key points referenced in the text and restated in the figure captions would be very helpful.

We now labelled the more salient features in most figures. Moreover, some particular key points were added in the captions.

Corrected *as suggested.*

1.3 Estimates of input observation error

Input data error estimates need to be stated more clearly and with more complete justification. For example, the authors use a mean value of 5 m for estimated thickness error for all experiments, based on a (convincing) paper in which GPR was applied to a relatively thin glacial system, with lower wavelength antennae. It is not tenable to assume the same error estimate for airborne radar measurement from the 1980s. Also, no real effort is made to justify the 0.2 m yr^{-1} estimate in apparent surface mass balance.

Concerning the measurement error associated with the used thickness data, we now decided to distinguish between GPR and airborne surveys on VIC. Petterrson et al. (2010) estimate the error for these surveys to be 9.3 and 23.1 m, respectively. For the formal error estimate on VIC, we now use 10 and 25 m. For WSB and THPB, we kept the 5-m estimate from Lapazaran et al. (2016), who relied on a WSB portion of the thickness measurements used in our manuscript.

Concerning the SMB uncertainty estimate, we rely on Lang et al. (2015) who compared their simulated SMB values to observations. This comparison gave the means to justify an uncertainty estimate. In the SMB input description, we now specify the following:

'*The difference between modelled SMB values and 10 used validation sites shows a low bias of -0.03 m i.e.* yr^{-1} *with a standard deviation of 0.14 m i.e.* yr^{-1}*. The latter value is considered as an uncertainty estimate for the SMB field.*'

Concerning the error in $\partial_t h$*, Moholdt et al. (2010) compute an average 0.3 m* yr^{-1} *at all cross-over points for their 'plane method'. In the section on the* $\partial_t h$ *input, we now added:*

'*Moholdt et al. (2010) report that the local root-mean-square deviation of several hundred*

surface-change estimates is 0.3 m yr^{-1}. .'

***Corrected** by adjusting the airborne and ground RES measurement uncertainty on VIC. Moreover, we now provide some motivation for a 0.4 m yr^{-1} input uncertainty for the apparent mass balance.*

For all of these error sources, the distinction between simple observational error and the error associated with the variables used in your equations (which are time averaged) needs to be discussed. See the methods section of Brinkerhoff et al. (2016) for a discussion of what I mean by this; in short, Eq. 1 assumes that all of the inputs are temporally consistent, but in reality they are not, and this induces an additional source of uncertainty.

In reponse to this appreciated comment we added a passage to the description of the formal error estimate (new Sect. 2.2.3; former Sect. 3.2.3)

'[...], the error analysis accounts for uncertainties in the observational record but does not comprise the error that stems from time-averaging of the input and temporal inconsistencies between different fields. A detailed assessment and treatment of various input errors within a Bayesian framework is presented in Brinkerhoff et al. (2016).'

***Corrected** by adding a brief discussion on this error source term and pointing to the suggested reference.*

1.4 Flow directions

I strongly suggest reading Kamb and Echelmeyer (1986), when approaching flow direction computations. They provide a strong theoretical basis for how to approach ice routing using only surface elevation observations in order to approximately recover higher-order directions. With the availability of these theoretical results, which have been used successfully many times throughout the balance flux literature, I find the ad-hoc method of smoothing by applying a contouring algorithm then using natural neigh- bors interpolation to degrade the surface elevation accuracy to be troubling. Barring the success of the smoothing proposed by Kamb and Echelmeyer (1986) at eliminating closed basins (which I understand to be the problem that elicited the ad hoc approach), there are plenty of basin filling algorithms that would also solve this problem in a somewhat more rigorous way.

This comment of the reviewer is most appreciated because the suggestion to refer to the balance flux literature did substantiate the calculation of the flux direction. We now decided to follow the approach presented in Brinkerhoff & Johnson (2015) for the determination of the flux direction (Eqs. 9 and 10) by solving a partial differential equation for a smoothed version of the driving stress. In this way, the direction choice is based on theoretical arguments and it is very convenient that the smoothing radius varies with the ice

thickness and thus naturally adjusts to different glacier sizes.

Corrected *by opting for the direction choice forwarded in Brinkerhoff & Johnson (2015).*

This consideredation should also be included when using the SIA to infer thickness fields from the balance flux. Contemporary surface DEMs often show topography at a much smaller scale than that which is relevant for determining driving stress in the Stokes' equations, and smoothing is necessary to avoid non-physical oscillations.

The smoothed driving stress solution is now also used in terms of a smooth surface topography entering the SIA equation.

Corrected *as suggested.*

1.5 $\dot{a}$ as a control variable

The $\dot{a}$ resulting from the inversion procedure needs to be presented, because the derived thickness field only conserves mass with respect to this augmented field, and in my experience performing these types of inversions for $\dot{a}$ without considerable explicit smoothing leads to an apparent mass balance that can look pretty weird. Indeed, it becomes the dumping ground for all manner of errors derived from other input fields and the model itself. One way of getting around this is to apply a regularization term to $\dot{a}$ (with a regularization parameter associated with the length scale of feasible spatial variability in apparent mass balance), just as it is already applied to H in Eq. 4.

Initially, we did not provide these fields because the article was already rather long and the information gained from this comparison is of interest to a rather limited community. Anyhow, differences are instructive and provide some intuitive understanding on how the optimisation works. Therefore, we provide now another figure showing the final apparent mass balance fields for both regions and a brief discussion, both in a separate Appendix section. The difference fields show no dominant spatial variability pattern, which would justify another regularisation term in the cost function. Moreover, a general bias/drift was already prevented by penalising differences between the initial and the final apparent mass balance. Therefore, we refrained from any modification of the cost function.

Corrected *by adding the requested figure and a brief discussion in the Appendix. We did not see the necessity to add the suggested regularisation term to the cost function.*

1.6 Boundary conditions

The PDE being solved here (Eq. 1) involves only first spatial derivatives and no

time derivative. As such, the number of boundary conditions allowed is limited to one per characteristic. An ice divide implicitly acts as a zero-flux boundary, meaning that specifying the flux at the margin is not well-defined. Nonetheless, the magic of numerical solutions allows it anyways. However, one needs to be quite careful to understand that this introduces a fictitious source term (as it must for mass to be conserved) that needs to be accounted for in error estimates and interpretation of results. This artifact is evident in Fig. 4, along the eastern margin of VIC, where thickness is around 300m right up until it reaches a land terminating boundary. In a sense, this is the opposite problem of that which you're trying to solve with the first term in Eq. 4, but rather than the flux running out before reaching the margin, it doesn't go to zero fast enough. Perhaps consider introducing another term to Eq. 4 that adjust the surface mass balance so that flux goes to zero along land terminating boundaries?

> *The reviewer rightly points out that there are fictitious source and sink terms in the ice flux at any boundaries. These terms accommodate inconsistencies particularly in areas where multiple Dirichlet conditions are set. These terms are not necessarily biased as values are both negative and positive for a single test geometry. We followed the reviewers suggestion and made several attempts to reduce these fictitious values by directly penalising them or by increasing the flux-solution smoothing around the land-terminated margin. The solution could actually be improved near the margin for some glaciers. Yet for others, a worthwhile reduction of the magnitude of these boundary source and sink terms could only be achieved at the expense of other terms in the cost. We could not find settings that resulted in an overall improvement for all test geometries. We therefore cannot offer a solution within this revision as more development is necessary.*
>
> ***Not corrected**. Several attempts to solve the raised issue did fail and require more development.*
>
> *The thickness artifact, the reviewer mentions (Fig. 4), is certainly associated with a flux field that does not necessarily decrease most gradually to zero as the margin is reached. Yet the mentioned area also shows that the surface elevation reaches 300m near the margin. We do not think that this is a real feature but rather some inconsistency between the chosen DEM and the glacier inventory margin position. Along other segments of the land-terminated margin, ice thickness decreases more gradually.*
>
> *Though not specifically asked here, we removed the Dirichlet condition on ice thickness at the measurements locations and replcaed it by another term in the cost function. In this way, further fictitious source and sink terms in the solution are avoided.*
>
> ***Replaced internal Dirichlet conditions** in second-step reconstruction by extra cost term.*

1.7 Formal error estimate

This section is mostly based on Morlighem et al. (2010), with the key difference that flux at measurement locations is directly imposed via Dirichlet boundary conditions rather than a best match found through an inverse procedure. This is problematic, for the same reason discussed in the above point about boundary conditions: imposing the value of the flux at more than one location along a flightline must lead to a fictitious numerical source in order for the condition to be upheld, because the PDE is first-order and only admits a single boundary condition per characteristic. Thus there is a hidden source term that needs to be included in the estimate of $\dot{a}$ that is likely to locally exceed the (already very optimistic) error estimate of 0.2m yr^{-1}.

On a related note, I think that the estimate of uncertainty in surface mass balance is probably incorrect following the inversion procedure. Consider the following line of reasoning: the PDE for error propagation is derived by stating that

$$\nabla \cdot (\mathbf{n} + \delta\mathbf{n})(F + \delta F) = \dot{a} + \delta\dot{a} \tag{1}$$

which is separated into

$$(\nabla \cdot \mathbf{n}F - \dot{a}) + (\nabla[\mathbf{n}F + \delta\mathbf{n}F] - \dot{a}) = 0, \tag{2}$$

where n is the true (error free) flow direction, F the true flux, and $\dot{a}$ the true apparent mass balance, and the -annotated quantities are the errors associated with each of these quantities. The first term is zero due to mass conservation, and the second is solved for δF to get the error in the flux. The problem arises in the definition of $\delta\dot{a}$. In the manuscript it is given a numerical value (0.2m yr^{-1}), which is supposed to represent the observational uncertainty. However, after the optimization procedure is complete, which makes significant modifications to $\dot{a}$ (I assume, which is why it needs to be reported), this variable is no longer the value for which that particular error estimate holds. Instead, it is a new and potentially non-physical field into which has been placed error in surface elevation, smoothing lengths, numerical error, etc. The field resulting from the optimization is neither the true value $\dot{a}$, nor the original field for which the error estimate was made, and as such $\delta\dot{a}$ must pick up the remaining difference. I presume that it would thus be substantially larger than the initial 0.2m yr^{-1} estimate and would be neither independent nor identically distributed.

As a final objection, I do not understand this business of taking the minimum of two error propagation PDEs, one with a reversed velocity field. Why should a more favorable error estimate propagate back upstream from an observation, given that hyperbolic PDEs transport information in one direction only (with respect to a characteristic). It is interesting to note that neither publication that initially stated this method (Morlighem et al., 2010, 2014) gives a reference for it, and I have never been able to find one in my own literature searches. I invite the authors to

take this opportunity to convince me of this idea's correctness.

Now, lest I appear too curmudgeonly on this issue: is all this a big problem? Probably not. My Bayesian treatment of the problem (Brinkerhoff et al., 2016) suggested that the error estimate suggested here isn't too bad in a practical sense, and the cross-validation presented in the latter parts of this manuscript suggest the same. Additionally, the additive model of errors used in the PDE error propagation equations would tend to overestimate uncertainty (for the same reason that adding two Gaussian random variables doesn't double their standard deviation). However, I would like to see a more robust defense of the theory behind the methods used, and a more transparent accounting of the simplifying assumptions.

> *The reviewer is rather critical about the presented error estimation, which was certainly never intended to be a strict probabilistic measure. Yet, the presented error estimation is of a practical use and it should be able to distinguish areas in which the thickness reconstruction is well constrained from others where this is not the case. In the most practical sense, the latter areas could be the target for future survey campaigns. We certainly do not want to promote the error estimate field as an input for further error analysis. Here, our concern is that the field could be picked up for assessing the sensitivity of glacier volume projections to bedrock changes. For such a purpose, more stringent statistical measures should be invoked and implemented. One of the next development steps certainly includes the implementation of a more stringent treatment of uncertainties from diverse sources.*
>
> *The reviewer also asked for a more robust defense of the error-estimate theory and its limitations/assumptions. This is not evident because our approach is informed by Morlighem et al. (2011), who did not provide any reference. Anyhow, we gladly try to provide more information on assumption and limitations. In this approach, we have a certain control on the error at the measurement location from the acquisition instruments/settings. The central assumption is then of course that the erroneous flux field also fulfills the mass conservation, which implies that the error is propagated along the flow downglacier. This assumption might not be too problematic as long as input uncertainties do not dominate. Exclusive downstream error propagation results in a sawtooth structure with error estimate that increase gradually until a next downstream measurement is reaches where values drop abruptly. To avoid this structure, we followed the upstream propagation presented in Morlighem et al. (2011). A first argument why this might anyhow hold comes from the mass conservation equation itself. A multiplication by (-1.0) is analytically identical though numerically different. In addition, the physical interpretation is upward motion with an inverted source and sink field. We however understand the concern that the error should not propagate upstream against the ice flux. The reviewer might however agree that*

a measurement constrains the thickness field also some way upstream. This would imply that the error has to decrease along a flowline the closer one gets to a measurement. The rate of this error decrease is certainly questionable. If we accept that errors are allowed to decrease with a certain rate along the flow, then upstream Dirichlet boundary conditions have to be set such that the error equals the measurement uncertainty at the survey locations (further downstream). To improve the conditioning of the problem, we multiply by (-1.0), which is physically interpreted as upstream propagation. Yet, there is a slight nuance in this because we have to deliberately decide now for a rate of error change valid for upstream propagation. This rate might differ from the downstream propagation but as we have no good reason for choosing a different value, we simply set magnitudes equal from the downstream propagation. A similar discussion is added to the text and the reader will be prominently informed about the limitations of upstream error propagation, using a disputable change rate.

Expanded discussion *on the assumptions in the formulation of upstream error propagation.*

The reviewer also raises concerns that the modification of the apparent mass balance field during the optimisation will affect the input uncertainty distribution (assumed constant). Even though a spatially variable input uncertainty field could be accommodated, it is far from evident how to generate such a field during the iterative update of the apparent mass balance within our rather basic error-estimation approach. A more stringent treatment of error distribution would be required, which we like to postpone to further development of our approach. Anyhow, we added a brief passage that the assumption of a constant input uncertainty of the apparent mass balance (and likewise for the surface velocities in the second step) might partially be undermined/corrupted or limited during the iterative update of the control parameters. In addition, the relevance of this concern can be assessed from the now provided comparison between the initial and the final apparent mass balance fields in the Appendix.

Added a brief passage on this particular concern *in the manuscript. Necessary development work for a stringent treatment of various error source terms (as for instance in Bayesian statistics), though not directly requested by the reviewer, goes beyond this revision and would justify another submission.*

1.8 Error estimate results

The formal error estimate should provide an upper bound on the actual mismatch, not a prediction of it. A good metric here would be to compute the frequency by which the actual mismatch falls below the predicted error. In the context of normal distributions, the actual misfit would be less than the predicted misfit 95% (or

whatever your definition of error is) of the time. This is more or less the definition of credibility intervals in Bayesian statistics. If the mismatch falls outside the estimated error much more frequently than this, then one begins to question what use the estimated error is. While it's sort of interesting to consider the median values, this neglects the aspect of error prediction which is likely to be of most interest to people who would use this product: spatial skill.

> *Again the reviewer had a good point on the spatial skill of the error-estimate maps. We therefore added all locations where the min/max interpretation of the error estimates is violated to Fig. 9 (now Fig. 8). Moreover a table is added giving the fraction of the withheld measurements for which the actual mismatch is smaller than the formal error estimate. We find that the min/max interpretation valid in more than 80% of the cases, except if the reconstruction is informed by very few measurments.*
>
> ***Corrected*** *by adding a Table with the requested information.*

1.9 Appendix A
If one cannot attribute the observed flux to deformation in a physically reasonable way (e.g. with a material parameter A that is physically justifiable), then doesn't it make sense to assume a certain amount of sliding? It seems to me that instead of allowing viscosity to be an order of magnitude less than temperate ice, one could adjust β^2 instead. This would make for a much more straightforward way of interpreting a figure like Fig. A1. I recognize that the authors may not wish to add the additional uncertainty of selecting a sliding law to the model, and I'm certainly fine with that. However, the notion that the viscosity parameter is aliasing unmodelled basal processes should at least be addressed.

> *We refrained from choosing an additional sliding law but rather invoke the notion that the viscosity parameter is aliased by unaccounted model physics.*
>
> ***Added*** *notion on unaccounted physics aliasing the tuning of the viscosity parameter.*

2 Minor Points and Technical Corrections
NOTE: This paper has a relatively high number of typos and grammatical errors. I will try to point them out where I see them, but the manuscript would benefit considerably from detailed copy editing.

P1L4 Please define what 'performs well' means.

> ***Reformulated*** *as follows.*
>
> *'The approach is applied to a variety of test geometries [...]'*

P1L12 'Withholding parts': the paper shows this in a median sense, not a spatially explicit one, which is an important point.

Corrected *by adding the adjective 'median'.*

P1L16 'are in fact'⟶ 'is'.

Corrected *as suggested.*

P2L4 Delete 'large' (and non-specific adverbs throughout the manuscript at large).

Done *during the copy-edit.*

P2L5 'thickness of the ice cover' ⟶ 'ice thickness'.

Corrected *as suggested.*

P2L11 'Antarctica Ice Sheet' ⟶ 'Antarctic Ice Sheet'.

Corrected *as suggested.*

P2L13 'thicknesses' ⟶ 'thickness'.

Corrected *as suggested throughout the manuscript.*

P2L35 Perhaps elaborate on what 'computationally less favorable' means.

Reformulated. *'[...] at the expense of computational costs.'*

P3L1 delete 'physical'.

Done.

P3L7 I don't understand the implication of this sentence.

Deleted sentence.

P3L14 'allows to estimate'⟶ 'allow estimation of'.

Done.

P3L15 Missing period.

Inserted *full stop.*

P3L15 'Much development ...' needs citation.

Inserted *relevant reference.*

P4L1 'For DEMs and elevation changes...' this sentence doesn't really say anything.

Deleted sentence.

P4L18 Citations are needed throughout.

Added relevant citations *for remote-sensing based DEM generation and velocity measurements.*

Introduction at large I suggest including a paragraph on the general availability of thickness observations for consistency.

Added *two sentences on the availability of thickness measurements referring to GlaThiDa 2.0.*

P4L2324 This sentence needs a bit more specificity.

Deleted sentence*.*

General characteristics at large This section should be compressed a bit to ensure that the information presented is relevant to the conclusions of the paper.

Paragraph was shortened*.*

Glacier outlines why not use the modern high-res DEM everywhere?

No action taken*. High-resolution DEM is not available for Southern Spitsbergen.*

P6L11 'For VIC, thickness measurements' $\longrightarrow$ 'VIC thickness measurements'.

Corrected *as suggested.*

P6L14 Delete 'there only'.

Done*.*

P6L23 Do borehole depths agree with GPR?

Values agree on view*. A direct comparison is difficult as the positioning of these icecores has an uncertainty of roughly 100m. For the deep borehole B closest to the ice front (bed contact after 206m; Jania et al., 1996), the GPR survey line shows a local thickness maximum of about 200m.*

Figure 2 Is $\partial_t h <$ SMB along ice divides? This was a problem I encountered in ITMIX.

No action necessary*. Panels (e) and (f) of Fig.2 show that the apparent mass balance is positive over most of the divide areas.*

P9L25 Olex needs a citation.

Removed sentence *because a co-author also commented that the Olex system is mentioned too prominently.*

P10L8 I think you can delete everything up to 'incompressibility can be written as ...'.

Corrected *as suggested.*

All equations The divergence operator is traditionally written as $\nabla\cdot$, rather than just ∇, which is typically thought to mean the gradient operator.

Corrected *as suggested.*

P10L28 'Inflow boundaries': I don't understand this sentence.

Reformulated sentence *as follows.*
'Inflow boundaries did not occur in our setup. These would require Dirichlet conditions on the ice flux.'

P11L18 I'm not sure I understand how using the spatial gradient in SMB solves the problem. Assuming that SMB is only a function of elevation, doesn't SMB also reach a maximum where slope goes to zero, i.e. SMB also has a very small slope where surface elevation does?

Sentence was removed *as SMB gradients are in fact only used where surface slopes become exactly zero. Initially, it was wrongly stated that the SMB gradients replace the surface slopes where their magnitude is less than α_0. Actually this emergency strategy is only necessary for some marine glacier snouts for which the DEM is completely flat for instance where the DEM and the glacier inventory are inconsistent). The SMB calculations rely on a different geometry and were therefore free of these artifacts.*

P11L24 Not sure what is meant by 'ice-flux direction is positive'.

Corrected *to 'flux magnitude is positive'.*

Eq. 4 I think that the integral should be

$$\int_F^{\infty} \delta(s)\mathrm{d}s\mathrm{d}\Omega \tag{3}$$

This means that if $F < 0$, then the integral crosses the origin, and the δfunction is activated. As it is, the function penalizes positive flux values. Writing that integral as a Heaviside function might be more clear.

Corrected *by rewriting the integral as a Heaviside function.*

P11L30 Maybe just state the parameter values and reasoning behind them, and forego subjective descriptions like 'good performance'.

Removed *the subjective description.*

P12L11 In glaciology, aspect ratios under which the SIA applies are usually referred to as small, rather than large. This derives from the aspect ratio being the small paramter in the asymptotic analysis of the SIA.

Corrected.

P12L24 Again, read Kamb and Echelmeyer (1986) for some theoretic basis for how to smooth for SIA applications.

Corrected. *We now consistently use a smoothed surface-slope field following Brinkerhoff and Johnson (2015).*

P12L29 A clearer sentence might read 'We apply a correction to the computed flux in order to avoid negative thickness values'.

Corrected *as suggested.*

P13L2 Would it be possible to explain why these particular functions and parameters were chosen?

The details of the flux correction is now presented in the Appendix. In this way, the general reader is not interrupted by the technicalities of this correction. The appendix now allows more space for explaining the choice of the functional dependence and the parameter choice. ***Paragraph was moved to the Appendix*** *where more specifications are given.*

P13L4 'If no observations ...' I don't understand this sentence.

Reformulated *the passage accordingly.*

Formal error estimate There should be at least a mention of additional error induced by using the SIA. This should include error in the surface gradient norm, among other things.

Added *not on these error sources.*

P14L27 'to' ⟶ 'too'.

Done.

P115L1 Maybe make a reference to L-curve analysis here.

No action undertaken. *We refrained from a strict L-curve analysis because it does neither give an objective criterion for parameter selection. The analysis will not be straight forward as 5 multipliers have to be considered.*

P16L12 'geoemetry' SIC.

Done.

P16L17 Maybe note that for a region bounded by two flowlines, flux is always at a maximum at the ELA.

No correction necessary. *We are not sure if this generally holds when* $\partial_t h \neq 0$.

P16L24-26 Is it that the old routing is still dominant on the surface topography, or that the velocity field and DEM aren't contemporaneous?

Reformulated paragraph. *The VIC surface geometry is from 2010 and our ice velocities from 2015-16 so both explanation hold. Yet 2008 velocities already show that both branches were active (Pohjola et al., 2011). Therefore, the reason is that the old routing is still dominantly imprinted on the topography.*

P17L1 This line makes a strong case that $\delta\dot{a} = 0.2$ everywhere might not be right.

We increased the input uncertainty $\delta\dot{a}$.

Ice thickness and bedrock elevation at large Is it possible to extend the results of your error analysis to integrated quantities like total sub-sea level area or total volume? It would make these numbers considerably more interesting if we could be sure that they represented a (statistically) significant departure from previous estimates.

The interpretation of median error-estimates as upper constraints on the aggregate mismatch can certainly be transferred to the ice volume and the area fraction below sea-level. Even if error estimates are rather high, the previous estimate for ice grounded below sea-level on VIC of 5% falls outside the maximum range of 6 - 23%. We also provide now maximum ranges for the mean ice thickness. These ranges are given for both the first and second step in the reconstruction approach.

Added maximum ranges for the integrated quantities.

P22L26 'Therefore ...' I don't understand this sentence.

Removed sentence.

Figure 8 A gradient, rather than random colorbar would be useful here. Also, linear axes would help to get a sense for the sizes of the error bars.

No action undertaken. *In the presented way, colours are clearly distinguishable. ColorBrewer does not advice the usage of a sequential or divergent (both gradual) colour map with 12 colours. Results cluster and overlap using linear axes .*

P24L4 'none'⟶ 'any'.

Done.

P25L23 Delete 'anyhow'.

Done.

Ice thickness at large Much of this section focuses on the differences between the first and second-step solution. Perhaps a figure showing the differences between the two predicted thickness fields would help the reader get a sense of how the differences are distributed?

We refrain from adding a difference plot because its interpretation is not necessarily more evident than comparing absolute values.

No action undertaken.

Figure 9 The transparency method for delineating which areas were subject to the second stage isn't very clear. Maybe switch colormaps or just draw a line around the areas that were updated. Error estimates at large If error estimates go up when using the second stage, please convince me why the second stage is useful. Perhaps a similar plot to Fig. 8 is in order, which would hopefully show that including velocity observations reduces the actual mismatch for withheld measurements.

Removed transparency and added median error-estimate/mismatch plot *similar to Fig. 8 (now Fig. 7).*

P27L11 There's no 'might' about it: ignoring sliding biases the result towards thicker ice.

Adjusted *as suggested.*

P28L14 Perhaps consider reading Brinkerhoff (2016), which discusses this point in somewhat more detail.

See above *corrections.*

P29L23 'mere' $\longrightarrow$ 'a mere'.

Done.

P30L6 'tend to overestimate mismatch values' when taken in aggregate, but not necessarily individually.

Corrected *by distinguishing between error estimates in terms of an aggregate median value and for individual measurements*.

P30L7 'Error estimates can here be considered upper and lower constraints of inferred thickeness values' $\longrightarrow$ is this not the operational definition of error? If we knew that error was the exact amount by which our estimates were off, then we could just subtract it and get perfect results.

Removed sentence.

P33L17 'For glaciers ...' this sentence is pretty awkward.

Removed sentence *because it held self-evident content.*

Figure A4 This might be better served by displaying a map of the difference in thickness between the two experiments.

Not adjusted *because zero thickness values are well visible in this map. Difference plots showed no improvement.*

References

Brinkerhoff, D. J., Aschwanden, A., and Truffer, M. (2016). Bayesian inference of subglacial topography using mass conservation. Frontiers in Earth Science, 4(8).

Farinotti, D., Brinkerhoff, D., Clarke, G. K. C., Fürst, J. J., Frey, H., Gantayat, P., Gillet-Chaulet, F., Girard, C., Huss, M., Leclercq, P. W., Linsbauer, A., Machguth, H., Martin, C., Maussion, F., Morlighem, M., Mosbeux, C., Pandit, A., Portmann, A., Rabatel, A., Ramsankaran, R., Reerink, T. J., Sanchez, O., Stentoft, P. A., Singh Kumari, S., van Pelt, W. J. J., Anderson, B., Benham, T., Binder, D., Dowdeswell, J. A., Fischer, A., Helfricht, K., Kutuzov, S., Lavrentiev, I., McNabb, R., Gudmundsson, G. H., Li, H., and Andreassen, L. M. (2016). How accurate are estimates of glacier ice thickness? results from itmix, the ice thickness models intercomparison experiment. The Cryosphere Discussions, 2016,1-34.

Kamb, B. and Echelmeyer, K. (1986). Stress-gradient coupling in glacier flow: I. longitudinal averaging of the influence of ice thickness and surface slope. Journal of Glaciology, 32(111).

Morlighem, M., Rignot, E., Mouginot, J., Seroussi, H., and Larour, E. (2014). High-resolution ice-thickness mapping in south greenland. Annals of Glaciology, 55(67).

Morlighem, M., Rignot, E., Seroussi, H., Larour, E., Ben Dhia, H., and Aubry, D. (2010). Spatial patterns of basal drag inferred using control methods from a full-stokes and simpler models for pine island glacier, west antarctica. Geophysical Research Letters, 37(14).

Response to the
Interactive comment on "Application of a two-step approach for mapping ice thickness to various glacier types on Svalbard" by Johannes Jakob Fürst et al.

F. Maussion (Referee #2)
fabien.maussion@uibk.ac.at
Received and published: 13 April 2017

First of all we want to thank the reviewer for constructive comments on our manuscript. All comments have been taken into account and a list of answers and undertaken actions is given below. Answers are indented and in italic type while a ***short summarising reply*** *is provided in italic, bold-face type.*

General comments

In their manuscript, the authors present a new method to estimate the ice thickness of glaciers and ice-caps. They rely on an established theoretical background, but the paper presents innovative ways to deal with limited or inconsistent data input. The study is solid, comprehensive, and I am confident that many readers will find the paper useful for their research. I agree with most (if not all) of the issues raised by D. Brinkerhoff, and there is no point in repeating them here. However, I will modestly try to offer a different perspective, driven by my personal interests (large scale glaciology and reproducible science).

Generalisation of the method to other glaciers/regions

The authors state two times (in the abstract and in the conclusion) that their method has "data requirements which are comparable to other approaches that have already been applied world-wide". I have to disagree with this statement, which unnecessarily raises the readers expectations. To my knowledge, we are still far away from a global dataset of surface mass-balance and $\partial h/\partial t$. The most promising method to estimate geodetic mass-balance (DEM differencing) is rarely applied to regions larger than a catchment or mountain chain, and the global methods (GRACE, Icesat) suffer from considerable drawbacks (coarse spatial resolution and high uncertainties). Therefore, I suggest to remove this statement from the abstract. My understanding of the study is that it presents a way to deal with uncertainties in the boundary conditions and in the observations to which the model is tuned. Most efforts, it seems, are spent into correcting $\dot{a}$ to avoid singularities and in defining a formal way to propagate observational uncertainties. In the end, I feel like the paper would benefit from a more thorough discussion about the benefits and drawbacks of their method for large scale experiments, i.e. without any observation and/or without an observational dataset for $\dot{a}$.

> *We agree with the reviewer that reconstruction approaches that are applied world-wide comprise an approximation for unknown input fields as SMB and*

surface elevation changes. Such a parametersiation is indeed not presented here. So, our approach is not directly transferable worldwide. We therefore rephrased sentences in the abstract and the conclusion. In this way, no expectations on global applicability are raised. Therefore, a discussion on benefits and drawbacks of the presented approach in terms of global application become dispensable.

***Corrected** by rephrasing sentences in the abstract and conclusion.*

Structure of the paper

Like D. Brinkerhoff, I notice that the paper could gain in readability. I am however unsure how to proceed. One the one hand, I truly appreciate the authors thoroughness, and I am sure that the interested reader will find most of the information s/he needs to reproduce the steps listed here. On the other hand, the paper is long and sometimes difficult to follow. A change along the lines proposed by D. Brinkerhoff will surely improve the papers readability, but I would refrain from cutting too much text out of the paper: instead, move some details to the appendix or the suppl. material. (take the paragraph about the slope angle threshold for example: a specialist will probably be interested in this information, but a more general audience would rather skip these details).

We restructured the article according to the suggestions by reviewer #1. The passage on surface slope averaging was removed as we no follow another approach to determine flux directions. See answers to reviewer #1

***Corrected** by re-structuring the article.*

Case study?

To test a new method, one should rely on the best possible data input for calibration/validation. When looking at the fields in Fig. 02 I cant really imagine that this is the case in Svalbard. It is too late for this study, but in the future I would suggest to look at more appropriate benchmark glaciers (right at our doorstep?), where data denial experiments can be realised much more easily and with much more confidence in the boundary conditions.

We understand the reviewers concern on the input data quality on Svalbard. In ITMIX phase 2, we anticipate test glaciers for which reliable input fields will be made available in the near future. Once available, the ITMIX setup will certainly serve as a standardised benchmark for model validation.

***No action undertaken**.*

Specific comments

P2, L2 "**virtually complete coverage**" none of the cited studies (apart maybe from Paul et al, which is rather a methodological review paper) states that surface elevation change products have reached complete coverage. This is related to my general comment: the method presented in this paper is promising, but still belongs to the demanding ones in terms of data availability.

The specific passage, the reviewer points at, was misleading as we tried to condense to many aspects. We therefore reformulated the respective sentences giving more details and trying to be more specific.

***Corrected** accordingly.*

P2 L27 "**apparent flux divergence**" I also think that this new terminology makes no sense. One can argue about whether apparent mass-balance is the best term or not, but "apparent flux divergence" is definitely more confusing than helping.

Reverted terminology back to 'apparent mass balance'. For details see answers to reviewer #1.

***Corrected**. We now use 'apparent mass balance'.*

Figure 5 Obviously, both the observations and the ice divides (zero flux locations) are way too visible on the bedrock topography. This calls for a more constrained tuning, either by changing the way B is allowed to vary or by changing the way the model is dealing with small slopes?

The slope definition was changed in response to a comment from reviewer #1. This new definition will partially accommodate the slope problem. We do not see a problem with having thickness measurements imprinted in our reconstructed field. If these should be not consistent or show too high spatial variability, data pre-selection or a-priori homogenisation could be anticipated. We do not see the necessity for this here. We refrain from the suggestion to put limits on the tuning parameter B, as it accommodates for uncertainties and discrepancies in the input data as well as assumption in the approach. Therefore limits are hard to derive and they are not necessarily encountered near the divide. The slope threshold is another adjustable parameter but it is already chosen rather small as compared to other reconstruction approaches.

***Adjusted slope computation**.*

Figure 8 I understand the reason for using normalized values here, but from a volume estimation perspective (e.g. sea level rise), other metrics are much more important: bias and absolute error (i.e. small relative errors for large thickness values can be more relevant than large relative errors for small thickness values). Have you considered looking at absolute values, too?

This comment was very helpful because this figure changed often during the writing process. In its final form, it was actually again possible to present absolute values.

***Corrected**.*

Editorial comments

P3 L15 dot is missing

***Removed**.*

Fig. 02 intuitively, I associate blue values with positive mass-balance / surface change and red with the opposite. Consider reversing your colortable.

***Corrected** by inverting colourmap.*

All figures consider damping the topographical shading, which is currently very strong without a clear added value.

***Corrected** by removing transparency from most figures. Only exception is the presentation of the second-step results.*

All figures consider using another colormap. Rainbow (or "jet" in python) is now considered by many as being misleading (e.g. https://www.climate-lab-book.ac.uk/2014/end-of-the-rainbow/ and many further refs online)

***Corrected** by changing rainbow colourbar to another colourbar provided by ColorBrewer2.0.*

Application of a two-step approach for mapping ice thickness to various glacier types on Svalbard

Johannes Jakob Fürst[1], Fabien Gillet-Chaulet[2], Toby J. Benham[3], Julian A. Dowdeswell[3], Mariusz Grabiec[4], Francisco Navarro[5], Rickard Pettersson[6], Geir Moholdt[7], Christopher Nuth[8], Björn Sass[1], Kjetil Aas[8], Xavier Fettweis[9], Charlotte Lang[9], Thorsten Seehaus[1], and Matthias Braun[1]

[1]Institute of Geography, University of Erlangen-Nuremberg, Wetterkreuz 15, 91058 Erlangen, Germany
[2]University of Grenoble Alpes, CNRS, IRD, Institut des Géosciences de l'Environnement (IGE), CS 40 700, Grenoble, France
[3]Scott Polar Research Institute, University of Cambridge, Lensfield Road, Cambridge CB2 1ER, United Kingdom
[4]Faculty of Earth Sciences, University of Silesia in Katowice, ul. Bankowa 12, 40-007 Katowice, Poland
[5]Departamento de Matemática Aplicada a las Tecnologías de la Información y las Comunicaciones, desp. A302-4, ETSI de Telecomunicación. Universidad Politécnica de Madrid, Av. Complutense 30, 28040 Madrid, Spain
[6]Department of Earth Sciences, Uppsala University, Geocentrum, Villav. 16, 752 36 Uppsala, Sweden
[7]Norwegian Polar Institute, Fram Centre, Postbox 6606 Langnes, 9296 Tromsø, Norway
[8]Department of Geosciences, University of Oslo, Postboks 1047, Blindern, 0316 Oslo, Norway
[9]Department of Geography, University of Liège, Quartier Village 4, Clos mercator 3, 4000 Liège, Belgium

Correspondence to: Johannes Fürst (johannes.fuerst@fau.de)

Abstract. The basal topography is largely unknown beneath most glaciers and ice caps and many attempts have been made to estimate a thickness field from other more accessible information at the surface. Here, we present a two-step reconstruction approach for ice thickness that solves mass conservation over single or several connected drainage basins. The approach ~~performs well for~~ is applied to a variety of test geometries with abundant thickness measurements including marine- and land-terminating glaciers as well as a 2 400km^2 ice cap on Svalbard. Input requirements are kept to a minimum for the first step~~are comparable to other approaches that have already been applied world-wide. In the first~~ . In this step, a geometrically controlled, non-local flux solution is converted into thickness values relying on the shallow ice approximation. In a second step, the thickness reconstruction is improved along fast-flowing glacier trunks on the basis of velocity observations. ~~In both steps , thickness measurementsare assimilated as internal boundary conditions~~Both steps account for available thickness measurements. Each thickness field is presented together with ~~a map of error estimates which stem from~~ an error-estimate map based on a formal propagation of input uncertainties. These error estimates point out that the thickness field is least constrained near ice divides or in other stagnant areas. ~~The error-estimate map also highlights key regions for future thickness surveys as well as a preference for across-flow acquisition. Withholding parts~~ Withholding a share of the thickness measurements~~indicates that error estimates show a tendency to overestimate actual mismatch values . For very sparse or non-existent thickness information, our reconstruction approach indicates that we~~ , error estimates tend to overestimate mismatch values in a median sense. We also have to accept an ~~average~~ aggregate uncertainty of at least 25% in the reconstructed thickness field for glaciers with very sparse or no observations. For Vestfonna, a previous ice volume ~~estimates have~~ estimate based on the same measurement record as used here has to be corrected upward by 22%. We also find that a ~~12~~13% area fraction of the ice cap ~~are~~ is in fact grounded

below sea-level~~as compared to the previous~~ . The former 5% ~~estimate~~estimate from the direct measurement interpolation exceeds the maximum range of 6 - 23% as inferred from the map of thickness error-estimates.

1 Introduction

For the 210'000 glaciers and ice caps ~~that we find~~ on this planet (Bishop et al., 2004), satellite remote sensing based on optical or radar instruments ~~has recently enabled us to measure changes in glacier extent and in surface elevation with virtually complete coverage (e.g. Zwally et al., 2011; Rankl et al., 2014; Paul et al., 2015; Zwally et al., 2015) . Yet~~enables us to monitor glacier surface geometry (e.g. Farr et al., 2007; Tachikawa et al., 2011) and glacier extent variations (e.g. Raup et al., 2007; Rankl et al., 2014) . Recent studies have shown that surface elevation changes can be produced on a regional basis (e.g. Berthier et al., 2010; Zwally et al., 2011; However, for the ~~large~~ majority of these ice geometries, there is no information ~~available on the thickness of the ice cover (Gärtner-Roer et al., 2016)~~ on ice thickness (Gärtner-Roer et al., 2014, 2016) . Any attempt to predict the glacier demise under climatic warming and estimate the future contribution to sea-level rise (Radić and Hock, 2011; Radić et al., 2014; Marzeion et al., 2012, 2014; Huss and Hock, 2015) is limited as long as the glacier thickness is not well known. Moreover, the ignorance of the bed topography inhibits the applicability of ice-flow models, which could help to understand dominant processes controlling the ice-front evolution of marine-terminating glaciers. This is because the basal topography exerts a major control on the dynamic response of grounded ice (Schoof, 2007, 2010; Favier et al., 2014). A reason for further concern is that grounded parts of the ~~Antarctica~~ Antarctic Ice Sheet are assumed to respond to climatic warming primarily by outlet glacier acceleration ~~,~~as the floating ice-shelves thin (Paolo et al., 2015) and loose their buttressing ability (Fürst et al., 2016). As it is impractical to measure ice ~~thicknesses everywhere~~thickness for most glaciers, reconstruction approaches have been proposed that can infer thickness fields from available geometric, climatic and ice-velocity information.

In terms of input requirements, reconstruction approaches always need information on the geometric setting. This normally comprises the glacier outline and the surface topography. In the "Ice Thickness Models Intercomparison eXperiment" (ITMIX; Farinotti et al., 2016), two types of reconstruction approaches rely exclusively on this geometric information. The first type ~~stems from a perfect plasticity~~~~assumption~~assumes perfect plasticity, relating ice ~~thicknesses~~ thickness to a glacier-specific ~~yields~~ yield stress, which itself is inferred from the elevation range of the glacier (Linsbauer et al., 2012; Frey et al., 2014; Carrivick et al., 2016). The second type assumes that characteristics of the ice-covered bed topography resemble the nearby ice-free landscape (Clarke et al., 2009). Under this premise, an artificial neural network is trained with digital elevation models (DEM) of the surrounding area. ~~Once sufficiently trained, this approach can efficiently compute glacier bed topographies.~~ Another reconstruction approach (Gantayat et al., 2014) uses additional information on surface velocities and relies on the shallow ice approximation (SIA; Hutter, 1983; Morland, 1986). Under this assumption, surface velocities directly translate into ice-thickness values dependent on glacier-surface slopes. Most of the participating approaches rely, however, on mass conservation. This implies that they need information on the difference between the actual surface mass balance (SMB) and the contemporaneous surface elevation changes. This difference is ~~often~~ referred to as the "apparent mass balance" ~~(Farinotti et al., 2009b)~~ (AMB; Farinotti et al., 2009b) . A large subset of ~~these approaches generates a generic apparent mass~~

balance field the mass-conserving approaches assume a generic AMB informed by the geographic location and the continental character of the prevailing climate assuming specific linear relations to the surface elevation below and above a preset equilibrium line altitude (Farinotti et al., 2009a; Huss and Farinotti, 2012; Clarke et al., 2013). In addition, these approaches rely on the SIA and require an input ice-discharge value for marine-terminating glaciers. As standard procedure, many of the above approaches dissect glacier outlines into a number of centrelines along which the actual reconstruction is performed. Consequently, these approaches are computationally efficient but they require a final interpolation of the thickness values between these centrelines. To avoid such an interpolation, computationally less favorable mass conservation approaches were adopted that find a physical other mass-conservation approaches determine a solution over entire glacier basins (Morlighem et al., 2011; McNabb et al., 2012; Brinkerhoff et al., 2016) at the expense of computational costs. Two strategies are pursued for these reconstruction types. For the one type, ice-flow models are applied in a pseudo-transient way such that the actual surface elevation remains close to observations optimising the bed topography (van Pelt et al., 2013). Dependent on the dynamic complexity, these forward modelling approaches become very expensive in terms of computing resources. For the other type, ice velocities are taken from observations and enter the mass conservation equation, which is then directly solved for ice thickness (Morlighem et al., 2011; McNabb et al., 2012; Mosbeux et al., 2016). Thickness measurements are more or less well accounted for in all of the above approaches. Overview map of the Svalbard archipelago showing ice coverage (blue shading). The two test sites (red shading and rectangles) are Vestfonna Ice Cap (VIC) on Nordaustlandet and the glacier complex comprising the marine-terminating Austre Torell-, Hans-, Paierlbreen (THPB) and the land-terminating Werenskioldbreen (WSB) in Wedel Jarlsberg Land. Background: grey-scale hill-shaded topography based on a 50m from the Norwegian Polar Institute (NPI).

From an observational perspective, operational and regular satellite imagery acquisition has become an indispensable and continuously growing source of information. Therefore, automated procedures have been brought in place providing products such as glacier outlines (Bishop et al., 2004; Atwood et al., 2010; Nuth et al., 2013; Rankl et al., 2014; Paul et al., 2015), digital elevation models (ArcticDEM; ASTER GDEM2, Tachikawa et al. (2011); SRTM, Farr et al. (2007),TanDEM-X, Rankl and Braun (2016)) and surface velocities (Joughin et al., 2010; Rignot et al., 2011; Rignot and Mouginot, 2012; Rosenau et al., 2015; Seehaus DEM differencing then allows to estimate surface elevation changes (Joughin et al., 2010; Rignot et al., 2011; Rignot and Mouginot, 2012; Surface elevation changes can be inferred from DEM differencing. Much development effort is now put into reducing associated uncertainties in these measurements. Glacier outlines are accessible globally and regular updates can be generated with existing methods. For DEMs and elevation changes, different data sources and methods existuncertainties associated with signal penetration and not well known firn properties (e.g. Gardelle et al., 2012; Berthier et al., 2016) . Depending on the missions, the products mission, surface elevation changes can be generated almost operationally for large areas . Surface velocities are somewhat more challenging to infer, certainly where magnitudes are smallor (Gardelle et al., 2013; Rankl and Braun, 2016) . Concerning surface velocities from remote sensing, a good coverage is challenging in areas where displacements are small, where the glacier surface is featureless , such as in the accumulation area, or during periods of rapid changes in surface characteristics(for instance when first melt or snowfall sets in). Consecutive image pairs can then de-correlate leaving gaps in the measurements. In addition, measurement uncertainties become relatively more important where velocities are small. In terms of mass conservation, spatial velocity gradients are required which are susceptible to small measurement uncertainties.

Moreover, associated uncertainties generally exceed 10 m yr^{-1} (Seehaus et al., 2015; Schwaizer, 2016, e.g.) , which limits the reliability in slow moving areas. The SMB field is another prerequisite for mass conservation. It is not directly measurable by remote sensing techniques. Sparse SMB records can be used to determine elevation gradients that are then extrapolated according to a regional DEM (Farinotti et al., 2009b). Otherwise, SMB records are exploited to validate parametric SMB approaches (Möller et al., 2016) or more physically-based ~~, low-resolution~~ regional climate models ~~could be applied (Lang et al., 2015; Aas et al., 2016) .~~ (Lang et al., 2015; Aas et al., 2016) . For ice-thickness measurements, a standardised, open-access database has recently been launched (Gärtner-Roer et al., 2014) and its gradual growth already justified an updated release (Gärtner-Roer et al., 2016) . Despite this international effort, many thickness measurements still remain unpublished.

In light of this continuously growing body of information, input fields for relatively complex thickness-reconstruction approaches are ~~readily~~ becoming more available. In this regard, we present a two-step approach that provides, in the first step, a physically based thickness field over entire glacier basins, ice fields or ice caps with few input requirements (Sect. 2.3). In the second step, velocity information is exploited to update and improve the thickness reconstruction in specific areas (Sect. 2.1). A final interpolation of the basal topography is not required. For a set of three test geometries on Svalbard, the necessary input data were gathered (Sect. 3) and thickness maps ~~were inferred .~~ are inferred (Sect. 4). A rich thickness record is available on these test glaciers and serves to constrain both the ice-thickness distribution and the associated map of error estimates~~(Sect. 4).~~ .

2 ~~Test geometries~~Methods

~~The two-step~~ The thickness reconstruction approach is ~~tested on three ice geometries on Svalbard where an abundant record of thickness observations was available (Fig. 1). These three test geometries comprise Vestfonna ice cap (VIC) on Nordaustlandet, the glacier complex composed of the marine-terminating Austre Torellbreen, Hansbreen, Paierlbreen (THPB) in Wedel Jarlsberg Land and in the same region the land-terminating Werenskioldbreen (WSB). This choice allows an assessment of how the approach performs under different glacier geometries. The reconstruction approach requires as input the glacier outline, the surface geometry, the surface mass balance as well as surface elevation changes. Optionally, ice velocity information can be used to improve the thickness reconstruction in a second step. Fjord bathymetry information and thickness measurements are used to constrain the inferred thickness values.~~

2.1 ~~General characteristics~~

~~VIC is one of the two major ice caps on Nordaustlandet (Dowdeswell, 1986a) , being the largest in the Svalbard archipelago (Fig. 1). According to the 2002-2010 glacier inventory, it covers an area of 2366 km^2 with its summit area lying at 630m above sea level (a.s.l.). Ice flow is channeled through several elongate outlet glaciers, which drain radially from a central crest and export ice to the surrounding ocean (Fig. 2g). For the outlet glaciers on the south side of Vestfonna (Dowdeswell and Collin, 1990) , ice front positions have retreated in the period 1984-2010 (Braun et al., 2011) after more variable terminus fluctuations in the 1970s (Dowdeswell, 1986b) . Despite the steady retreat for most outlet glaciers, Søre and especially Nordre Franklinbreen on~~

the west side advanced notably. This re-advance coincided with a strong acceleration reaching far inland. Surface velocities doubled and now exceed 100 m yr^{-1} over a large area (Pohjola et al., 2011) . Prior to the speed-up, most of the ice was exported via the northern branch of Nordre Franklinbreen based on mass conservation and largely originates from ideas presented in Morlighem et al. (2011) . We opted for a two-step approach because surface velocity information from satellite remote sensing often fails to cover entire drainage basin. Therefore, the first-step, glacier-wide thickness reconstruction can optionally be updated in areas where velocity measurements are available. In the first step, an ice flux is calculated from the difference between SMB and surface elevation changes. The flux solution is translated into thickness values assuming the SIA (Hutter, 1983) . In the meantime, ice velocities indicate that the southern branch is the more prolific export path (Fig. 2g). The bi-modal pattern in ice dynamics is overprinted by cyclic surges with the last active phase observed in 1952 along Søre Franklinbreen (Błaszczyk et al., 2009) . Surges are quasi-periodic cycles of an active phase, during which extremely fast flow can transfer an immense ice volume downglacier, followed by a quiescent phase during which the ice cover in the accumulation area gradually regains its former height. Two other surge-type glaciers are known in the eastern part of Vestfonna. Active phases were reported in 1939 and 1992 for Rijpbreen and during the period 1973-1980 for Bodleybreen (Dowdeswell, 1986b; Błaszczyk et al., 2009) . second step, the mass conservation equation is directly solved for ice thickness in a sub-domain with reliable velocity information.

Austre Torellbreen is a marine-terminating glacier in Wedel Jarlsberg Land, southern Spitsbergen (Fig. 2b). The glacier drains into Skoddebukta on Hornsundbanken and spans altitudes from sea-level to about 900m a.s.l. The most elevated parts of the accumulation area belong to Amundsenisen (above 700m a. s.l.) and are drained by Bøygisen and Løveisen. Before reaching the ocean, Austre Torellbreen is further fed by Vrangpeisbreen from the south, which shares an ice divide with Hansbreen. Hansbreen, in turn, has a dominant main branch receiving important lateral inflow from two prominent tributaries in the southwest, i.e. Deileggbreen and Tuvbreen (Grabiec et al., 2012) . The glacier shows a somewhat reduced elevation range of only up to 500m a.s.l. Beyond the mountain range to the east lies Paierlbreen covering again the full elevation range. This glacier also connects to Amundsenisen in the north via Nornebreen. Kvitungisen provides a large passage to Hansbreen in the west. Lågberisen reaches up to the central divide areas of the glacier complex whereas Perlebreen joins further downstream from the eastern side, just before the ocean is reached. Paierlbreen was not only classified as marine-terminating in the 2002-2010 glacier inventory but the glacier also exhibited surge behaviour in 1993-1999 Błaszczyk et al. (2009); Nuth et al. (2013) . During the surge, the ice front position was, however, not much affected. The reason might be that the surge event was superimposed on the well-documented retreat of all marine-terminating glaciers in the Hornsund area over the last century (Błaszczyk et al., 2013) . Austre Torellbreen, Hansbreen and Paierlbreen cover areas of 141, 64 and 99 km^2, respectively. West of the THPB complex lies Werenskioldbreen (Ignatiuk et al., 2014) . It is land-terminating and somewhat smaller with 27 km^2. It covers an elevation range from 40 to just above 700m a.s.l.

2.1 Mass conservation

Over the ice covered domain Ω, the material incompressibility can be written as follows (p. 333 in Cuffey and Paterson, 2010) .

$$\frac{\partial H}{\partial t} + \boldsymbol{\nabla} \cdot (\boldsymbol{u} H) = \dot{b}_\mathrm{s} + \dot{b}_\mathrm{b} \,. \tag{1}$$

Here, ∇ is the divergence operator in two dimensions, H is the ice thickness, $\boldsymbol{u} = (u_1, u_2)$ are the vertically-averaged, horizontal velocity components and $\partial H / \partial t$ are temporal surface elevation changes. Surface and basal mass balance are denoted with $\dot{b}_\mathrm{s}$, $\dot{b}_\mathrm{b}$, respectively. The flux divergence $\nabla \cdot \boldsymbol{F} = \nabla \cdot \boldsymbol{u} H$ is a-priori unknown and we rearrange accordingly.

$$\boldsymbol{\nabla} \cdot \boldsymbol{F} = \dot{a}. \tag{2}$$

2.2 ~~Glacier outlines~~

~~Glacier outline information is taken from the 2002-2010 glacier inventory described in Nuth et al. (2013) . As THPB is a well-connected glacier complex, adjacent glacier boundaries were removed and joined into one single outline. WSB was not merged with the THPB complex because the shared ice divide is short and shallow (Kosibapasset has only ~15m depth)~~ All source and sink terms are combined in the 'apparent mass balance' (AMB) field $\dot{a} = \dot{b}_\mathrm{s} + \dot{b}_\mathrm{b} - \partial H / \partial t$. Throughout this manuscript, we assume that the basal mass balance $\dot{b}_\mathrm{b}$ is negligible. ~~VIC is treated as a single entity by merging all its individual drainage basins. In this way, we avoid discontinuities in the anticipated thickness solution across ice ridges and divides.~~

2.2 ~~Surface elevation~~First step: Flux-based solution

~~Concerning the Svalbard surface elevation, we rely on a 50m digital elevation model (DEM) from the 1990s[1] provided by the Norwegian Polar Institute (NPI). This map was produced from areal photos using photogrammetry as well as from contour lines in earlier elevation maps, which were digitised and interpolated. We refrained from using this DEM on VIC because it mainly stems from contour-line information resulting in a characteristic wave pattern in the slope field. Therefore, we use a more recent 10m DEM inferred from 2010 radar data acquired by the TanDEM-X mission, operated by the German Aerospance Center (DLR; Krieger et al., 2013) . The DEM was processed from bi-static Synthetic Aperture Radar (SAR) data using a differential interferometric approach (Seehaus et al., 2015; Rankl and Braun, 2016; Vijay and Braun, 2016, ; Saß et al., (in preparation)) .It was referenced to sea level by means of ICESat (Schutz et al., 2005) .~~

2.3 ~~Thickness measurements~~

~~For VIC, thickness measurements (Fig. 4a) were obtained from 60MHz airborne radio-echo sounding surveys between 1983 and 1986 (Dowdeswell et al., 1986) . Five flightlines run north-south across the ice cap and two from east to west. All profiles follow centrelines of prominent outlet glaciers. Unfortunately, no bed reflector could be identified for a large portion of these airborne data, including most of the ice-divide area. There only recently (2008-2009), ground-based pulsed radar data~~

[1] ~~Norwegian Polar Institute (2014). Terrengmodell Svalbard (S0 Terrengmodell) Data set. Norwegian Polar Institute. doi:10.21334/npolar.2014.dce53a47~~

were collected by (Pettersson et al., 2011) . Following Pettersson et al. (2011) , the early airborne measurements were adjusted assuming a constant thinning rate of ~ 0.16m yr^{-1} over the entire ice cap.

In the Hornsund area, Hansbreen is well studied and an ice-core drilling team reached the bed at three locations already in 1994 (Jania et al., 1996) . Between 2004 and 2013, ground-penetrating radar profiles were collected both on THPB and WSB (Navarro et al., 2014) . These surveys provide a dense grid over most parts of these glaciers (Fig. 4b). For WSB, the measurement error was analysed in depth even accounting for the often ignored positioning-related ice-thickness uncertainty (Lapazaran et al., 2016) . Measurement errors fall into a range of 3.3 to 6.8 m with an average value of 4.5 m. The early ice-core information was ignored for In a first step, the mass conservation (Eq. 2) is solved for the ice flux $\boldsymbol{F}$ (Sect. 2.0.1) while prescribing the flux direction (Sect. 2.2.1). The flux solution is translated into a glacier-wide thickness field relying on the SIA (Sect. 2.0.3). In a last step, the error associated with the thickness reconstruction here because it only gives information at a few additional points and because it is not evident how the surface elevation has changed since the early 1990sis estimated (Sect. 2.0.4). Input fields to the ice thickness reconstruction for VIC (a,c,e,g) and THPB/WSB (b,d,f,h). Surface mass balance (SMB) input (a,b) is provided by MAR as an average over the period 1979-2014 (Lang et al., 2015) . Elevations changes (c,d) are inferred from 2003-2007 ICESat profiles on VIC and from a 2008 SPOT-HRS DEM in southern Spitsbergen. From this elevation information, we subtracted the 1990 from the Norwegian Polar Institute (NPI). For VIC, line information on elevation changes along the ICESat tracks was linearly interpolated (c). The difference between SMB and surface elevation changes (e,f) is referred to as the apparent mass balance. Surface velocity magnitudes (g,h) were inferred from 2015/2016 Sentinel-1 imagery. Background: grey-scale hill-shaded topography based on a NPI 50m .

(continued)

2.3 Surface mass balance

For the SMB information, we rely on the regional climate model MAR (Modèle Atmopshérique Régional; Lang et al., 2015) . MAR combines a hydrostatic model for the atmospheric circulation with a physically based model for snow-pack evolution. The MAR-SMB simulations cover the entire archipelago (Fig. 2a,b)and were validated by Lang et al. (2015) against available climatic variables as well as SMB measurements from Pinglot et al. (1999, 2001) . Simulation were conducted on a regular 7.5km grid but a downscaled output was provided on 200m spacing using an interpolation strategy that distinguishes the various SMB components (Franco et al., 2012) . The components are interpolated according to locally defined, vertical gradients. For the reconstruction, the annual SMB record was averaged over 1979-2015.

To assess the sensitivity of the thickness reconstruction to the SMB input (Appendix C1), results from the Weather Research and Forecasting (WRF) model were considered (Aas et al., 2016) . The WRF-SMB field represents the period 2003-2013 and has a 3km resolution. The field could not be downscaled as the above routines were not implemented by ourselves. Therefore, the SMB sensitivity is only assessed on the large VIC geometry.

2.2.1 Flux direction

With prior knowledge only on à, the single mass conservation equation is insufficient to determine the two unknown flux components. To close the system, ice flux is separated into its magnitude F and its direction vector $\boldsymbol{r}$.

$$\boldsymbol{F} = F \cdot \boldsymbol{r}. \tag{3}$$

2.3 ~~Surface elevation changes~~

~~Over VIC, 2003-2007 elevation changes (Fig. 2c) were inferred from laser altimetry measurements with the Ice, Cloud, and Land Elevation Satellite (ICESat). ICESat measurements were referenced to the 1990 20m NPI DEM[1] (Moholdt et al., 2010) . The laser altimetry system has a footprint of 70m diameter with 170m along-track spacing. Across-track spacing is irregular and much larger with several kilometres. A Natural-Neighbour Sibsonian interpolation[2] (Fan et al., 2005) is used to estimate elevations changes in between these scattered ICESat measurements.~~ The direction is specified following Brinkerhoff and Johnson (2015) as the solution to

$$\boldsymbol{\tau}_s = \boldsymbol{\nabla}\left[(l \cdot H)^2 \nabla \cdot \boldsymbol{\tau}_s\right] + \boldsymbol{\tau}_d \tag{4}$$

Here, $\boldsymbol{\tau}_s$ is a smoothed version of the driving stress $\boldsymbol{\tau}_d = (\rho g) \cdot H \cdot \nabla h$. Other parameters needing specification include the ice density $\rho = 917\,\mathrm{kg\ m^{-3}}$, the gravitational acceleration $g = 9.18\,\mathrm{m\ s^{-2}}$ and the surface elevation h. The flux direction vector $\boldsymbol{r}$ is computed by normalising $\boldsymbol{\tau}_s$. Along the lateral glacier margin Γ, the following boundary condition is set:

$$(\boldsymbol{\nabla} \cdot \boldsymbol{\tau}_s) \cdot \boldsymbol{n}_\Gamma = 0. \tag{5}$$

~~For Wedel Jarlsberg Land, elevation changes were calculated by differencing the NPI 20m DEM[1] from 1990 with a 40m DEM inferred from 2008 imagery acquired by the high resolution stereoscopic (HRS) sensor on-board SPOT 5 (Korona et al., 2009) . The DEMs were first co-registered (Nuth and Kääb, 2011) before subsequent differencing and resampling to 100m (Fig. 2d).~~ Here, $\boldsymbol{n}_\Gamma$ is perpendicular to Γ. The solution to Eq. (4) is equivalent to an averaging of the driving stress using a variable length scale (lH). This scaling stems from theoretical work on the influence of longitudinal stress gradients on glacier flow (Kamb and Echelmeyer, 1986) . These stress gradients are comparable to membrane stresses in thin body mechanics (Hindmarsh, 2006) . Membrane stresses can instantly transmit perturbations upglacier but this transmission was shown to be a secondary factor in terms of centennial ice-sheet volume evolution (Fürst et al., 2013) . The associated scaling length is usually expressed as a multiple l of the ice thickness H. For $l = 10$, we find that resultant flux streamlines are inappropriately averaged over adjacent branches of a single valley glacier. For $l = 1$ however, the routing remained locally defined. We therefore decided to prescribe $l = 3$, in agreement with the suggestion by Kamb and Echelmeyer (1986) , who expected coupling lengths for valley glaciers between $l = 1$ and $l = 3$.

2.3 ~~Surface velocities~~

[2] ~~source code available at~~

Using satellite imagery acquired between January 2015 and September 2016 by the C-band Synthetic Aperture Radar (SAR) onboard Sentinel-1, we apply intensity offset tracking to consecutive image pairs (Strozzi et al., 2002; Seehaus et al., 2016) . The time series of displacement fields is first filtered for obvious outliers within a certain kernel area in terms of the prevailing flow direction and magnitude (Seehaus et al., 2016) . Then, fields are stacked using median-averaging to obtain maximum coverage and to reduce effects from short-term or seasonal fluctuations (Fig. 2g, h). Velocity maps are provided at 100m resolution. The uncertainty associated to the inferred velocity maps is estimated on 70 stable reference areas without ice cover. We find an average uncertainty of 19 m yr^{-1}, which is comparable to independent uncertainty estimates for merged Sentinel-1 imagery with minimum values of $\sim$ 17m yr^{-1} (Schwaizer, 2016) .

2.3 Fjord bathymetries

Information on the fjord bathymetry is used to further constrain the thickness reconstruction at marine ice fronts. The new International Bathymetric Chart of the Arctic Ocean holds a wealth of new measurements around the Svalbard archipelago (Jakobsson et al., 2012) . It comprises several recent multibeam surveys that entered deep into some major fjords and collected high-resolution seafloor information (Ottesen et al., 2007) . Around the archipelago, the new IBCAO map is provided at high spatial resolution of 500m. To some extent, this fine spacing is possible because of high-resolution input data from the *Olex* seabed mapping system.

3 Methods

The thickness reconstruction approach is ultimately based on mass conservation and largely stems from ideas presented in Morlighem et al. (2011) . We opted for a two-step approach because surface velocity information from satellite remote sensing often fails to cover an entire glacier basin. The two-step approach, first provides a thickness field over the entire glacier surface which can be updated in areas where reliable velocity information is available. In the first step, a balance flux is calculated from the difference between SMB and surface elevation changes, i. e. the apparent mass balance. Relying on the SIA (Hutter, 1983) , the local By construction, the ice thickness is calculated from the resultant ice-flux field and the surface topography. In a second step, the mass conservation equation is directly solved for ice thickness in a sub-domain where reliable velocity information is available. The first step thickness field then serves as lateral boundary condition.

2.1 Mass conservation

Assuming that ice is an incompressible material, the 3D velocity field $\boldsymbol{v}$ is free of divergent or convergent flow. Any divergence in the vertically-averaged, horizontal velocity components $\boldsymbol{u} = (u_1, u_2)$ translates directly into thickening or thinning. Accounting for the kinematics of the upper and lower boundary surfaces (p. 333 in Cuffey and Paterson, 2010) , incompressibility can be rewritten as follows.

$$\frac{\partial H}{\partial t} + \boldsymbol{\nabla}(\boldsymbol{u}H) = \dot{b}_\mathrm{s} + \dot{b}_\mathrm{b}$$

Here, Ω is the 2D ice-covered domain. The flux divergence term is a-priori unknown and we rearrange accordingly.

$$\nabla \boldsymbol{F} = \dot{a}$$

Here, ∇ is the divergence operator in two dimensions, H is the ice thickness and $\boldsymbol{F} = \boldsymbol{u}H$ is the horizontal ice-flux vector. Sources and sinks in the flux divergence arise from the surface $\dot{b}_\mathrm{s}$ and bottom mass balance $\dot{b}_\mathrm{b}$, as well as from surface elevation changes $\partial H/\partial t$ over time. We avoid the terminology of apparent mass balance for the combined effect of all source and sink terms $\dot{a} = \dot{b}_\mathrm{s} + \dot{b}_\mathrm{b} - \partial H/\partial t$ and rather refer to it as apparent mass balance (Fig. 2e, f). Except for glacier geometries that are in equilibrium with the climatic conditions ($\partial H/\partial t = 0$), $\dot{a}$ is not directly associated with the mass balance neither for a glacier as a whole nor at the surface. Throughout this manuscript, we assume that the basal mass balance $\dot{b}_\mathrm{b}$ is negligible as compared with the other terms in the apparent mass balance

a priori unknown and so is the coupling length scale (lH). Therefore, we initially assume $H = 100$ m to compute a first flux direction field $\boldsymbol{r}$. Then, a first estimate is available for the thickness field and flux directions are updated accordingly. Thereafter, directions are kept fixed during the optimisation (Sect. 2.0.2). The reasons for fixing the direction are to limit the degrees of freedom during the optimisation and because the first-step thickness field already captures the general magnitude of the observations giving a reasonable (lH)-field.

2.1 First step: Flux-based solution

In a first step, the mass conservation is solved for the ice flux (Eq. 2), which itself is assumed to follow the steepest descent in the surface topography.

$$\tilde{\boldsymbol{F}} = \tilde{F} \cdot \boldsymbol{n}$$

Here, $\boldsymbol{n}$ is the normalised negative surface slope vector. Along all land-terminating segments of the glacier outline, we impose a zero-flux condition. A free boundary condition is chosen across marine ice fronts, providing an ice-discharge estimate consistent with the apparent mass balance. Inflow boundaries are avoided because a Dirichlet condition on the ice flux would become necessary there. To solve Eq.

2.0.1 Flux magnitude

To determine the flux magnitude F according to Eqs. (2) and (3), we use the Elmer finite-element software developed at the Center for Science in Finland (CSC-IT, http://www.csc.fi/elmer/) and more specifically the mass conservation solver implemented in its glaciological extension Elmer/Ice (Gagliardini and Zwinger, 2008; Gillet-Chaulet et al. , 2012; Gagliardini et al., 2013). (Gagliardini and Zwinger, 2008; Gillet-Chaulet et al., 2012; Gagliardini et al., 2013) . For the discretisation of the problem, we select the stabilised streamline upwind Petrov-Galerkin (SUPG) scheme (Brooks and Hughes, 1982).

The assumption that the ice-flux points into the opposite direction of surface gradients has important consequences for the solution to Eq. (2). The flux solution becomes highly dependent on the surface elevation information. Independent of the quality or the resolution of the input DEM, singular source or sink points are introduced over the entire glacier domain where the DEM shows local minima or maxima. At these locations, flowlines have to either start or end resulting in a highly partitioned and

~~erratic flux field. Even a topography smoothing using various kernel sizes could not suppress this effect. Searching for an effective way to avoid such singular points, we decided to first extract surface elevation contours each 50m intervals. This contour information is then interpolated and gridded using a Natural Neighbours Sibsonian interpolation (Fan et al., 2005) . This decision largely guarantees that the flux solution changes gradually and is free of most singular points.~~

~~In areas near the ice divide or near~~ Along all land-terminating segments of the glacier outline, we impose a zero-flux condition. A free boundary condition is chosen across marine ice fronts, ~~surface slopes can locally become very small. As a consequence, the ice-flux solution can diverge. Therefore, we decided to introduce a slope threshold α_0 of 1°. If this value is not reached, the normalisation of the slope vector uses this threshold. The chosen threshold value is small as compared to the two-fold values chosen in the original thickness reconstruction approach by Farinotti et al. (2009b) . Both their thresholds lie higher at 5° and 20°. For VIC, THPB and WSB, the DEM surface slopes do not reach the 5°-threshold over most of the respective glaciated area (97.2, 86.3 and 53.1%, respectively).The 1°-threshold slope implies that this fraction reduces to 18.7, 4.8 and 0.1% of their respective surfaces and that this area disintegrates into many small patches distributed over the domain. Where the slope magnitude falls below the α_0-threshold, the ice-flux direction is taken from the spatial gradient in the input SMB. The choice for a smaller threshold value, here, is in agreement with a thickness reconstruction on the Patagonian ice fields (Carrivick et al., 2016) , for which a value of 1.7° was applied~~providing an ice-discharge estimate consistent with the AMB. Inflow boundaries did not occur in our setup. These would require Dirichlet conditions on the ice flux.

2.0.2 Cost function and single-variate optimisation

The direct flux solution to all input fields often shows wide-spread negative values and high spatial variability. Therefore, we chose to iteratively update the ~~apparent mass balance~~ AMB-field $\dot{a}$, as control variable, such that undesired characteristics in the flux field are reduced. We anticipate that the ~~ice-flux direction~~ flux magnitude F is positive and ~~that it is~~ smooth. For the purpose of the iterative optimisation, we introduce the following cost function J.

$$J = \lambda_{\text{pos}} \cdot \int_{\Omega} F^2 \int_{-\infty}^{F} \delta(s) ds \cdot \mathrm{H}\left[-F\right] d\Omega + \lambda_{\text{reg}} \cdot \int_{\Omega} \left(\frac{\partial F}{\partial x}\right)^2 + \left(\frac{\partial F}{\partial y}\right)^2 d\Omega + \lambda_{\dot{a}} \cdot \int_{\Omega} \left(\dot{a} - \dot{a}^{\text{init}}\right)^2 d\Omega \tag{6}$$

Here, ~~$\delta(s)$ is the Dirac delta functionwith~~ $\mathrm{H}[s]$ is the Heaviside function, being zero for negative and one for positive $s \in \mathbb{R}$. The first term is thus zero for positive flux values but penalises negative flux solutions. The second term is a regularisation, which favours smooth flux solutions. The last term ~~increases the more the iteratively updated apparent mass balance~~ adds up differences between the iteratively updated $\dot{a}$ ~~deviates from~~ and the initial input $\dot{a}^{\text{init}}$. The cost J should primarily be considered as a function of $\dot{a}$. As the ~~control variable~~ AMB is iteratively updated, the cost should decrease. ~~Good performance was achieved with the following multiplier choice:~~ Multipliers values are $\lambda_{\text{pos}} = 10^2$, ~~$\lambda_{\text{reg}} = 10^0$~~ $\lambda_{\text{reg}} = 10^1$ and $\lambda_{\dot{a}} = 10^{-2}$. ~~The parameter~~ For WSB, we chose $\lambda_{\text{reg}} = 10^0$ to compensate for resolution differences. The multiplier choice aimed at a balance between improving the smoothness of the flux field and reducing areas with negative flux values by adapting λ_{pos} and λ_{reg}. The solution showed not much sensitivity to changes in $\lambda_{\dot{a}}$.

For the optimisation of the cost function, we rely on the "m1qn3" module (Gilbert and Lemaréchal, 1989) that can solve large-scale unconstrained minimisation problems. It requires first derivatives of the cost with respect to the single control variables $\dot{a}$. For a precise calculation of these derivatives, we rely on the adjoint system associated ~~to~~ with Eq. ~~2~~(2). The stopping criterion for the iterative optimisation is non-dimensional at 10^{-14} and computed as a ratio between the current and the initial norm of the cost derivatives.

2.0.3 Inferring ice thickness

Once a flux field is determined over the glacier domain, the ice thickness is inferred in a post-processing step. ~~Having assumed that the ice flux follows the surface topography, a natural choice for relating it to ice thickness is the SIA (Hutter, 1983) . This ice-dynamic approximation~~ Flux values are locally translated into thickness values assuming the SIA (Hutter, 1983) .

$$F^\star = \frac{2}{\mathrm{n}+2} B^{-\mathrm{n}} (\rho g)^{\mathrm{n}} \, \|\nabla h\|^{\mathrm{n}} \cdot H^{\mathrm{n}+2} \tag{7}$$

Here, the flow law exponent is $n = 3$ and the superscript * denotes a flux correction (see below and Appendix C3). Note that in this way, the first-step reconstruction neglects effects from basal sliding, which limits its applicability to areas of slow ice flow. The SIA is typically applied to geometries with ~~large~~ small aspect ratios (~~horizontal vs. vertical scales). It implies that the ice-flux magnitude is given by the local geometry.~~

$$F^\star = \frac{2}{n+2} B^{-n} (\rho g)^{n} \, \|\nabla h\|^{n} \cdot H^{n+2}$$

~~Other parameters needing specification include the ice density $\rho = 917\,\mathrm{kg\,m^{-3}}$~~, vertical vs. horizontal scales), which is not necessarily the case for our test geometries. Accounting for the influence of membrane stresses on ice flow, we correct the local surface slope magnitude $\|\nabla h\|$ informed by the smoothed driving stress $\boldsymbol{\tau}_s$ (Eq. 4), assuming $\|\boldsymbol{\tau}_s\| = (\rho g) H \cdot \|\nabla h\|$. In areas near the ice divide, surface slopes can locally become very small and thickness values diverge. Therefore, we decided to impose a slope threshold $\alpha_0 = 1°$ as a lower limit on ∇h. The chosen threshold is small as compared to other reconstruction approaches. For a similar reconstruction approach, combining mass conservation with the SIA along glacier flowlines, Farinotti et al. (2009b) apply a 5° limit. Assuming perfect plasticity to infer glacier thickness in Patagonia, Carrivick et al. (2016) a lower limit of 1.7°. Even though our choice for α_0 is somewhat lower, the limit is still applied over a 17% area fraction of the ~~gravitational acceleration $g = 9.18\,\mathrm{m\,s^{-2}}$ and the flow law exponent $n = 3$.In this way, the ice thickness becomes highly dependent on gradients in surface elevation ∇h. Note that this assumption implies zero basal sliding and thus limits the applicability to areas of slow ice flow. This constraint will be reduced during the second step of this reconstruction (Sect. 2.1), which is informed by ice velocity measurements.~~ ice-cap test geometry. For the 1.7 and 5° limits, this area fraction increases to 46% and 94%, respectively.

The ice-viscosity parameter B is a-priori unknown. Yet, where thickness measurements are available, B can be computed from Eq. (7). Thereafter, the scattered information on ~~the ice-viscosity parameter~~ B ~~, at the thickness measurement locations,~~ is interpolated over the entire glacier domain. To avoid unreliable extrapolation effects, we prescribe a mean ~~value for the~~

~~viscosity parameter~~ B value from all measurements around the lateral domain margin. ~~Per domain, the mean value is the average viscosity inferred at all measurement locations.~~ If no thickness measurements ~~had been~~ were available, an a-priori choice of the viscosity parameter ~~would have been~~ B is required.

~~Here, surface slopes are computed from a somewhat smoothed variant of the DEM. First, the original topographic map on 50m resolution (12 m for VIC) is downsampled to 100m (500m for VIC and THPB). Thereafter, a least-square difference parabola is fitted to each point, considering neighbouring DEM points within 300m (1500m for THPB and VIC). Local slopes are then calculated from the parabolic fit. This smoothing is an attempt to account for the SIA assumption on small aspect ratios.~~

~~In~~ We apply a correction to the computed flux before computing the ice thickness from Eq. (7)~~, the flux solution does not enter directly but is corrected to avoid negative thickness values~~. Details of this flux correction and the sensitivity of the results are given in Appendix C3. The reason is that despite the cost term on negative ice flux (Sect. 2.0.2), negative values ~~persist in some small areas. On VIC and THPB, the area fraction with negative ice flux is 0.5 and 1.7%, respectively. On WSB however, the flux solution over the main branch is generally very small and shows many zero transitions. Consequently, the area-fraction is higher at 4.4% . The reason is that the apparent mass balance shows no dominant source area in the upper glacierranges. The zero~~ prevail in limited areas, which transmit into the thickness field. When the input à shows only few source areas with net accumulation, ice flux remains small and negative values were found over as much as 5% of the only land-terminating test glacier. Zero transitions in the flux solution ~~would~~ directly transmit into the ice thickness field. To ~~avoid these oscillations~~prevent such spurious variations, we correct the flux ~~as follows: $F^\star = (1-\kappa)\cdot\|F\| + \kappa\cdot F_{\text{crit}}$ with $\kappa = 1 - 2/\pi \cdot \text{atan}(F^2/F_{\text{crit}}^2)$. F_{crit} is equal 10% of the average flux magnitude over the domain. Along the lateral land-terminating domain margin, we keep $F = F^\star = 0$. In the case of abundant thickness measurements, the effect of this flux correction on the inferred thickness is compensated by the ice-viscosity choice~~solution according to Eq. (C1), which guarantees positive values. In areas of more pronounced ice flux, where the correction is a priori not necessary, its effect is inherently compensated by adapting the viscosity parameter B where thickness measurements were collected. If no ~~observations are availableand for $F > F_{\text{crit}}$, the functional dependence implies that the reduction effect on the inferred thickness field remains below~~ thickness measurements are available, inferred thickness values are reduced by at most 2% ~~as compared to the uncorrected case. Where the ice flux exceed the domain average ($10 \cdot F_{\text{crit}}$), the effect on the ice thickness falls below 0.15%. Below F_{crit}, thickness values are effectively increased. The sensitivity of the results to this flux correction is assessed in Appendix C3.~~ for pronounced ice flow.

2.0.4 Formal error estimate

Together with the thickness map, we ~~want to~~ present a formal error map. For this purpose, the uncertainty on the input fields, i.e. the SMB and $\partial H/\partial t$, are propagated in two steps. Uncertainties are first transmitted through the mass conservation equation (Eq. 2) and the resulting estimate of the flux error is then scaled by a SIA flux-thickness conversion (Eq. 7). For the first step, we follow the ideas presented in Morlighem et al. (2014), who assume that the inaccurate flux field $F + \delta F$ also satisfies mass

conservation.

$$\boldsymbol{\nabla}\left[(F+\delta F)\cdot(\boldsymbol{n}+\delta\boldsymbol{n})\right]=\dot{a}+\delta\dot{a} \tag{8}$$

Here, $\delta\dot{a}$ is the uncertainty of the AMB and $\delta\boldsymbol{n}$ is the error on the prescribed flux direction. Neglecting second order terms and accounting for the fact that F satisfies Eq. (2), the flux error is a solution of:

$$\boldsymbol{\nabla}\left[\boldsymbol{n}\delta F_1\right]=\|\delta\dot{a}-\boldsymbol{\nabla}\left[F\delta\boldsymbol{n}\right]\| \tag{9}$$

Along the land-terminating domain margin, we assume zero flux and the thickness error estimate implicitly becomes zero. At the thickness measurement locations, we assume that the ice flux is known with a precision that is equivalent to the uncertainty in the thickness measurements δH_{obs}. ~~For this purpose, the above reported 5m~~ The thickness-measurement uncertainty is translated into a flux-equivalent value using Eq. (7) without ~~correction~~ the flux correction, thus $F^\star = F$. ~~Along the land-terminating domain margin, we assume zero flux and the thickness error estimate implicitly becomes zero.Despite~~ The solution to Eq. (9) shows a sawtooth pattern along the ice flow, as error estimates increase downglacier until another measurement is reached. There the value drops to a small magnitude and starts again to increase. We however expect that measurements also constrain the ice thickness upglacier. Therefore, we assume that the uncertainty can also decrease at a certain rate along the flow. This generic decrease rate is not known but we assume the same magnitude as for the above error increase rate in Eq. (9).

$$\boldsymbol{\nabla}\left[(\quad\boldsymbol{n})\,\delta F_2\right]=(-1.0)\cdot\|\delta\dot{a}+\boldsymbol{\nabla}\left[F\delta\boldsymbol{n}\right]\| \tag{10}$$

This equation requires appropriate upstream boundary conditions, ~~the flux error estimate is actually constrained from measurementsupstrean and downstream. This is readily accounted for by solving the following two problems~~ such that the error reaches δH_{obs} at the next observation downglacier. Yet this is impractical and we rather restate the problem as an upstream error increase well constrained at the measurements.

$$\boldsymbol{\nabla}\left[(+\boldsymbol{n})\,\delta F_1\right]=\delta\dot{a}+\|\boldsymbol{\nabla}\left[F\delta\boldsymbol{n}\right]\|$$
$$\boldsymbol{\nabla}\left[(-\boldsymbol{n})\,\delta F_2\right]=\delta\dot{a}+\|\boldsymbol{\nabla}\left[F\delta\boldsymbol{n}\right]\|$$

~~These two problems~~

$$\boldsymbol{\nabla}\left[(-\boldsymbol{n})\,\delta F_2\right]=\qquad\|\delta\dot{a}+\boldsymbol{\nabla}\left[F\delta\boldsymbol{n}\right]\| \tag{11}$$

The two problems Eqs. (9) and (11) are structurally identical to Eq. (1) and thus numerically solved as described in Sect. 2.3. ~~These~~ The two formal error estimates $\delta F_1, \delta F_2$ subsequently enter a linear error propagation within the SIA thickness-flux relation (Eq.7). This yields:

$$\delta H_i=\frac{1}{n+2}\frac{1}{\mathrm{n}+2}\left[-\frac{2}{n+2}\frac{2}{\mathrm{n}+2}B^{-1/n-1/\mathrm{n}}(\rho g)^{n\mathrm{n}}\,\|\boldsymbol{\nabla}h\|^{n\mathrm{n}}\right]^{-1/(n+2)-1/(\mathrm{n}+2)}\cdot\|F\|^{-(n+1)/(n+2)-(\mathrm{n}+1)/(\mathrm{n}+2)}\cdot\|\delta F_i\| \tag{12}$$

~~Finally, the~~ In this way, the error analysis is limited by the assumptions inherited from the SIA. Uncertainties in B, ρ, g and ∇h are not accounted for. The final thickness error estimate δH is the minimum of ~~the two values stemming from up- and downwards propagation $\min(\delta H_1, \delta H_2)$~~ δH_1 and δH_2.

Input ~~fields to the calculation of this formal error map are~~ uncertainties for the test geometries are presented in Sect. 3.9. These uncertainties are chosen constant which is problematic in terms of the control variable $\dot{a}$. This variable changes during the optimisation and all uncertainties of other input fields and underlying assumptions of the reconstruction approach are placed into $\dot{a}$. Yet, it is not evident how to iteratively update the uncertainty associated with the ~~thickness measurements (Lapazaran et al., 2016) , the flux direction and the apparent mass balance. These uncertainties are assumed to be constant: $\delta H_{\text{obs}} = 5.0\,\text{m}$, $\delta n = 0.2$ and $\delta \dot{a} = 0.2\,\text{m i.e. yr}^{-1}$.~~ control parameter and we accept some limitations here. The importance of this assumption can be assessed from a comparison of the initial and the final AMB field (Appendix B). Apart from this limitation, the error analysis accounts for uncertainties in the observational record but does not comprise the error that stems from time-averaging of the input and temporal inconsistencies between different fields. A detailed assessment and treatment of various input errors within a Bayesian framework is presented in Brinkerhoff et al. (2016) .

2.1 Second step: Velocity-based solution

In a second step, the ice thickness map is updated in areas where reliable surface velocity information is available by solving Eq. (1) directly for the ice thickness. Equation (1) is vertically integrated and the surface velocity information needs to be ~~translated~~ converted into a vertical mean value. Within the scope of this methodological study, we apply this second step exclusively where velocity magnitudes exceed $100\,\text{m yr}^{-1}$ (details of the sub-domain delineation in Sect. 2.2). In these sub-domains, basal sliding is assumed to dominate over internal deformation, and therefore vertical mean and surface velocities are set equal. We rely on the same Elmer/Ice routine to discretise and solve the mass conservation problem as above (Sect. 2.3). ~~Thickness measurements are imposed as internal Dirichlet boundary conditions, whereas the previously inferred~~ Previously inferred first-step thickness values are prescribed as Dirichlet conditions around the lateral domain margin~~. If the sub-domain comprises a marine ice front, no boundary conditions are imposed~~ , whereas no condition is imposed along marine ice front.

2.1.1 Cost function & ~~Multi-parameter~~ multi-parameter optimisation

~~Again, the~~ The ice thickness solution is optimised as we cannot anticipate that input fields are consistent in terms of the mass balance equation. Yet in this step, the optimisation makes use of three control variables. The ~~apparent mass balance~~ AMB is complemented by ~~the~~ both horizontal velocity components u_i. For this second-step optimisation, a new and more elaborate cost function N is defined.

$$N = \gamma_{\text{pos}} \cdot \int_\Omega H^2 \cdot \text{H}\left[-H\right] d\Omega + \gamma_{\text{obs}} \cdot \int {}^{H}_{-\infty}\delta_\Omega(sH - H_{\text{obs}}) ds^2 \, d\Omega + \gamma_{\text{marine}} \cdot \int_{\Gamma_{\text{marine}}} H^2 \int_{-\infty}^{H} \delta(s - H_{\text{min}}) ds \int_{H}^{\infty} \delta(s - H_{\text{max}}) ds \cdot \text{H}\left[H_{\text{min}}\right.$$

$$\gamma_{\text{reg}} \cdot \int_\Omega \left(\frac{\partial H}{\partial x}\right)^2 + \left(\frac{\partial H}{\partial y}\right)^2 d\Omega + \gamma_{\dot{a}} \cdot \int_\Omega \left(\dot{a} - \dot{a}^{\text{init}}\right)^2 d\Omega + \gamma_{\text{U}} \cdot \sum_{\text{i}=1}^{2} \int_\Omega \left(u_\text{i} - u_\text{i}^{\text{init}}\right)^2 d\Omega$$

Most of the terms have equivalents in Eq. (6). As before, we penalise a negative solution, high variability of the control variables and the control-variable mismatch to initial values. ~~The only new term is the~~ New terms are the penalty for thickness values that differ from the measurements H_{obs} and the line integral along ~~any~~ the marine boundary Γ_{marine}. ~~It~~ The latter integral penalises thickness values outside a certain range. The lower limit of this range stems from the fact that marine-terminating glacier margins on Svalbard are mostly grounded (Dowdeswell, 1989). Therefore, H_{min} is given by the flotation criterion $H_{\text{min}} = h \cdot \rho_{\text{water}}/(\rho_{\text{water}} - \rho_{\text{ice}})$. The upper limit is calculated from the IBCAO bathymetry. We assume that the bed topography does not significantly decrease inland and thus that the bathymetry along the ice front should be shallower than the maximum depth at all ocean points within a 5-km radius. ~~We mostly experienced that the lower limit is not reached.~~ The multiplier choices are motivated as follows~~. The~~ : First, the most decisive multiplier is γ_{reg}~~as it determines the smoothness~~. If chosen to high, boundary thickness values and measurements are simply smoothed without much consideration for the ice dynamic influence. If chosen too low, the thickness solution of adjacent flow lines decouples. The choice $\gamma_{\text{reg}} = 10^{-2}$ represents a trade-off between the two extremes. Second, we deemed it appropriate to set ~~$\gamma_{\text{pos}} = \gamma_{\text{marine}}$. This multiplier~~ $\gamma_{\text{pos}} = \gamma_{\text{marine}} = \gamma_{\text{obs}}$. The value was gradually increased until the solution was ~~affected, suggesting~~ appropriately affected, giving $\gamma_{\text{pos}} = 10^2$. As before, the remaining two multipliers $\gamma_{\dot{a}} = 10^{-4}$ and $\gamma_{\text{U}} = 10^{-8}$ are not very decisive and they were mostly added to prevent ~~general divergence~~divergent behaviour.

As above (Sect. 2.0.2), cost derivatives with respect to the control variables $\dot{a}$ and ~~u_i~~ u_{i} were computed from the adjoint system to Eq. (2). Without further modifications, the iterative optimisation preferentially modifies $\dot{a}$ because the control variables have different magnitudes. To align relative change values, a scaling factor of 0.05 for the velocity derivatives was introduced. Convergence of this second-step optimisation is reached using the same threshold criterion as above (Sect. 2.0.2).

2.1.2 Error estimate

Errors are again estimated following the ideas presented in Morlighem et al. (2014). As the ice thickness is calculated directly from mass conservation, errors have only to be propagated through Eq. (1). By analogy with Sect. 2.0.4, two systems of equations limit the error estimate~~from upstream and downstream~~.

$$\begin{aligned} \boldsymbol{\nabla}\left[(+\boldsymbol{u})\,\delta H_1\right] &= \delta\dot{a} + \|\boldsymbol{\nabla}\left[\mathrm{F}\delta\boldsymbol{u}\right]\| \\ \boldsymbol{\nabla}\left[(-\boldsymbol{u})\,\delta H_2\right] &= \delta\dot{a} + \|\boldsymbol{\nabla}\left[\mathrm{F}\delta\boldsymbol{u}\right]\| \end{aligned} \tag{14}$$

The minimum value of the absolute values of these two error estimates gives the actual thickness error $\delta H = \min(\|\delta H_1\|, \|\delta H_2\|)$. Input uncertainties are $\delta u = 20.0\,\text{m yr}^{-1}$ and $\delta\dot{a} = 0.2\,\text{m i.e. yr}^{-1}$

2.2 Gridding & Boundary conditions

The individual glacier outlines from Nuth et al. (2013) are first partitioned into marine and land-terminating segments by searching if the surface elevation is zero within ~~150m~~ 150 m of the outline point. ~~For the THPB complex, the~~ Where the DEM showed more advanced glacier fronts than ~~in~~ the glacier inventory~~. For these glaciers, an acceptable choice for detecting marine termination was to use a 100m~~ , a marine termination is inferred within the same search radius but with 100 m as surface-

elevation threshold~~instead~~. Subsequently, nunataks ~~were~~ are automatically accounted for in the mesh, if resolved by the target grid spacing. ~~The target mesh resolution was 200m for THPB and VIC and 100m for WSB.~~ In addition, we added grid points at each location where thickness measurements were available. This was necessary to prescribe internal boundary conditions on ~~ice thickness and~~ the error estimates. ~~The observations are very densely spaced and we decided to only keep measurements that are more than 50m apart, which is half of the minimum grid spacing. The initial 20792, 44921 and 21273 measurements of VIC, THPB and WSB were thus reduced to 4475, 5945 and 1189 points, respectively.~~ High-resoltuion thickness measurements were a-priori subsampled in accordance with the grid resolution. From the outline and measurement locations, a 2D mesh with triangular elements was generated using the open source finite element grid generator Gmsh (Geuzaine and Remacle, 2009). Nodal values for all input fields are determined relying on a standard Natural Neighbours Sibsonsian interpolation procedure (Fan et al., 2005).

In the first-step reconstruction, two external boundary conditions ~~were~~ are necessary around the glacier domain. At outflow boundaries along marine ice fronts, no conditions ~~were~~ are set on either the ice flux or the ice thickness. ~~Also the shared ice divide between Austre and Vestre Torellbreen is an outflow boundary for Torellbreen.~~ Where glaciers terminate on land, a zero flux Dirichlet condition ~~was~~ is imposed. Internal boundary conditions ~~were~~ are applied where measurements were available. There, flux error estimates $\delta \mathrm{F}_1, \delta \mathrm{F}_2$ ~~were~~ are set in accordance to ~~the reported 5m mean error on the thickness measurements~~ reported measurement errors (Sect. ~~2.0.4~~3.9). In the ~~second step reconstruction~~second-step, the domain is reduced to sub-domains with reliable velocity information. In each drainage basin, the largest sub-domain ~~was~~ is chosen from all areas in which velocity observations exceed 100 m yr^{-1}. At the lateral boundaries of this sub-domain, ice-thickness values as well as thickness error estimates ~~were~~ are prescribed from the first-step reconstruction. No boundary conditions ~~were~~ are imposed along marine ice fronts. Where thickness measurements were acquired, Dirichlet conditions ~~were~~ are imposed on the ~~thickness solution (Eq. 2)while valueswithin the up- and downstream error propagation (Eq. 14)were set~~ up- and downstream error propagation. However, the uncertainty δH_{obs} varies with the inferred thickness field. It is chosen as the minimum of the actual mismatch ($H - H_{\mathrm{obs}}$) and the reported measurement error.

3 Test geometries

The two-step reconstruction approach is tested on three ice geometries on Svalbard where an abundant record of thickness observations was available (Fig. 1). The three test geometries are Vestfonna ice cap (VIC) on Nordaustlandet, the land-terminating Werenskioldbreen (WSB) and the glacier complex composed of the marine-terminating Austre Torellbreen, Hansbreen and Paierlbreen (THPB). The latter two geometries are located in Wedel Jarlsberg Land. Input requirements are glacier outline, the surface geometry, the surface mass balance, surface elevation changes as well as surface velocities. Fjord bathymetry information and thickness measurements are used to constrain the inferred thickness values.

3.1 General characteristics

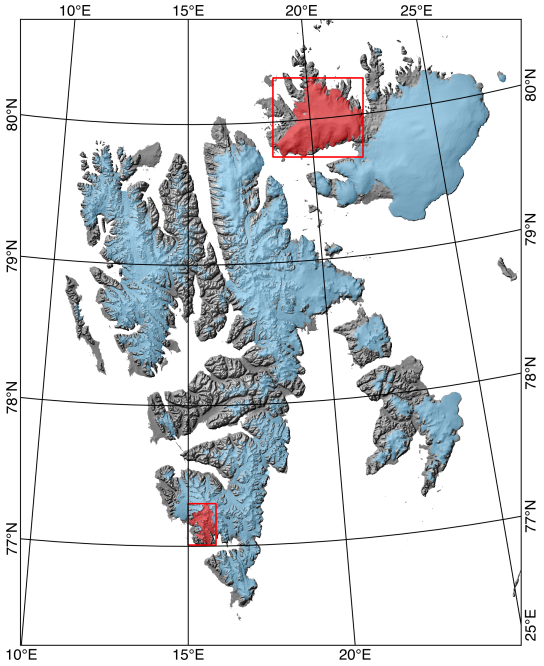

Figure 1. Overview map of the Svalbard archipelago showing ice coverage (blue shading). The two test sites (red shading and rectangles) are Vestfonna Ice Cap (VIC) on Nordaustlandet and the glacier complex comprising the marine-terminating Austre Torell-, Hans-, Paierlbreen (THPB) and the land-terminating Werenskioldbreen (WSB) in Wedel Jarlsberg Land. Background: grey-scale hill-shaded topography based on a 50 m DEM from the Norwegian Polar Institute (NPI).

VIC is the second largest ice caps on the Svalbard archipelago (Fig. 1; Dowdeswell, 1986a) . According to the 2002-2010 glacier inventory, it covers an area of 2366 km^2 with its summit area lying at 630 m above sea level (a.s.l.). Ice flow is channeled through several elongate outlet glaciers, which drain radially from a central crest and export ice to the surrounding ocean (Fig. 2g). Despite the steady retreat of most outlet glaciers since the 1970s (Dowdeswell, 1986b; Braun et al., 2011) , Søre and especially Nordre Franklinbreen advanced notably. This re-advance coincided with a strong acceleration reaching far inland. Surface velocities doubled and now exceed 100 m yr^{-1} over a large area (Pohjola et al., 2011) . Prior to the speed-up, most of the ice was exported via the northern branch of Nordre Franklinbreen. In the meantime, ice velocities indicate that the southern branch is the more prolific export path (Fig. 2g). The bi-modal pattern in ice dynamics is overprinted by cyclic surges with the last active phase reported in 1952 for Søre Franklinbreen (Błaszczyk et al., 2009) . Surges are quasi-periodic cycles of an active phase, during which extremely fast flow can transfer an immense ice volume downglacier, followed by a quiescent phase during which the ice cover in the accumulation area gradually regains its former height. Two other surge-type glaciers are known in the eastern part of Vestfonna. Active phases were reported in 1939 and 1992 for Rijpbreen and during the period 1973-1980 for Bodleybreen (Dowdeswell, 1986b; Błaszczyk et al., 2009) .

Austre Torellbreen is a marine-terminating glacier (Fig. 2b) that calves into Skoddebukta and spans altitudes from sea-level to about 900 m a.s.l. The most elevated parts of the accumulation area belong to Amundsenisen (above 700 m a.s.l.). This area is drained by Bøygisen and Løveisen. Before reaching the ocean, Austre Torellbreen is fed by Vrangpeisbreen from the south. Across the divide in the south lies Hansbreen, which has a dominant main branch receiving important lateral inflow from two prominent tributaries in the southwest, i.e. Deileggbreen and Tuvbreen (Grabiec et al., 2012) . The glacier shows a somewhat reduced elevation range, only up to 500 m a.s.l. Beyond the mountain range to the east lies Paierlbreen. Both glaciers are well connected via Kvitungisen. Paierlbreeen connects again back to Amundsenisen in the north via Nornebreen. The glacier was not only classified as marine-terminating in the 2002-2010 inventory, but it also exhibited surge behaviour in 1993-1999 (Błaszczyk et al., 2009; Nuth et al., 2013) . During the surge, the ice front position was, however, not much affected. The reason might be that the surge event was superimposed on the well-documented retreat of all marine-terminating glaciers in the Hornsund area over the last century (Błaszczyk et al., 2013) . Austre Torellbreen, Hansbreen and Paierlbreen cover areas of 141, 64 and 99 km^2, respectively. West of the THPB complex lies Werenskioldbreen (Ignatiuk et al., 2014) . It is land-terminating and somewhat smaller with 27 km^2.

3.2 Glacier outlines

Glacier outline information is taken from the 2002-2010 glacier inventory described in Nuth et al. (2013) . As THPB is a well-connected glacier complex, adjacent glacier boundaries were removed and joined into one single outline. WSB was not merged with the THPB complex because the shared ice divide is short and shallow (Kosibapasset has only $\sim$ 15m depth). VIC is treated as a single entity by merging all its individual drainage basins. In this way, we avoid discontinuities in the anticipated thickness solution across ice ridges and divides.

3.3 Surface elevation

Concerning the Svalbard surface elevation, we rely on a 50 m digital elevation model (DEM) from the 1990s[1] provided by the Norwegian Polar Institute (NPI). This map was produced from areal photos using photogrammetry as well as from contour lines in earlier elevation maps, which were digitised and interpolated. We refrained from using this DEM for VIC where it is based on contour-line information resulting in a characteristic wave pattern in the slope field. Therefore, we use a more recent 10 m DEM inferred from 2010 radar data acquired by the TanDEM-X mission, operated by the German Aerospance Center (DLR; Krieger et al., 2013) . The DEM was processed from bi-static Synthetic Aperture Radar (SAR) data using a differential interferometric approach (Seehaus et al., 2015; Rankl and Braun, 2016; Vijay and Braun, 2016) . It was referenced to sea level by laser altimetry measurements with the Ice, Cloud, and Land Elevation Satellite (ICESat) (Schutz et al., 2005) .

3.4 Thickness measurements

[1] Norwegian Polar Institute (2014). Terrengmodell Svalbard (S0 Terrengmodell) [Data set]. Norwegian Polar Institute. doi:10.21334/npolar.2014.dce53a47

VIC thickness measurements (Fig. 4a) were obtained from 60MHz airborne radio-echo sounding (RES) surveys between 1983 and 1986 (Dowdeswell et al., 1986) . Five flightlines run north-south across the ice cap and two from east to west. All profiles follow centrelines of prominent outlet glaciers. Unfortunately, no bed reflector could be identified for a large portion of these airborne data, including most of the ice-divide area. Recently in 2008-2009, ground-based pulsed radar (GPR) data were collected by (Pettersson et al., 2011) . Following Pettersson et al. (2011) , the early airborne measurements were adjusted assuming a constant thinning rate of ~ 0.16m yr^{-1} over the entire ice cap. In addition, they estimate the measurement error for the early airborne surveys from Dowdeswell et al. (1986) to be 23.1 m, whereas the more recent GPR data shows a 9.3 m uncertainty.

In the Hornsund area, Hansbreen is well studied and an ice-core drilling team reached the bed at three locations already in 1994 (Jania et al., 1996) . Between 2004 and 2013, ground-penetrating radar profiles were collected both on THPB and WSB (Navarro et al., 2014) . These surveys provide a dense grid over most parts of these glaciers (Fig. 4b). Therefore, the early ice-core information was discarded here because it only gives information at three additional points and because it is not evident how to reliably estimate surface-elevation changes since the early 1990s. For WSB, the GPR measurement error was analysed in depth accounting for positioning-related ice-thickness uncertainty (Lapazaran et al., 2016) . Measurement errors fall into a range of 3.3 to ~~the 5m measurement uncertainty (Sect. 2.0.4).~~ 6.8 m with an average value of 4.5 m. These error values ignore, however, a known uncertainty term originating from 2D data migration (Moran et al., 2000) . This migration is common practice but it ignores transversal bedrock slopes. This processing uncertainty attains up to 14 m for a certain part of a small and shallow Alaskan valley glacier. It is impossible to a-priori determine this uncertainty for each measurement on Svalbard and we therefore ignore this source term here.

3.5 Surface mass balance

For the SMB information, we rely on the regional climate model MAR (Modèle Atmopshérique Régional; Lang et al., 2015) . MAR combines a hydrostatic model for the atmospheric circulation with a physically based model for snow-pack evolution. The MAR-SMB simulations cover the entire archipelago (Fig. 2a,b) and were validated by Lang et al. (2015) against available climatic variables as well as SMB measurements from Pinglot et al. (1999, 2001) . The difference between modelled SMB values and 10 used validation sites shows a low bias of -0.03m i.e. yr^{-1} with a standard deviation of 0.14m i.e. yr^{-1}. The latter value is considered as an uncertainty estimate for the SMB field. Simulation were conducted on a regular 7.5 km grid but a downscaled output was provided on 200 m spacing using an interpolation strategy that distinguishes the various SMB components (Franco et al., 2012) . The components are interpolated according to locally defined, vertical gradients. For the reconstruction, the annual SMB record was averaged over 1979-2015.

To assess the sensitivity of the thickness reconstruction to the SMB input (Appendix C1), results from the Weather Research and Forecasting (WRF) model were considered (Aas et al., 2016) . The WRF-SMB field represents the period 2003-2013 and has a 3 km resolution. The field could not be downscaled as above for the MAR results. Therefore, the SMB sensitivity is only assessed on the large VIC geometry.

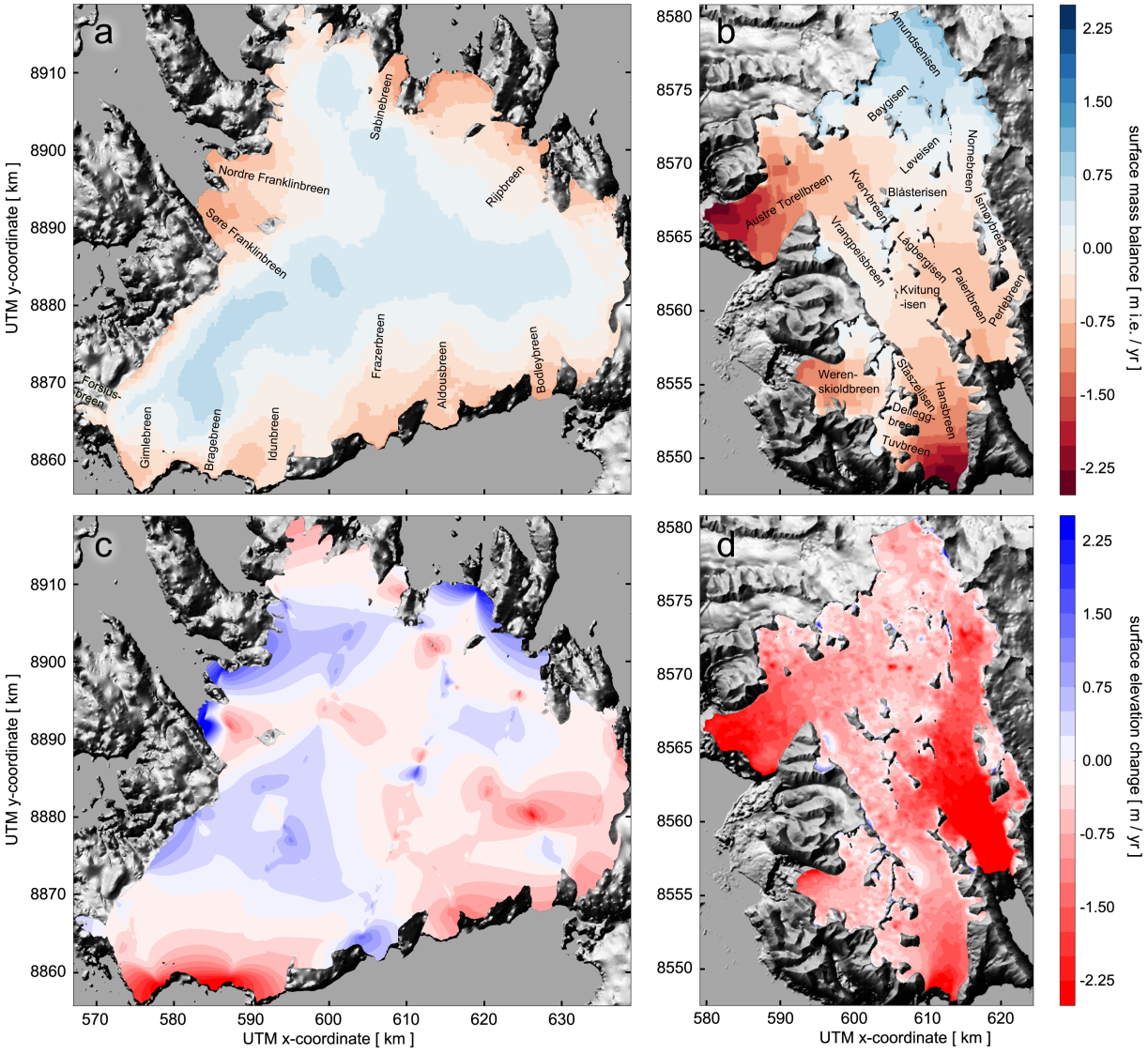

Figure 2. Input fields to the ice thickness reconstruction for VIC (a,c,e,g) and THPB/WSB (b,d,f,h). Surface mass balance (SMB) input (a,b) is provided by MAR as an average over the period 1979-2014 (Lang et al., 2015) . Elevations changes (c,d) are inferred from 2003-2007 ICESat profiles on VIC and from a 2008 SPOT-HRS DEM in southern Spitsbergen. From this elevation information, we subtracted the 1990 DEM from the Norwegian Polar Institute (NPI). For VIC, line information on elevation changes along the ICESat tracks was linearly interpolated (c). The difference between SMB and surface elevation changes (e,f) is referred to as the AMB. Surface velocity magnitudes (g,h) were inferred from 2015/2016 Sentinel-1 imagery. Background: grey-scale hill-shaded topography based on a NPI 50 m DEM.

3.6 Surface elevation changes

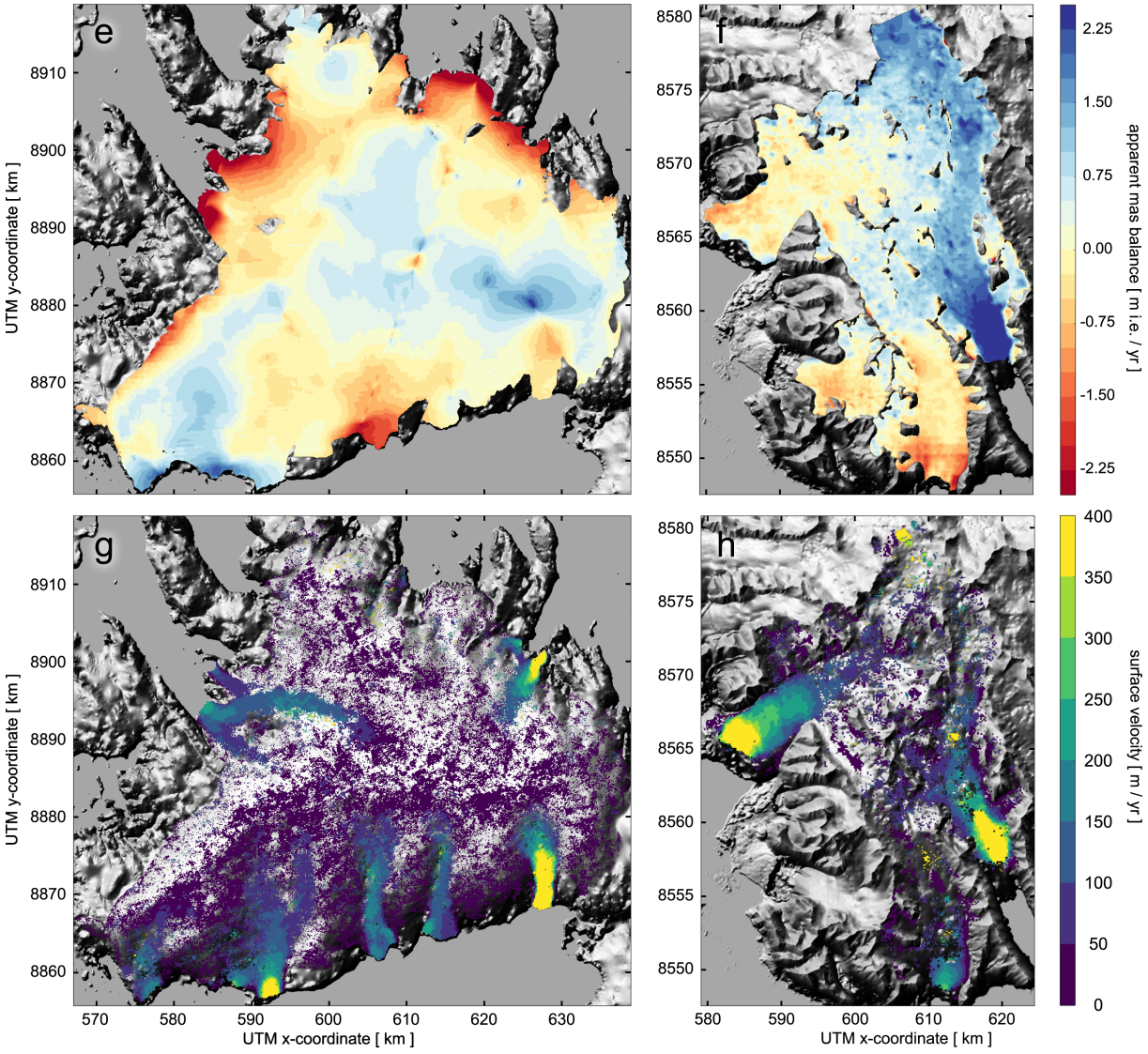

Figure 2. **(continued)**

Over VIC, 2003-2007 elevation changes (Fig. 2c) were inferred from ICESat altimetry measurements (Moholdt et al., 2010) . The laser altimetry system has a footprint of 70 m diameter with 170 m along-track spacing. Across-track spacing is irregular and much larger with several kilometres. A Natural-Neighbour Sibsonian interpolation[2] (Fan et al., 2005) is used to estimate elevations changes in between these scattered ICESat measurements. Moholdt et al. (2010) report that the local root-mean-square deviation of several hundred surface-change estimates is 0.3m yr^{-1}.

[2] source code available at https://github.com/sakov/nn-c/tree/master/nn

For Wedel Jarlsberg Land, elevation changes were calculated by differencing the NPI 20 m DEM[1] from 1990 with a 40 m DEM inferred from 2008 imagery acquired by the high resolution stereoscopic (HRS) sensor on-board SPOT 5 (Korona et al., 2009) . The DEMs were first co-registered (Nuth and Kääb, 2011) before subsequent differencing and re-sampling to 100 m (Fig. 2d). No information on the DEM differencing uncertainty was available.

3.7 Surface velocities

Using satellite imagery acquired between January 2015 and September 2016 by the C-band Synthetic Aperture Radar (SAR) onboard Sentinel-1, we apply intensity offset tracking to consecutive image pairs (Strozzi et al., 2002; Seehaus et al., 2016) . The time series of displacement fields is first filtered for obvious outliers within a kernel size scaling with the prevailing flow direction and magnitude (Seehaus et al., 2016) . Then, fields are stacked using median-averaging to obtain maximum coverage and to reduce effects from short-term or seasonal fluctuations (Fig. 2g, h). Velocity maps are provided at 100 m resolution. The uncertainty associated to the inferred velocity maps is estimated on 70 stable reference areas without ice cover. We find an average uncertainty of 19m yr^{-1}, which is comparable to independent uncertainty estimates for merged Sentinel-1 imagery with minimum values of $\sim$ 17m yr^{-1} (Schwaizer, 2016) .

3.8 Fjord bathymetries

Information on the fjord bathymetry is used to further constrain the thickness reconstruction at marine ice fronts. The new International Bathymetric Chart of the Arctic Ocean (IBCAO Version 3.0) holds a wealth of new measurements around the Svalbard archipelago (Jakobsson et al., 2012) . It comprises several recent multibeam surveys that entered deep into some major fjords and collected high-resolution seafloor information (Ottesen et al., 2007) . Around the archipelago, the new IBCAO map is provided at a spatial resolution of 500 m.

3.9 Grid specifications & Input uncertainties

The target resolution for the meshing is set to 200 m for THPB and VIC and 100 m for WSB. Observations for all test geometries are very densely spaced and we decided to only keep measurements that are more than 50 m apart, which is half of the minimum grid spacing. The initial 20792, 44921 and 21273 measurements collected on VIC, THPB and WSB were thus reduced to 4475, 5945 and 1189 points, respectively.

From the above presentation of the input fields available for the test geometries, we define appropriate input uncertainties for the formal error propagation in Sects. 2.0.4 and 2.1.2. First, the Dirichlet conditions on the error on the WSB and THPB thickness measurement δH is set to 5 m (Lapazaran et al., 2016) . For VIC, we prescribe 10 m and 25 m for the ground and airborne RES data, respectively (Pettersson et al., 2011) . Second, the AMB uncertainty is estimated to be $\delta\dot{a} = 0.4$m yr^{-1}, which is the sum of the individual error estimate reported for SMB and surface elevation changes (Sects. 3.5 and 3.6). For the first-step reconstruction, we estimate a 20% error in the flux direction δn. Only a scalar estimate is necessary here because of

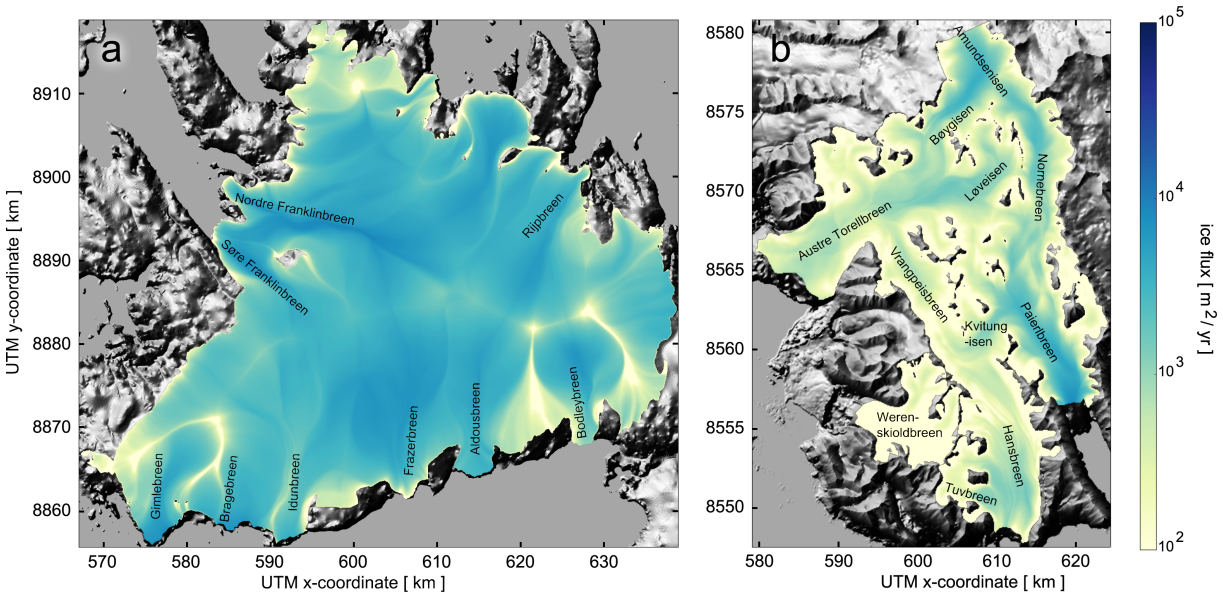

Figure 3. Ice-flux solution after cost optimisation for VIC (a), THPB and WSB (b). The ice flux gradually increases and converges into several distinct outlet glaciers. Ice flux converges over major drainage basins and is channeled through several major outlet glaciers. Flux values at marine ice fronts are therefore part of the solution~~whereas a zero condition is prescribed along the land-terminating margin~~. Background: grey-scale hill-shaded topography based on a NPI ~~50m~~ 50 m DEM.

the normalisation of the direction vector $\boldsymbol{n}$. The surface-velocity uncertainty is directly inferred from ground control points: $\delta u = 20\text{m yr}^{-1}$.

4 Results & Discussion

4.1 ~~First step~~ First-step reconstruction

This section covers the presentation and discussion of the ice-flux solution, the reconstructed thickness and bedrock elevation fields as well as the error estimates. In the error analysis, actual mismatch values from a fraction of withheld measurements are compared to the formal error estimate (Sect. 2.0.4). In the appendix, interested readers find a brief discussion of the viscosity parameter (Appendix A) and a sensitivity assessment with respect to changes in SMB, surface ~~geoemetry and to the flux correction term~~ geometry and to a flux correction (Appendix C).

4.1.1 Ice flux

For Vestfonna ice cap, the ice-flux field is very instructive (Fig. 3). For many drainage basins, ice flux is small near the ice divide and gradually increases downglacier. The increase ~~stems~~ results from ice accumulated along flow lines as well as from flow

convergence towards the lateral margin. Often, ice flux is highest ~~at or below~~ near the equilibrium line altitude. For Gimlebreen, ~~Frazerbreen, Aldousbreen, Søre and Nordre Franklinbreane~~Braggebreen, Idunbreen, Aldousbreen and Bodleybreen, ice flux remains elevated up to the marine ice fronts. For Gimlebreen, Braggebreen abd Idunbreen, these high values are explained by an increasingly positive ~~apparent mass balance~~ $\dot{a}$ towards the ice front (Fig. 2e). Also for Aldousbreen, $\dot{a}$ stays positive near the glacier tongue. Unlike these examples, the ~~apparent mass balance~~ AMB turns negative long before the margin is reached for Nordre Franklinbreen and Frazerbreen. There, elevated ice-flux values are maintained by strong convergence. For Nordre Franklinbreen, the ice flux mainly follows the ~~northern branch, whereas the 2015-2016 velocity information indicates that the southern branchis currently more active. The reason for this ice-flux deflection is that Franklinebreen was primarily drained through the northern branch in the 1990s (Schäfer et al., 2012) and that this route is still dominantly imprinted in the surface geometry. For most of the ice cap, flux values decrease towards the margin and level out to zero in land-terminating areas.~~ southern branch.

For WSB and THPB, the ice flux is small all along the land-terminating margin and increases towards centrelines. For Austre Torellbreen, we find strong flux convergence along Bøygisen and Løveisen. Further downstream, ice-flux magnitudes remain constant as the ~~apparent mass balance~~ AMB is close to zero. Unlike this balanced situation, a large surface lowering signal on Paierlbreen remains unexplained by the SMB, resulting in a positive ~~apparent mass balance~~ AMB over the entire catchment area. This imbalance is compensated by extensive downwasting implying a gradual flux increase up to the marine ice front. The imbalance itself might partially reflect the long-term geometric adjustment of Paierlbreen to the surge in 1993-1999. Yet, we cannot exclude that the SMB model underestimates the magnitude of surface melting or that a bias is introduced by the DEM differencing (Sect. 3.6). In any case, the Paierlbreen setup is challenging because there is almost no sink in the ~~apparent mass balance implying that ice mass is largely~~ AMB and ice is primarily lost via the marine ice front. The ~~tongue of Hansbreen shows less elevated flux valuesinstead which are explained by the small source area~~ main branch of WSB shows however very small flux values. The reason is that source areas ($\dot{a} > 0$ in Fig. 2f) ~~. The situation is even more extreme on WSB, where such source areas are mostly limited to~~ are very limited and located on two small glacier branches joining ~~the main branch~~ from the north. Though they provide a certain in-flux, values along the main branch remain close to zero. Under the ~~imposed~~ input SMB and elevation-change fields, no important ice-dynamic balancing is ~~needed. Accepting a certain uncertainty in the imposed fields, we expect that WSB is stagnant at lower elevations because of the general glacier retreat on Svalbard.~~ required.

4.1.2 Ice thickness and bedrock elevation

The first-step thickness map (Fig. 4) depends on surface slopes, thickness measurements and the ice-flux solution. The latter reflects both climatological and geometric information. For VIC, we find a mean thickness of ~~226m~~ 228 m (Table A1). This value is significantly higher than the previously reported ~~185m~~185 m, which was inferred from a direct kriging interpolation ~~of the observations (Pettersson et al., 2011)~~ (Pettersson et al., 2011) of the same observations that entered our reconstruction. One reasons for differences is that our reconstruction produces thicker ice along outlet glaciers troughs. Such deep and often over-deepened channels (Frazerbreen and Franklinbreen in Fig. 5) are explained by convergent ice flow draining large zones of the ice-cap accumulation area (Dowdeswell and Collin, 1990). For Braggebreen and Gimlebreen, the reconstruction suggests

deep troughs which arise from a very positive ~~, apparent mass balance~~AMB. The troughs are absent in the kriging interpolation as no observations were collected in this region. Another reason for differences is that kriging is expected to underestimate the ice thickness along the land-terminating margins away from observations because of ice-free conditions outside the domain. For our approach, ~~margin thicknesses are~~ the margin thickness is affected by physical quantities such as ice flux and surface geometry. An illustrative example for this effect is the dome-like surface topography of Forsiusbreen in the southwest of VIC~~(Fig. 2a).~~ . This glacier is almost deconnected from the main ice cap and the closest thickness measurements were taken more than ~~10km~~ 10 km away. As a consequence, Pettersson et al. (2011) generate limited thickness values from kriging. In our reconstruction, a small ice dome is predicted (Fig. 4a) that is even grounded slightly below sea level in its central areas (Fig. 5a). In ~~addition, the thickest ice is no longer suspected beneath the main crest but our reconstruction suggests a maximum east of Frazerbreen, where values locally exceed 450m. In~~ general, the first-step thickness map suggests that more than ~~12~~13% of the ice-covered area is grounded below sea level. Previously, it was thought that only a 5% ~~area fraction lay~~ area fraction lays below sea-level, due to limited measurements from the outer part of the ice cap. In terms of total ice volume, the first-step thickness map yields ~~534.7km^3~~ 540.2km^3 as compared to the 442km^3 from kriging (Pettersson et al., 2011). ~~Ice thickness (a,c,e) as in Fig. 4 and bedrock topography (b,d,f) as in Fig. 5 for Nordre and Søre Franklinbreen on VIC. To facilitate visual comparability, the outline of the subdomain of Franklinbreen that is updated in the second-step reconstruction is highlighted (non-transparent lurid colours). First (a,b) and second rows (c,d) show the inferred geometries using 1% or all thickness measurements during the reconstruction respectively. The last row depicts the updated geometry after the second-step. Partially transparent areas in these maps (unsaturated colours) stem from the associated first-step reconstruction.~~

For the THPB and WSB systems in southern Spitsbergen (Fig. 4b), an abundant observational record was available. Therefore, we expect that relative differences between thickness maps from a direct interpolation and the first-step reconstruction should be small. From a direct kriging interpolation by Navarro et al. (2014), the mean thickness estimate for the THPB system is 184 m as compared to ~~182~~ 176 m, here (Table A1). For the land-terminating WSB, ~~mean thicknesses~~ a mean thickness of 119 and ~~109 m are~~ 112 m is found, respectively. Relative differences ~~in~~ between these values are ~~small with 1.1% for THPB and 8.4% for WSB~~smaller than 6% for both. The slightly updated volume estimates are then ~~55.5km^3 and 2.9km^3~~53.5km^3 and 3.0km^3, respectively. Despite the similarity in these values, we see several systematic differences in the thickness maps from these two approaches. First, the kriging map shows that the measurements were interpolated ignoring the presence of some ice-free nunataks (for example above the confluence of Bøygisen and Løveisen in Fig. 4 in Navarro et al., 2014). Similarly, ice thickness does not tend to zero along some land-terminating margins. These positive biases are compensated in other areas, where thickness measurements are not reproduced after kriging. A clear difference is seen along Vrangpeisbreen~~(Fig. 2b).~~ . In its upper reaches, the direct interpolation shows values below ~~100m~~ 100 m (Fig. 4 in Navarro et al., 2014), whereas the thickness measurements along the centreline readily exceed ~~200m~~ 200 m (Fig. 4b). These measurements are by construction reproduced here. Turning to the basal topography, we find elongate troughs reaching far upglacier from the marine terminus (Fig. 5b). The bedrock elevation is below zero over ~~14~~12% of the entire THPB area. For Hansbreen, the bed remains below sea-level almost up to Kvitungisen~~(Fig. 2b). Even up at Nornebreen, a main tributary of Paierlbreen, the ice is grounded well below sea-level.~~ .

We For many glaciers, only few or even no thickness measurements are available and, therefore, we want to asses a lack of in situ measurements. For this purpose, we re-computed the VIC, THPB and WSB all thickness fields relying on a random 1%-sample of all thickness measurements (Fig. 4c,d). The idea is to assess the consequences of a lack of in situ measurements. For many glaciers around the globe, only few or often even no measurements are available. We therefore briefly discuss consequences from a lack of measurement constraints. For For VIC, we find somewhat reduced values a slightly larger value for the mean ice thickness of 216m 230 m and the total ice volume of 510.6 km^3 543.3 km^3 (Table A1). Despite this reduction, general characteristics of the basal topography are already imprinted in the poorly informed reconstruction (Fig. 5c). Along the central survey track at the northern branch of Nordre Franklinbreen (Fig. 6a,b,c,d), the reconstruction provides an acceptable estimate of the withheld thickness measurement profiles. For THPB and WSB, the mean ice-thickness values are reduced to 129 and 108m from previously 182 and 109m145 and 100 m from previously 176 and 112m, respectively. For THPB, the relative thickness reduction is substantial with 29%. As a consequence, this reconstruction only finds a 5% area fraction being substantial thickness reduction implies that the area-fraction grounded below sea level as compared to 14%, beforefalls from 12 to 8%. In many places, the sparsely informed reconstruction underestimates the depth of elongate, narrow bed troughs (e.g. Nornebreen, Vrangpeisbreen). Hansbreen is The densely spaced GPR grid measured on Hansbreen provides an ideal test case to estimate how well the reconstruction performs without much thickness constraints because it is there that the GPR survey net is densest. Withholding 99% of the thickness measurements, the reconstruction suggest an elongate deep trough . Considering all measurements, the trough is actually somewhat deeper (especially close to the divide with Vrangpeisbreen) and ice-covered many measurements. Though an elongated bed trough is predicted, thickness values and the slope of lateral valley sides are steeperunderestimated. Moreover, ice in tributary glaciers is found to be thicker. Despite the magnitude,the patterns in the well-informed thickness reconstruction shows more spatial variability in central areas, which is not produced when almost no thickness measurements are consideredbedrock topographies differ (Fig. 5b,d). This implies that small-scale some observed features in the bedrock topography are not necessarily well imprinted in the glacier surface nor the flux field. Admittedly, a certain degree of details has been removed by a-priori smoothing of the surface topography.in the slope field is removed by the geometric smoothing (Sect. 2.2.1).

4.1.3 Thickness error estimates

The following error analysis is two-fold: we first present and discuss error-estimate maps from the formal error propagation of input uncertainties as described in Sect. 2.0.4. Secondly, we split the abundant thickness measurement record into two subsets. One subset is used in the reconstruction (Sect. 2.0.3), whereas the remainder is withheld for validation. The validation subset is used to infer actual mismatch values at the respective measurement location. Average values for the actual mismatch are then compared with the respective formal error estimates.

4.1.4 Estimates from error propagation

Relying on a formal error propagation (Sect. 2.0.4), it becomes possible to provide an error map (Fig. 76a,b). Using all thickness observations, the survey tracks are clearly discernible visible as small values in all error maps. The 5m-constraint along these

tracks (Lapazaran et al., 2016) is propagated along flux streamlines both upstream and downstream. ConsequentlyAway from these measurements, error estimates only gradually increase along flow, whereas more abrupt variations appear gradually increase in both direction along streamlines. More abrupt variations are found perpendicular to the inferred flux direction. Moreover, error estimates We therefore suggest that future measurement campaigns should give priority to across-flow profiles. Values are highest in areas where ice flux is small as, for example near unconstrained divides along the southwestern part of the VIC divide and on a large portion of WSBpart of the land-terminating WSB. For the latter area, error estimates are largest. We therefore suggest that future measurement campaigns should give priority to across-flow profiles as well as to stagnant areas. From gaps in the available cross profiles, we anticipate that a measurement spacing appropriate for thickness reconstructions should be in accordance with the target thickness map resolution. Once measurement gaps exceed the nominal resolution, error streaks start propagating through cross profiles. The by-far largest error estimates amongst all test geometries are found for the land-terminating WSB. These extreme values are caused by negligible ice flux over a major part of the domain (Sect. 4.1.1). The error-estimate map of VIC also highlights that measurements should ideally be acquired on both sides of an ice divide. For Idunbreen(Fig. 2a), no measurements were obtained (Fig. 4a), which leads to elevated error estimates over most of this drainage basin (Fig. 76a). Thickness measurements collected just across the ice divide were not transmitted over the crest to the Idunbreen catchment area.

Considering only 1% of all thickness measurements, the error estimates become larger (Fig. 7c,d). In this case, the 6c). The ice-cap setup shows largest errors along the ice divide. The increase in the error estimates are unproportional with respect to the actual differences in the thickness values values along ice divides and ridges where flux values are smallest. On WSB and THPB (Fig. 4a,c). Therefore, the fact that error estimates exceed the actual thickness value near the ice divide should not be overrated. For the valley glaciers THPB and WSB, 6d), maximum error estimates are found in areas with small ice flux. Errors are most prominent for WSB and Hansbreen , which both were found to exhibit small or even negligible ice flux. In addition, errors tend to be higher along central flow lines as a result of convergent ice flux. For sparse measurements again found in the stagnant areas on WSB but also on Hansbreen and Austre Torellbreen values are elevated. In critical areas on ice caps and glaciers, we confirm that local error estimates error estimates can readily reach 50% of the inferred thickness valuesice thickness if thickness measurements are sparse.

4.1.5 Actual thickness mismatch

A pressing question is whether the magnitude of these error-estimate maps is reliable and falls into a realistic range. For this purpose, we withheld a random sample of all thickness measurements from the reconstruction and computed an absolute thickness mismatch for comparison. The sample size is defined as a fraction of all measurements and we investigated the range from 1 to 99%.

In a first attempt, we directly compared the formal error estimates to the in situ absolute mismatch values. Ideally, these two values would show a positive correlation. Yet, no clear dependence was discernible for none any of the sample sizes. Both data distributions, for mismatch values and error estimates, are not normaland we therefore . Being robust to outliers, we decided to quantify them these distributions in terms of medians and quartiles . These measures are more robust to outliers than mean

values and standard deviations. Medians and quartiles are normalised to the average thickness of all withheld observations (Fig. 8). First and foremost, medians and quartiles suggest that 7). In this aggregate sense, error estimates tend to overestimate the absolute mismatch. For small fractions of withheld measurements, the overestimation is stronger. This bias does not surprise as formal error estimates cannot fall below a 5m limit Lapazaran et al. (2016) preset measurement error (Sect. 3.9), whereas high correlation between thicknesses thickness values at adjacent location results in very low mismatch values. If only 1% of the measurements is withheld, normalised medians of the absolute mismatch range from 0.5 to 1.4%, whereas equivalent values for the error estimates range between 4 and 22%. As more and more data is withheld, normalised median mismatches increasemedian mismatch values do not exceed 3 m, which simply reflects spatial data correlation. For this case, median error estimates are about 20 m for VIC and THPB. Error estimates are problematic on the stagnant WSB setup, where we find a median of 149 m, which exceeds the mean ice thickness. For a withheld data fraction of 99%, we find values of 8% mismatch medians of 21 m for VIC, 24% 47 m for THPB and 23% 36 m for WSB. These values could give a first indication of the maximum overall uncertainty associated to the presented thickness reconstruction for glaciers for which no measurements are available. The normalised Again these are overestimated by the median error estimates are 43%, 11% and 51%of 102 m, 66 m and 360 m, respectively. Again , the value on WSB stands outhere because formal error estimates diverge over a large portion of the glacier area where flux values are very small. From this comparison, we take that . We conclude that aggregated values of formal error estimates show a tendency to exceed mismatch values. This tendency suggests that error estimates, here, can be interpreted in terms of an upper constraint. Admittedly, magnitudes of these error estimates depend on the choice of te input uncertainty, which will affect the interpretation . We strongly want to discourage that this error estimates are interpreted in terms of a standard deviation because of two reasons. First, mismatch values and error estimates are not correlated and, secondly, both distributions are not normal.

4.2 Second-step reconstruction

The second step of this reconstruction is optional and depends on the availability of velocity information. Knowing surface velocities,the mass conservation equation can be solved directly for the unknown ice thickness (Morlighem et al., 2014) .

The above aggregate assessment suggested that the error estimates could serve as upper constraints for the actual mismatch. It remains however unclear how reliable this interpretation is at individual measurement locations. We therefore compute the data fraction of all withheld measurements for which the actual mismatch is less than the predicted error estimate (Table 1). If only a 1% fraction of the measurements is withheld, more than 90% of the actual mismatch values fall into the error bounds. On VIC, even 100% are reached. As before, these high values simply reflect the strong spatial correlation in the measurements. Withholding gradually more data for validation, the data fraction for which the upper error constraints are valid decrease. The second-step thickness field is anticipated to be an improvement. The reason is that minimum of 64% is reached for THPB. These numbers give a first indication on the spatial reliability of the flow direction is no longer geometrically prescribed but follows the observed surface velocity field. In addition, the pattern of velocity magnitudes enters the reconstruction and modulates the thickness field accordingly. We decided to limit the thickness update to areas in which the observed velocity magnitude exceeds error-estimate map. Looking at the spatial distribution of violated error bounds (Fig. 6c,d), a clustering is

Table 1. Fraction of all validation measurements for which the absolute mismatch is less than the predicted error estimate. Values are given in per cent.

fraction of withheld measurements [%]	test geometries		
	VIC	THPB	WSB
99	84.0	63.9	88.7
95	89.0	80.0	87.0
90	93.0	79.4	91.1
80	94.7	82.8	94.1
70	96.2	86.0	93.4
60	97.3	88.6	96.1
50	97.3	88.7	95.6
40	97.9	89.2	96.8
30	97.9	89.5	96.9
20	97.5	89.5	98.0
10	98.4	91.2	96.6
1	100.0	93.1	90.9

visible. For the ice-cap setup, we find violations along the land-terminating margin, where inferred thickness values tend to underestimate the measurements. Concerning violation in the interior, a tendency for overestimating the thickness values is discernible. For the more constrained valley glacier setups (THPB, WSB), these tendencies are not confirmed.

We conclude that median error-estimates overestimate the mismatch values and could therefore serve as an upper error constraint. Accepting this interpretation, we can provide an aggregate error range. Mean thickness values for VIC, THPB and WSB fall into a range of 172 - 320 m, 141 - 217 m and 46 - 508 m, respectively. For the area fraction of ice grounded below sea-level, we find ranges of 7 - 23% for VIC and 7 - 22% for THPB. This maximum range on VIC is clearly exceeded by the 5% area fraction inferred by a direct interpolation of measurements. Despite this aggregate assessment, the spatial reliability of interpreting the error-estimate map in terms of an upper constraint for local measurements become increasingly difficult the fewer measurements are available.

4.2 Second-step reconstruction

The second step of this reconstruction is applied in one sub-domain for each test geometry, where velocity measurements exceed 100 ~~m yr^{-1}. Below this threshold, the velocity information becomes increasingly fragmented~~ m yr^{-1} (Fig. 2g,h). In these sub-domains, mass conservation is directly solved for the unknown ice thickness. As this solution is additionally informed by velocity observations, we expect an improved thickness field.

4.2.1 Ice thickness

On VIC, ice thickness is updated along 8 fast-flowing outlet glaciers (~~Figs. 6e and 9~~8a,c). In these areas, the new thickness field can differ considerably from the first-step reconstruction (Fig. 4), particularly in areas with sparse observational constraints as for Idunbreen and Rijpbreen. The reason is that velocity streamlines deviate from the ~~slope-prescribed~~ geometrically prescribed flux direction. Consequently, the ice is distributed differently. For Idunbreen and Rijpbreen, deeper troughs are found somewhat away from the ice front ~~which is explained by a convergent surface velocity field. Therefore, velocity measurements seem more valuable in areas where no thickness measurements are available. Along the southern branch of Nordre Franklinbreen, some measurements were collected, constraining the reconstruction. The updated thickness fieldis anyhow thicker downstream of the junction between the southern branch and~~ and a larger ice volume is inferred. For all other outlet glaciers, the ~~not-updated northern branch~~ ice volume estimate decreases. In addition, spurious along-flow variations in the geometrically controlled first-step thickness field, for instance on Bodleybreen and Rijpbreen (Fig. ~~6e). The updated bedrock topography now shows asomewhat deeper trough (Fig. 6f). The reason for this difference is that ice flow follows the 2014-2015 surface velocities, which favoured the southern branch, while the geometrically imposed first-step flux direction showed a preference for northward outflow (Fig. 3).~~ 4a), are not visible in the second-step field. Accounting for the second-step reconstruction, both the total ice volume and the mean ice thickness slightly decrease to 538.8km^3 and 227 m, respectively. This also reduces the area fraction grounded below sea-level to 13.0%.

In Wedel Jarlsberg Land, thickness fields are updated for the three fast-moving frontal areas of ~~each glacier in~~ the THPB complex. The wealth of thickness observations implies that the first- and second-step reconstructions are very similar (Fig. ~~9~~8b). This is certainly the case for ~~the fast portions of Hansbreen and~~ Paierlbreen. Differences become largest near the calving fronts because of the free boundary condition. For Hansbreen, the bed trough near the ice front becomes both deeper and wider~~whereas the updated Paierlbreen geometry only shows a wider trough~~. For Austre Torellbreen, differences are more apparent as only two along-flow measurement profiles constrain the thickness field at low elevations. Along ~~the centreline of Austre Torellbreen, two overdeepened spots~~ its centreline at the confluence with Vrangpeisbreen, an overdeepened spot in the first-step reconstruction ~~are flattened out~~ is flattened in the updated basal topography (Fig. ~~9~~8d). The frontal area is also thinner than in the first-step reconstruction. For the entire THPB complex, we find a small reduction in average thickness to 173 m.

4.2.2 ~~Error~~ Mismatch & error estimates

The updated error-estimate ~~fields are~~ map (Fig. 9) is informed by first-step values at lateral boundaries~~except for marine ice fronts (Fig. 10). Owing to this inheritance, a repetition of the above error analysis (Sect. 4.1.3) seems redundant . In the subdomains, error estimates are simply~~ . These estimates are now propagated along velocity streamlines~~and further modified. For~~ , which themselves are inferred from measurements. On Frazerbreen and Hansbreen, large first-step error estimates near the ice front are reduced because of high velocities. In the sub-domains on VIC, magnitudes of the updated error estimates tend, however, to increase as compared to the first-step values. ~~This might imply that the~~ A possible reason is the relatively large input velocity uncertainty of 20 m yr^{-1}~~was chosen relatively high. Yet, this tendency is not confirmed for the THPB~~

complex. Along the survey tracks, error estimatesare identical as we again prescribe the 5m value associated to the thickness measurements (Lapazaran et al., 2016) .

We repeat the aggregate error assessment from above (Fig. 10). For VIC and THPB, we find that median mismatch values are higher than in the first step. So despite the additional velocity information, the second-step reconstruction is not necessarily able to produce a more reliable thickness map. Another trend is seen in the interquartile error-estimate range, which is often reduced, certainly for THPB. Yet no trend is visible in the median error estimates, which are smaller for THPB and higher for VIC than in the first step. Following the above interpretation of these aggregated error estimates in terms of a maximum range, we can update the mean thickness ranges to 171 - 320 m and 142 - 212 m for VIC and THPB, respectively. The maximum ranges for the area fraction below sea-level become 6 - 23% and 6 - 18%, respectively.

5 General Discussion

In this section, we discuss the central assumptions and caveats of the presented reconstruction approach. For the first step, sliding is inherently neglected, assuming that ice motion is an exclusive result from internal deformation. In areas without thickness and velocity information, this assumption is likely the dominant source of uncertainties and might even bias biases the results towards high higher thickness values. Other reconstruction approaches use an empirical scaling relation (e.g. Farinotti et al., 2009b) or incorporate a transiently resolved relation for basal water availability (van Pelt et al., 2013). In either case, formulations are basic because of our limited knowledge of basal conditions. Although these approaches are valuable attempts to address the issue of unknown basal conditions, it remains questionable whether uncertainties in the reconstructed thickness field are in fact reduced. Here, we instead address basal sliding by relying on direct measurements of the surface velocities but limited to sub-domains where magnitudes exceed $100\,\mathrm{m\ yr^{-1}}$. These velocity measurements comprise motion arising from both internal deformation and basal sliding. For THPB and VIC we find reduced values for the mean glacier thickness when using velocities. This concurs with the expected high bias in the first step.

Another caveat in the first-step reconstruction is the assumption that the ice flux follows the steepest surface slope a smoothed version of the surface-slope field (Sect. 2.3). Although this assumption The smoothing is spatially variable accounting for non-local flow coupling via membrane stresses. Although the direction choice might be appropriate in slow-moving areas, the actual velocity vector can point into a different directionelsewhere. The situation becomes even more complex for surging glaciers, for which the surface topography is significantly notably modified during these short-term events. An examples is Franklinbreen on VIC. Here, , for which velocity information from the early 1990s show main outflow via the geometrically imposed flux direction prefers the northern outlet branch(Fig. 3) . Although this is consistent with velocities in the early 1990s, the 2015 state shows that more ice is currently . Using the 1990 DEM (Sect. C2) for the first-step reconstruction, most ice is also exported via the southern branch (not shown). Therefore, the surface topography is not necessarily the best indicator for the flow direction. In the second step, we were able to update the thickness field in consistency with the recent velocity fields2015-2016 velocity fields, with preferential outflow also via the southern branch. Yet even for the second-step this reconstruction, it is

not evident how to account for important, non-regular dynamic changes, such as surging, as for instance on Franklinbreen and Paierlbreen (Błaszczyk et al., 2009).

~~From the perspective of mass conservation, uncertainties from temporal inconsistencies could be reduced by contemporaneous input fields. If some input fields are representative for very different time periods than others, a not-well assessable bias is introduce in th reconstruction . Despite time consistency, input fields should also be averaged over a certain period. The reason is that input variables can show strong seasonal and inter-annual variability, which alter the inferred thickness fields. This effect was also seen for Franklinbreen for which ice preferred different export paths in the two reconstruction steps. Therefore, some inherent response time of glacial systems has to be accounted for~~ The provided error-estimate map is shown to be a practical measure for a first error assessment. The underlying error analysis inherits all assumptions made in the mass-conserving reconstruction and thereby accounts for various input uncertainties. A fundamental assumption is that the error estimate is the minimum value of two solutions (Sect. 2.0.4). These two solutions stem from an error increase or an error decrease along the flow, both assumed to change at the same rate. We argue that the latter solution is necessary to constrain the error estimate upstream of measurements. The assumed magnitude of the decrease rate is however disputable. Furthermore, the error analysis neglects other sources of uncertainty. First, not all input fields are contemporaneous and therefore an inconsistency is introduced in the mass conservation equation. Second, the control parameters à, u_1 and u_2 are updated during the optimisation. These changes are unaccounted for in the ~~averaging. For the test cases described in this manuscript, time consistency could not be prioritised because of limited data availability. Resultant time inconsistencies therefore add to the uncertainties associated with the presented thickness fields.~~ constant input uncertainties. Third, input fields are time averaged. Such averaging suppresses seasonal signals for instance in the velocity measurements or is simply a necessity to obtain a climatologically meaningful SMB field. Yet, the averaging adds further to the uncertainty. Finally, uncertainties in some SIA parameters and variables remain unconsidered, including surface-slope magnitude and the viscosity parameter. The latter is even unconstrained if no thickness measurement is available. All these unconsidered source terms reduce the reliability of the presented error-estimate map. In a stringent Bayesian framework, Brinkerhoff et al. (2016) were able to account for the above terms.

Concerning the sensitivity of the thickness map of VIC to changes in the input ~~fields~~ SMB and the input DEM (Appendix C), we find that integrated values as mean ice thickness and ice volumes are rather insensitive. On VIC, relative differences in our analysis remain ~~below 3~~within 5% (Table A1). Differences in these integrated values reduce as more and more thickness measurements are available. Locally, differences can however become large~~and the explanation is not always evident~~. Without thickness measurements for correction, we found that an offset in the specific SMB directly translates into a thickness bias. Concerning the flux correction, we confirm that it is most influential for stagnating areas. Ice flux values on Werenskioldbreen are very small and the relative volume difference when applying the flux correction reaches ~~8%. Yet the effect reduces both with the~~ 14%. Differences again reduce with increasing availability of thickness measurements~~and with an increasing mass overturning as prescribed by the apparent mass balance~~. For VIC, ice-volume or mean-thickness estimates change by less than ~~0.3~~2.0% after applying the flux correction. For THBP, the relative difference is slightly larger at ~~2.4~~5.0%. For ~~these cases~~VIC and WSB, these relative differences are ~~comarably small as compared to~~ often smaller than the sensitivity to measurement

availability. Using either all or only 1% of all available measuremetns in the reconstruction results in larger relative changes in the mean ice thickness by ~~5% for VIC and 29~~11% for WSB and 17% for THPB.

~~For~~ The central assumption in the second-step ~~in this reconstruction , we found that it is impractical to use the velocity observations over entire drainage basins. The primary reason is that the reconstruction approach is very sensitive to inconsistencies~~ reconstruction is that surface velocities equal vertical mean values. This assumption is justified as this step is only applied in areas where ~~velocity magnitudes are small. Therefore, we decided to spatially limit the reconstruction using a 100 m yr^{-1} velocity threshold. This choice ensured that fragmented areas in the velocity field were avoided and that relative input uncertainties remain below 20%. Another reason was that the ice thickness reconstruction can only perform well where ice flow is linked to a designated source area. Sources can either be an area of dominant surface accumulation or an important upstream inflow boundary. When applied to entire drainage basins on VIC, some isolated flow systems (e.g. the northern branch of Nordre Franklinbreen) were not linked to any source area. As a consequence,~~ surface velocities exceed 100 m yr^{-1}. There, basal sliding is likely dominant. An aggregate assessment of the thickness mismatch indicates that the ~~velocity informed thickness reconstructionproduced almost no ice cover in these areas. We are convinced that~~ second-step thickness update is not necessarily more reliable than the first step. Though the updated field is consistent with the actual flow field, mismatch values tend to be larger than in the first-step reconstruction. Reasons for a worse match are that velocity measurements also introduce further uncertainty and that thickness measurements enter a cost term during the second-step ~~reconstruction could be extended to larger sub-domains. We think that such an extension is possible by lowering the velocity threshold while assuring that most velocity streamlines connect to an upstream inflow boundary. Yet, the actual choices involved are not evident and need further investigation which exceeds the scope of this study~~optimisation rather than being imposed in the first. In addition, the sub-domain delineation might not be optimal.

6 Conclusions

We ~~have presented~~ present a two-step, mass-conserving reconstruction approach to infer ~~ice~~ glacier thickness maps with prior knowledge on source and sink terms in the mass budget. The ~~first step is intended for glaciers for which input information is limited. Requirements are comparable to other reconstruction approaches that have been applied successfully to glaciers world-wide (Huss and Farinotti, 2012) . In fast-flowing areas, available velocity information is used, in a second step, to improve the thickness field along outlet glacier sub-domains~~two steps guarantee applicability in absence of velocity measurements. In the first step, a glacier-wide thickness field is inferred from a balance flux calculation on the basis of an input AMB. The second step requires velocity measurements, which are often not reliable all over the glacier. Therefore, the glacier thickness is only updated over a sub-domain. This updated field is consistent with the observed flow field and shows a seamless transition into the glacier-wide first-step map. In both steps, available thickness measurements are readily assimilated to constrain the reconstruction. ~~The approach is tested on different~~ Moreover, the inferred thickness field is provided together with an error-estimate map, based on a formal propagation of input uncertainties. Here, we present and apply this approach to various

glacier geometries on Svalbard where an abundant thickness record was available. On these test geometries, we show that the approach performs well for entire ice caps as well as for marine- and land-terminating glaciers.

For the land-terminating Werenskioldbreen in southern Spitsbergen, measurement tracks are densely spaced. Therefore, average thickness values from a direct interpolation (Navarro et al., 2014) and from the first-step reconstruction are very similar at 119 and 109m, respectively. Dense measurement tracks were also acquired on the adjacent Austre Torellbreen, Hansbreen and Paierlbreen complex for which the average thickness value of 186m deviates by mere 2% from the direct interpolation. However, reconstructed thickness values along the land terminated margin are somewhat smaller than from the direct interpolation whereas ice tends to be thicker along central flow lines and away from constraining observations . For the three marine-terminating glaciers, the mean ice-front thickness is just above 100m, which is loosely confirmed by the rough archipelago-wide estimate of 100m which was necessary as no measurements or reconstructions were available (Błaszczyk et al., 2009) . The thickness field of an ice cap is considered a more challenging task for reconstruction because of an increasingly flat topography near the ice divide. For Vestfonna ice cap, we find a mean first-step thickness value of 226m, about 22% larger than the previously reported glacier-mean of 186m (Pettersson et al., 2011) . In addition, the fraction of ice grounded below sea-level needs substantial upward correction, from 5% to 14%. Consequently, ice loss under future climatic warming will be intensified by iceberg calving to the surrounding oceans over a much larger area. In The approach is found to be most beneficial in areas where thickness observations are sparse or unavailable. There, our reconstruction is informed by glacier geometry and the second step of our approach, the ice thickness field was updated using ice velocity measurements over prominent marine-terminating glaciers. The resultant thickness field is more consistent with the actual AMB both constraining the produced thickness values. A direct measurement interpolation ignores such information and fills such gaps according to distant thickness information. The associated error map estimated from our reconstruction additionally highlights areas with least constrained ice thickness, namely away from observations and especially where ice-flow pattern and therefore considered an improvement. In areas without thickness measurements, the second step reconstruction can produce thicker ice in confluence areas.

The reconstructed thickness field is provided together with an error-estimate map, which stems from a formal propagation of input uncertainties through the underlying equations. For the first-step reconstruction, the magnitude of these error estimates was validated against mismatch values computed from withheld measurements. We find that formal error estimates tend to overestimate mismatch values. Analysing their distribution, error estimates can here be considered upper and lower constraints of inferred thickness values. The error-estimate maps highlight that survey tracks should preferentially be planned in across-flow direction. The error map is also valuable as it points out the regions that were thickness values are least well constrained and should therefore be target areas when planning future surveys. Generally error estimates diverge over ice divides and in stagnant areas. The fact that we withheld fractions of all thickness measurements could further be exploited in terms of a first overall uncertainty estimate for glacier for which not many or even no thickness observations are available. From the analysis of resultant mismatch values, we expect a is small or even stagnates. In an aggregate, glacier-wide median uncertainty in the reconstructed thickness field of about sense, the actual thickness mismatch is shown to reach 25%, normalised to the

~~mean glacier thickness~~ % for glaciers with only few thickness measurements. In absence of such measurements, the aggregate mismatch freely scales with a-priori choices for not well-constrained parameters.

In light of the growing body of information on glacier changes with satellite remote sensing, reconstruction approaches for mapping glacier ice thickness are less and less limited from the input side. Therefore, 2D approaches become increasingly attractive and favourable because a final interpolation, which fills gaps between reconstruction profiles, can be avoided. However, the largest limitation on the applicability of 2D approaches is the availability of regional information on surface elevation changes and surface mass balance. Elevation change maps from stellite remote sensing have already been presented for several regions but further development is necessary to reduce uncertainties associated with signal penetration and firn properties. Concerning regional SMB fields, we can either rely on parametric approaches or on regional climate models. In absence of both SMB and $\partial_t h$, a most basic parametric approach was already forwarded to infer distributed thickness fields world wide (Huss and Farinotti, 2012) .

Appendix A: Viscosity parameter

To translate the ice-flux solution into an ice-thickness field, the ice-viscosity parameter B has to be defined (Fig. A1). Parameter values are inferred at locations where thickness measurements are available via Eq. (7). The resultant point information is then interpolated over the entire glacier domain (Sect. 2.0.3). For VIC, we find values covering a spectrum from 0.02 to ~~0.54 MPa yr$^{1/3}$~~ $0.55 \cdot 10^6$ Pa yr$^{1/3}$, which corresponds to a rate-factor range from ~~$1.97 \cdot 10^{-25}$ to $1.98 \cdot 10^{-21}$~~ $1.90 \cdot 10^{-25}$ to $3.07 \cdot 10^{-21}$ Pa^{-3}s^{-1}. For ice temperatures between -20 and 0°C, we would expect rate-factor values between $1.0 \cdot 10^{-25}$ and $2.4 \cdot 10^{-24}$ Pa^{-3}s^{-1} (e.g. p. 75, in Cuffey and Paterson, 2010). The inferred values for VIC clearly exceed this meaningful range and should therefore not be interpreted in terms of a material property. The ice viscosity is a tuning factor, which compensates for any ~~deficiencies or inconsistencies~~ assumptions in the reconstruction or deficiencies and inconsistencies of input fields. The parameter is ~~also affected by the flux correction in stagnant areas~~further aliased by not accounting for basal sliding. The highest viscosities are inferred in areas next to land-terminating boundaries. These areas are also characterised by small flux values. As observations show some non-negligible thickness values there, B has to be high. The lowest values are seen in the northern part of the ice cap and along the lower trunk of Aldousbreen. For this glacier, one might interpret these low values in terms of sliding. However, for other outlet glaciers, the viscosity parameter is not necessarily decreased as compared with the surrounding area. This inconsistency also suggests that a physical interpretation of the viscosity parameter is delicate.

For the THPB and WSB area, the B-field also shows strong variations (Fig. A1). Values cover a range from ~~0.03 to 1.95 MPa yr$^{1/3}$~~ 0.02 to $2.20 \cdot 10^6$ Pa yr$^{1/3}$, corresponding to a rate factor range between ~~$4.26 \cdot 10^{-27}$ and $2.61 \cdot 10^{-21}$ Pa^{-3}s^{-1}~~ $2.97 \cdot 10^{-27}$ and $2.28 \cdot 10^{-21}$ Pa^{-3}s^{-1}. The inferred range is even larger than for VIC and again exceeds the physical range. Yet for these glaciers, a pattern might be discernible. High viscosities are often concentrated along central glacier flowlines. One explanation could be that the flux solution shows a low bias along these trunks as a result of systematic inconsistencies between the input SMB and the surface elevation changes. Such a systematic effect would naturally cumulate as ice flow converges towards centrelines. ~~This explanation is certainly supported on Hansbreen and Werenskioldbreen. There, the ice-flux solution shows comparatively small magnitudes, which likely explains unproportionally elevated viscosity values.~~ Lowest viscosity values are concentrated along the ridges and in the flat area between the nunataks separating Paierlbreen and Austre Torellbreen.

In summary, the interpretation of this viscosity field B in terms of ice dynamics is rather limited because values exceed the physical range. The field should rather be seen as a multiplier for tuning purposes as it can compensate for uncertainties in and inconsistencies between input fields as well as for assumptions within this first-step reconstruction. B is presented here to visualise that a single viscosity parameter might not be sufficient to capture all spatial variations in the thickness field. Initially, a best-fit single viscosity value over entire drainage basins was used, but the thickness pattern could not be explained by variations in ice flux and surface slopes alone (Eq. 7). A single viscosity parameter resulted in underestimated ~~thicknesses~~ ice thickness for the thick parts of the glacier and overestimated values for shallower parts (not shown). Other comparable state-of-the-art approaches often use a constant value for entire glacier basins (Farinotti et al., 2009b; Huss and Farinotti, 2012; van Pelt et al., 2013).

Appendix B: Apparent mass balance

In this section, we will briefly discuss how the AMB-field ȧ is adapted during the first-step optimisation when all thickness measurements are taken into account (Figs. 2e,f and A2). On the ice cap geometry, differences between the initial and the final AMB field are most expressed along the ice divide and ridges but also along some centrelines, as for instance on Frazerbreen. The reason for pronounced changes along these features is that they are focal areas in terms of flux convergence or divergence. AMB modifications there can efficiently correct for flux deficiencies (as defined by the cost function) over a large area of influence (either up- or downstream). The initial AMB shows only negative values over the little ice dome feeding Forsiusbreen. Yet after optimisation a small source area was created which explains the presence of ice in this area. Despite these most pronounced changes, the average AMB over the ice cap is initially $0.02\,\mathrm{m\,yr^{-1}}$ while finally we find $0.03\,\mathrm{m\,yr^{-1}}$. This is an increase of 35%. For WSB, even the sign of the AMB average changes as initially the main branch of the glacier shows hardly any source region with positive AMB. As ice flux is expected to be positive and as no inflow is possible along the upper land-terminated margin, the optimisation guides the system to a more equilibrated AMB state over this glacier. For THPB, the input AMB shows an area average of $4.1\,\mathrm{m\,yr^{-1}}$, differing by less than one permille from the final average. For THPB, differences between the final and the initial AMB field are again most expressed along certain flowlines.

Appendix C: Sensitivity analysis

C1 Surface mass balance

Here, the sensitivity of the first-step reconstruction to the SMB input is briefly discussed for VIC (Fig. ~~9~~8). For this purpose, we exchange the 1975-2015 MAR-SMB with the 2003-2013 WRF-SMB (Sect. 3.5). A fundamental discrepancy between the simulated time periods becomes apparent when integrating the SMB fields over the ice cap. We obtain mean SMB values of -0.08 for MAR and ~~-0.3 m i.e. yr^{-1}~~ −0.3 m i.e. yr^{-1} per unit area for WRF. For the WRF-SMB, more ice is removed at low elevations consistent with the warmer climatic conditions of the more recent period. When using all thickness measurements, the new thickness field (Fig. A1a) is very similar (Fig. 4a) showing a slightly reduced mean value of ~~222m~~ 225 m as compared to 228 m (Table A1). Consequently, the new volume estimate is also reduced to ~~525.2 km^3~~ 531.9 km^3 (about 2%). Reduced thickness values are ~~visible~~ best discernible near the ice fronts of Gimlebreen, Idunbreen and Bodleybreen. Due to a lack of observations in these regions, the reconstruction is not well constrained and as the WRF-SMB removes more ice, glacier thickness estimates become smaller. This reduction is important as the ice cliff height determines the unknown ice discharge. The frontal reduction is less clear for the land-terminating margin because steeper surface slopes limit the ablation-zone extent. The reduction becomes even more evident when only 1% of the thickness measurements is used (Fig. A1b). Thickness values near the ice divide are however not necessarily smaller. On average, the ice volume estimate is reduced to ~~497.9 km^3~~ 515.9 km^3 and a mean thickness value of ~~210m~~ 218 m is found (~~-3%~~).

as compared to 230 m). In general, the reconstruction is capable of compensating poorly constrained SMB data where the thickness record has ~~high~~ good spatial coverage. ~~For glaciers where no information is available neither on ice thickness nor on surface mass balance or elevation changes, the reconstruction is largely unconstrained. Without thickness information, the error estimates can be reduced by investing in consistent, contemporaneous and well-informed fields for SMB and surface elevation changes.~~

C2 Surface topography

The sensitivity of the first-step thickness field to the DEM choice is ~~somewhat smaller for VIC~~smaller as compared to the SMB sensitivity. The exchange of the 2010 DEM (Sect. 3.3) with the NPI 1990 DEM results in ~~mean~~ relative thickness and ice-volume ~~reduction~~ difference of less than ~~3~~1.3% (Table A1). ~~The difference reduces below 1% if all thickness measurements are used during the reconstruction. Moreover, the reduction in maximum thickness values is comparably larger with more than 10%. This latter reduction is symptomatic for an overall less variable thickness field~~ Maximum thickness values increase slightly. The new thickness field is comparably smooth because the NPI DEM on VIC was computed from contour ~~lines and is therefore rather smooth. In the~~ line information. As a consequence, some pattern change in the reconstructed ice thickness map (Fig. A4)~~, there are many small changes in the pattern~~. One more prominent difference is that the lower trunk of Franklinbreen becomes more elongate and deep. Pattern differences are again more expressed in the case ~~that~~ when less thickness observations ~~were~~ are used. Locally~~relative~~ , thickness differences can become very high. Therefore, the DEM choice is ~~certainly important for inferring local thickness values. Yet relative differences in the total ice-volume estimates are small~~ important for a reliable reconstruction. However, volume differences are relatively small (<1.3%) as compared to expected mismatch values of more than 25%, if no observations were available.

C3 Negative ice flux

~~The flux correction applied during the first-step reconstruction (Sect. 2.0.3) could be considered an important bias. Note howeverthat, the correction is not added to the flux solution itself (Fig. 3) and that it does not enter the error calculations (Sect. 2.0.4). The correction is only applied when inferring ice thickness values for the purpose of avoiding~~ On VIC and THPB, the area fraction with negative ice flux is 1.2 and 3.1%, respectively. On WSB however, the flux solution over the main branch is generally very small and shows many zero transitions. Consequently, the area-fraction is higher at 4.1%. The reason is that the AMB shows no dominant source area in the upper glacier ranges. The zero transitions in ~~areas where flux values turn negative. In this way, it only affect~~ the flux solution would directly transmit into the ice thickness ~~and the viscosity parameter. For VIC, negative flux values occur on a 0.5% area fraction. For THPB and WSB , this values is more elevated with 1.5 and 4.4%, respectively. In these areas, the flux solution and the geometrically imposed flux direction cannot be reconciled. The negative values prevail despite the penalty in the cost function during the optimisation (Sect. 2.0.2). An increase of the respective multiplier in the cost function resulted only in a limited improvement on WSB and came at the expense of a more variable flux field on all geometries. Therefore we rather decided to introduce a correction term that guarantees positive flux values in the SIA equation (Eq. 7). The correction is primarily required for WSB for which magnitudes of the flux solution are very small. Anyhow, we applied it to all geometries to keep uniformity in the approach.~~ field. To avoid such transitions, we correct the flux as follows:

$$F^\star = (1-\kappa)\cdot\|F\| + \kappa \cdot F_{\text{crit}}, \qquad \text{with} \qquad \kappa = 1 - 2/\pi \cdot \text{atan}(F^2/F_{\text{crit}}^2) \tag{C1}$$

The exact functional dependence for κ is not decisive but the choice has to assure a smooth transition. F_{crit} is set to 10% of the average flux magnitude over the domain. This value proved reasonable for the WSB setup. For smaller values, the flux field in the vicinity of negative values is less and less affected resulting in a more abrupt transition. Along the lateral land-terminating domain margin, we keep $F = F^\star = 0$. When thickness measurements are available, the effect of this flux correction on the inferred thickness is compensated by the calculation of the ice-viscosity. Without measurements and for $F > F_{\text{crit}}$, the functional dependence implies that the reduction effect on the inferred thickness field remains below 2%. Where flux magnitudes exceed the domain average ($10 \cdot F_{\text{crit}}$), the effect on the ice thickness falls below 0.15%. For $F < F_{\text{crit}}$, thickness values are effectively increased. ~~Here, we want to present the thickness solution in the case that no flux correction is applied (Fig. A5). For VIC and THPB, differences in the thickness maps are spatially very confined and thus difficult to discern.~~

The flux correction applied during the first-step reconstruction (Sect. 2.0.3) could be considered an important bias. Note however that the correction is not added to the flux solution itself (Fig. 3) and that it does not enter the error calculations (Sect. 2.0.4). The correction is only applied when inferring ice thickness values for the purpose of avoiding zero transitions in areas where flux values turn negative. In this way, it only affects the ice thickness and the viscosity parameter. Where negative values occur, the flux solution and the geometrically imposed flux direction cannot be reconciled. The negative values prevail despite the penalty in the cost function during the optimisation (Sect. 2.0.2). An increase of the respective multiplier in the cost function resulted only in a limited improvement on WSB and came at the expense of a more variable flux field on all geometries. Therefore we rather decided to introduce a correction term that guarantees positive flux values in the SIA equation (Eq. 7).

Table A1. Reconstruction sensitivity as quantified by the mean and maximum ice thickness, the ice volume and the area fraction grounded below sea-level. The ‡-symbol separates values stemming from a reconstruction using either all or only a 1% fraction of the available thickness measurements.

setting	glacier geometry abbr.	mean thickness thickness [m]	maximum thickness thickness [m]	ice volume [km^3]	b
reference	VIC	~~226.0~~ 228.3 ‡ ~~215.8~~ 229.6	~~452.6~~ 448.5 ‡ ~~461.3~~ 452.7	~~534.7~~ 540.2 ‡ ~~510.6~~ 543.3	~~12.4~~ 1
	THPB	~~182.0~~ 175.7 ‡ ~~129.2~~ 145.3	~~642.8~~ 611.1 ‡ ~~564.9~~ 563.6	~~55.5~~ 53.5 ‡ ~~39.4~~ 44.3	~~14.4~~ 1
	WSB	~~109.2~~ 112.1 ‡ ~~108.0~~ 100.3	~~378.3~~ 279.0 ‡ ~~301.9~~ 210.8	~~2.92~~ 3.00 ‡ ~~2.89~~ 2.68	~~0.27~~ 0.
WRF-SMB	VIC	~~222.0~~ 224.8 ‡ ~~210.4~~ 218.0	~~467.2~~ 467.0 ‡ ~~454.4~~ 424.7	~~525.2~~ 531.9 ‡ ~~497.9~~ 515.9	~~10.7~~ 1
NPI ~~50m~~ 50 m DEM	VIC	~~224.0~~ 225.5 ‡ ~~211.1~~ 230.5	~~425.2~~ 451.0 ‡ ~~413.7~~ 475.7	~~530.1~~ 533.6 ‡ ~~499.4~~ 545.5	~~12.2~~ 1
no flux correction	VIC	226.1 ‡ ~~215.2~~ 223.2	~~490.6~~ 451.6 ‡ ~~582.0~~ 440.2	534.9 ‡ ~~509.1~~ 528.1	~~12.5~~ 1
	THPB	~~180.8~~ 166.4 ‡ ~~126.2~~ 125.6	~~664.0~~ 614.1 ‡ ~~598.7~~ 567.1	~~55.1~~ 50.7 ‡ ~~38.5~~ 38.3	~~14.6~~ 1
	WSB	~~109.7~~ 106.0 ‡ ~~116.5~~ 87.76	~~408.3~~ 282.2 ‡ ~~385.8~~ 210.8	~~2.94~~ 2.84 ‡ ~~3.12~~ 2.35	~~1.45~~ 0.

The correction is primarily required for WSB, for which magnitudes of the flux solution are very small. Anyhow, we applied it to all geometries to keep a uniformity approach. The first-step thickness solution is most sensitive to the flux correction in small areas along divides and ridges (Fig. A5). For VIC, streak features with small thickness values appear for instance on Braggebreen (in the southwest) ~~. A similar feature is seen on Hansbreen just north of the confluence with Staszelbreen.~~ and northeast of Bodleybreen. Similar features are difficult to discern for THPB. More prominent are the effects on WSB. There, a noise pattern of near-zero values appears ~~on~~ for the thickness field of the main trunk where flux values are small (Fig. 3). The bogus noise pattern is not acceptable as we expect that the thickness field shows more gradual changes. For ~~VIC, changes~~ all test geometries, differences in mean ice thickness and ice volume ~~remain below 1~~reach 5% (Table A1)~~. This also holds for all test geometries~~ , when all available thickness measurements ~~were used during the first-step reconstruction~~are considered. Using only 1% of the thickness measurements, relative differences increase to ~~2.5% on THPB and 7.9~~5% on VIC, 14%on THPB and 13.0% on WSB. ~~For THPB, a reduction of ice volume is found without flux correction while thicker ice is predicted for WSB. A welcome side-effect of~~ In all cases the flux correction ~~is a general decrease in the maximum thicknessvalues which also appear in stagnant areas. Ice thickness for VIC (a,c) and THPB/WSB (b,d) as in Fig. 4. Here, the first-step flux solution is not corrected to avoid negative flux values in the SIA-equation used to infer the ice thickness (Sect. 2.0.3). For WSB, you see that many patches appear with very small thickness values. These bogus variations are a consequence of zero transitions in the flux field. For VIC and THPB such bogus variations are limited to some few small areas.~~results in a reduction of the mean ice thickness.

In summary, the effect of the flux correction can lead to a considerable difference in ice volume in the case that no thickness measurements are available and that small flux values prevail over a large area. Yet, ~~the correction results not necessarily in an increase of ice volume because of possible compensating changes in the ice-viscosity parameter . In addition, the effect of this~~ where measurements are available, a compensation is possible via the ice viscosity parameter B. The effect of the flux correction is expected to be ~~large~~ largest for stagnating glaciers whereas for dynamically active glaciers, consequences will be negligible. The ice-flux field gives an indication on if consequences are expected to be large and where they will be most expressed. In any case, the error-estimate map will highlight areas ~~in which this correction is~~ where the correction is most important. For the main trunk of WSB, error estimates exceed by far the inferred thickness values (Fig. ~~7~~6b).

Author contributions. J.J.F. designed and implemented the reconstruction approach, applied it to the test cases and elaborated the details of the error estimation. The research aims and setup was developed in regular discussion with F.G.-C., T.S., B.S. and M.B. J.J.F. led the writing of the manuscript, in which he received support from all authors. F.G.-C. developed and provided the initial version of the optimisation routines. Input fields for the reconstruction are Sentinel-1 surface velocities from T.S., ice thickness measurements from T.J.B., J.A.D., R.P., F.N. and M.G., DEMs from C.N. and B.S., surface elevation changes from C.N. and G.M., and surface mass balance fields from X.F.,C.L. and K.A.

Competing interests. The authors declare that they have no conflict of interest.

Acknowledgements. This study received primary funding from the German Research Foundation (DFG) within the Svalbard - iFLOWbed project, grant number FU1032/1-1. Results presented in this publication are based on numerical simulations conducted at the high performance computing centre of the "Regionales Rechenzentrum Erlangen" (RRZE) of the University of Erlangen-Nuremberg. The reconstruction approach also benefits from co-development work of the Elmer/Ice team at the CSC-IT Center for Science Ltd (Finland). The velocity analysis on Svalbard was funded by DFG within the priority programme 1158 Antarctic Research under contract number BR2105/9-1 and received financial support from the Helmholtz Association of the German Research Centres (HGF) Alliance on Remote Sensing and Earth System Dynamics.Thickness data collection in Wedel Jarlsberg Land was funded by the Spanish R&D projects C11093001 and C150954001, the NCBiR/PolarCLIMATE-2009/2-2/2010 from the Polish National Centre for R&D, by the IPY/269/2006 from the Polish Ministry of Science and Higher Education, by Polish-Norwegian funding through the AWAKE (PNRF-22-AI-1/07) project, by the EU FP7 ice2sea programme (grant number 226375) and by funds of the Leading National Research Centre (KNOW) received by the Centre for Polar Studies of the University of Silesia, Poland. The DEM generation in Wedel Jarlsberg Land received financial support from the European Union/ERC (grant 320816) and from ESA (project Glaciers CCI, 4000109873/14/I-NB). TanDEM-X data was provided under AO XTIGLAC6770. The WRF-SMB field was produced within the PERMANOR project funded by the Norwegian Research Council (255331).

~~urlstyle~~

~~Aas, K., Dunse, T., Collier, E., Schuler, T., Berntsen, T., Kohler, J., and Luks, B.: The climatic mass balance of Svalbard glaciers: a 10-year simulation with a coupled atmosphere–glacier mass balance model, The Cryosphere, 10, 1089–1104, , 2016.~~

Atwood, D. K., Meyer, F., and Arendt, A.: Using L-band SAR coherence to delineate glacier extent, Canadian Journal of Remote Sensing, 36, S186–S195, , 2010.

Bishop, M., Olsenholler, J., Shroder, J., Barry, R., Raup, B., Bush, A., Copland, L., Dwyer, J., Fountain, A., Haeberli, W., Kääb, A., Paul, F., Hall, D., Kargel, J., Molnia, B., Trabant, D., and Wessels, R.: Global Land Ice Measurements from Space (GLIMS): Remote Sensing and GIS Investigations of the Earth's Cryosphere, Geocarto International, 19, 57–84, , 2004.

Błaszczyk, M., Jania, J., and Hagen, J.: Tidewater glaciers of Svalbard: Recent changes and estimates of calving fluxes, Polish Polar Research, 30, 85–142, 2009.

Błaszczyk, M., Jania, J., and Kolondra, L.: Fluctuations of tidewater glaciers in Hornsund Fjord (Southern Svalbard) since the beginning of the 20th century, Polish Polar Research, 34, 327–352, , 2013.

Braun, M., Pohjola, V., Pettersson, R., Möller, M., Finkelnburg, R., Falk, U., Scherer, D., and Schneider, C.: Changes of glacier frontal positions of Vestfonna (Nordaustlandet, Svalbard), Geografiska Annaler: Series A, Physical Geography, 93, 301–310, , 2011.

Brinkerhoff, D. J., Aschwanden, A., and Truffer, M.: Bayesian Inference of Subglacial Topography Using Mass Conservation, Frontiers in Earth Science, 4, 8, , 2016.

Brooks, A. and Hughes, T.: Streamline upwind/Petrov-Galerkin formulations for convection dominated flows with particular emphasis on the incompressible Navier-Stokes equations, Computer Methods in Applied Mechanics and Engineering", 32, 199 – 259, , 1982.

Carrivick, J., Davies, B., James, W., Quincey, D., and Glasser, N.: Distributed ice thickness and glacier volume in southern South America, Global and Planetary Change, 146, 122–132, , 2016.

Clarke, G., Berthier, E., Schoof, C., and Jarosch, A.: Neural Networks Applied to Estimating Subglacial Topography and Glacier Volume, Journal of Climate, 22, 2146–2160, , 2009.

Clarke, G., Anslow, F., Jarosch, A., Radi, V., Menounos, B., Bolch, T., and Berthier, E.: Ice Volume and Subglacial Topography for Western Canadian Glaciers from Mass Balance Fields, Thinning Rates, and a Bed Stress Model, Journal of Climate, 26, 4282–4303, , 2013.

Cuffey, K. and Paterson, W.: The Physics of Glaciers, Butterworth-Heinemann publications, Elsevier, 2010.

Dowdeswell, J.: Drainage-basin characteristics of Nordaustlandet ice caps, Svalbard, Journal of Glaciology, 32, 31–38, 1986a.

Dowdeswell, J.: Remote sensing of ice cap outlet glacier fluctuations on Nordaustlandet, Svalbard, Polar Research, 4, 25–32, 1986b.

Dowdeswell, J.: On the nature of Svalbard icebergs, Journal of Glaciology, 35, 224–234, 1989.

Dowdeswell, J. and Collin, R.: Fast-flowing outlet glaciers on Svalbard ice caps, Geology, 18, 778–781, 1990.

Dowdeswell, J., Drewry, D., Cooper, A., and Gorman, M.: Digital mapping of the Nordaustlandet ice caps from airborne geophysical investigations, Annals of Glaciology, 8, 51–58, , 1986.

Fahnestock, M., Scambos, T., Moon, T., Gardner, A., Haran, T., and Klinger, M.: Rapid large-area mapping of ice flow using Landsat 8, Remote Sensing of Environment, 185, 84–94, , 2016.

Fan, Q., Efrat, A., Koltun, V., Krishnan, S., and Venkatasubramanian, S.: Hardware-assisted Natural Neighbor Interpolation, In Proc. 7th Workshop on Algorithm Engineering and Experiments (ALENEX), 2005.

Farinotti, D., Huss, M., Bauder, A., and Funk, M.: An estimate of the glacier ice volume in the Swiss Alps, Global and Planetary Change, 68, 225–231, , 2009.

Farinotti, D., Huss, M., Bauder, A., Funk, M., and Truffer, M.: A method to estimate the ice volume and ice-thickness distribution of alpine glaciers, Journal of Glaciology, 55, 422–430, , 2009.

Farinotti, D., Brinkerhoff, D., Clarke, G., Fürst, J., Frey, H., Gantayat, P., Gillet-Chaulet, F., Girard, C., Huss, M., Leclercq, P., Linsbauer, A., Machguth, H., Martin, C., Maussion, F., Morlighem, M., Mosbeux, C., Pandit, A., Portmann, A., Rabatel, A., Ramsankaran, R., Reerink,

T., Sanchez, O., Stentoft, P., Singh Kumari, S., van Pelt, W., Anderson, B., Benham, T., Binder, D., Dowdeswell, J., Fischer, A., Helfricht, K., Kutuzov, S., Lavrentiev, I., McNabb, R., Gudmundsson, G., Li, H., and Andreassen, L.: How accurate are estimates of glacier ice thickness? Results from ITMIX, the Ice Thickness Models Intercomparison eXperiment, The Cryosphere Discussions, 2016, 1–34, , 2016.

Farr, T., Rosen, P., Caro, E., Crippen, R., Duren, R., Hensley, S., Kobrick, M., Paller, M., Rodriguez, E., Roth, L., Seal, D., Shaffer, S., Shimada, J., Umland, J., Werner, M., Oskin, M., Burbank, D., and Alsdorf, D.: The Shuttle Radar Topography Mission, Reviews of Geophysics, 45, , 2007.

Favier, L., Durand, G., Cornford, S., Gudmundsson, G., Gagliardini, O., Gillet-Chaulet, F., Zwinger, T., Payne, J., and LeBroeq, A.: Retreat of Pine Island Glacier controlled by marine ice-sheet instability, Nature Climate Change, 4, 117–121, , 2014.

Franco, B., Fettweis, X., Lang, C., and Erpicum, M.: Impact of spatial resolution on the modelling of the Greenland ice sheet surface mass balance between 1990–2010, using the regional climate model MAR, The Cryosphere, 6, 695–711, , 2012.

Frey, H., Machguth, H., Huss, M., Huggel, C., Bajracharya, S., Bolch, T., Kulkarni, A., Linsbauer, A., Salzmann, N., and Stoffel, M.: Estimating the volume of glaciers in the Himalayan-Karakoram region using different methods, The Cryosphere, 8, 2313–2333, , 2014.

Fürst, J., Durand, G., Gillet-Chaulet, F., Tavard, L., Rankl, M., Braun, M., and Gagliardini, O.: The safety band of Antarctic ice shelves, Nature Climate Change, 6, 479–482, , 2016.

Gantayat, P., Kulkarni, A., and Srinivasan, J.: Estimation of ice thickness using surface velocities and slope: case study at Gangotri Glacier, India, Journal of Glaciology, 60, 277–282, , 2014.

Gärtner-Roer, I., Andreassen, L., Bjerre, E., Farinotti, D., Fischer, A., Fischer, M., Helfricht, K., Huss, M., Knecht, T., Landmann, S. K. J., Li, I. L. H., Li, Z., Machguth, H., Naegeli, K., Navarro, F., Rabatel, A., Stentoft, P., and Zemp (eds.), M.: WGMS (2016): Glacier Thickness Database 2.0., World Glacier Monitoring Service, Zurich, Switzerland, , 2016.

Geuzaine, C. and Remacle, J.: Gmsh: a three-dimensional finite element mesh generator with built-in pre- and post-processing facilities, International Journal for Numerical Methods in Engineering, 79, 1309–1331, 2009.

Gilbert, J. and Lemaréchal, C.: Some numerical experiments with variable-storage quasi-Newton algorithms, Mathematical Programming, 45, 407–435, 1989.

Grabiec, M., Jania, J., Puczko, D., Kolondra, L., and Budzik, T.: Surface and bed morphology of Hansbreen, a tidewater glacier in Spitsbergen, Polish Polar Research, 33, 111–138, , 2012.

Huss, M. and Farinotti, D.: Distributed ice thickness and volume of all glaciers around the globe, Journal of Geophysical Research, 117, 10 pp., , 2012.

Huss, M. and Hock, R.: A new model for global glacier change and sea-level rise, Frontiers of Earth Science, 3, 1261–1273, , 2015.

Hutter, K.: Theoretical glaciology. Material science of ice and the mechanics of glaciers and ice sheets, Publishing Company/Tokyo, Terra Scientific Publishing Company, Dordrecht, Boston, Tokyo, Japan, and Hingham, 1983.

Ignatiuk, D., Piechota, A., Cieply, M., and Luks, B.: Changes of altitudinal zones of Werenskioldbreen and Hansbreen in period 1990-2008, Svalbard, AIP Conference Proceedings, 1618, 275–280, , 2014.

Jakobsson, M., Mayer, L., Coakley, B., Dowdeswell, J., Forbes, S., Fridman, B., Hodnesdal, H., Noormets, R., Pedersen, R., Rebesco, M., Schenke, H., Zarayskaya, Y., Accettella, D., Armstrong, A., Anderson, R., Bienhoff, P., Camerlenghi, A., Church, I., Edwards, M., Gardner, J., Hall, J., Hell, B., Hestvik, O., Kristoffersen, Y., Marcussen, C., Mohammad, R., Mosher, D., Nghiem, S., Pedrosa, M., Travaglini, P., and Weatherall, P.: The International Bathymetric Chart of the Arctic Ocean (IBCAO) Version 3.0, Geophysical Research Letters, 39, , L12609, 2012.

Jania, J., Mochnacki, D., and Gdek, B.: The thermal structure of Hansbreen, a tidewater glacier in southern Spitsbergen, Svalbard, Polar Research, 15, 53–66, 1996.

Joughin, I., Smith, B., Howat, I., Scambos, T., and Moon, T.: Greenland flow variability from ice-sheet-wide velocity mapping, Journal of Glaciology, 56, 415–430, , 2010.

Korona, J., Berthier, E., Bernard, M., Rémy, F., and Thouvenot, E.: SPIRIT. {SPOT} 5 stereoscopic survey of Polar Ice: Reference Images and Topographies during the fourth International Polar Year (2007-2009) , {ISPRS} Journal of Photogrammetry and Remote Sensing, 64, 204 – 212, , 2009.

Krieger, G., Zink, M., Bachmann, M., Bräutigam, B., Schulze, D., Martone, M., Rizzoli, P., Steinbrecher, U., Walter Antony, J., De Zan, F., Hajnsek, I., Papathanassiou, K., Kugler, F., Rodriguez Cassola, M., Younis, M., Baumgartner, S., López-Dekker, P., Prats, P., and Moreira, A.: TanDEM-X: A radar interferometer with two formation-flying satellites, Acta Astronautica, 89, 83–89, , 2013.

Lang, C., Fettweis, X., and Erpicum, M.: Future climate and surface mass balance of Svalbard glaciers in an RCP8.5 climate scenario: a study with the regional climate model MAR forced by MIROC5, The Cryosphere, 9, 945–956, , 2015.

Lapazaran, J., Otero, J., Martn-Espaol, A., and Navarro, F.: On the errors involved in ice-thickness estimates I: ground-penetrating radar measurement errors, Journal of Glaciology, 62, 1008–1020, , 2016.

Linsbauer, A., Paul, F., and Haeberli, W.: Modeling glacier thickness distribution and bed topography over entire mountain ranges with GlabTop: Application of a fast and robust approach, Journal of Geophysical Research, 117, n/a–n/a, , F03007, 2012.

Marzeion, B., Jarosch, A., and Hofer, M.: Past and future sea-level change from the surface mass balance of glaciers, The Cryosphere, 6, 1295–1322, , 2012.

Marzeion, B., Cogley, J., Richter, K., and Parkes, D.: Attribution of global glacier mass loss to anthropogenic and natural causes, Science, 345, 919–921, , 2014.

McNabb, R., Hock, R., O'Neel, S., Rasmussen, L., Ahn, Y., Braun, M., Conway, H., Herreid, S., Joughin, I., Pfeffer, W., Smith, B., and Truffer, M.: Using surface velocities to calculate ice thickness and bed topography: a case study at Columbia Glacier, Alaska, USA, Journal of Glaciology, 58, 1151–1164, 2012.

Moholdt, G., Nuth, C., Hagen, J., and Kohler, J.: Recent elevation changes of Svalbard glaciers derived from {ICESat} laser altimetry, Remote Sensing of Environment, 114, 2756–2767, , 2010.

Möller, M., Obleitner, F., Reijmer, C., Pohjola, V., Głowacki, P., and Kohler, J.: Adjustment of regional climate model output for modeling the climatic mass balance of all glaciers on Svalbard, Journal of Geophysical Research: Atmospheres, 121, 5411–5429, , 2016.

Morland, L.: Unconfined ice-shelf flow, in: Dynamics of the West Antarctic ice sheet, Kluwer Academic Publishers, 1986.

Morlighem, M., Rignot, E., H. Seroussi, H., Larour, E., Ben Dhia, H., and Aubry, D.: A mass conservation approach for mapping glacier ice thickness, Geophysical Research Letters, 38, , 2011.

Morlighem, M., Rignot, E., Mouginot, J., Seroussi, H., and Larour, E.: Deeply incised submarine glacial valleys beneath the Greenland ice sheet, Nature Geoscience, 7, 418–422, , 2014.

Mosbeux, C., Gillet-Chaulet, F., and Gagliardini, O.: Comparison of adjoint and nudging methods to initialise ice sheet model basal conditions, Geoscientific Model Development, 9, 2549–2562, , 2016.

Navarro, F., Martn-Espaol, A., Lapazaran, J., Grabiec, M., Otero, J., Vasilenko, E., and Puczko, D.: Ice Volume Estimates from Ground-Penetrating Radar Surveys, Wedel Jarlsberg Land Glaciers, Svalbard, Arctic, Antarctic, and Alpine Research, 46, 394–406, , 2014.

Nuth, C. and Kääb, A.: Co-registration and bias corrections of satellite elevation data sets for quantifying glacier thickness change, The Cryosphere, 5, 271–290, , 2011.

Nuth, C., Kohler, J., König, M., von Deschwanden, A., Hagen, J., Kääb, A., Moholdt, G., and Pettersson, R.: Decadal changes from a multi-temporal glacier inventory of Svalbard, The Cryosphere, 7, 1603–1621, , 2013.

Ottesen, D., Dowdeswell, J., Landvik, J., and Mienert, J.: .

Paolo, F., Fricker, H., and Padman, L.: Volume loss from Antarctic ice shelves is accelerating, Science, , 2015.

Paul, F., Bolch, T., Kääb, A., Nagler, T., Nuth, C., Scharrer, K., Shepherd, A., Strozzi, T., Ticconi, F., Bhambri, R., Berthier, E., Bevan, S., Gourmelen, N., Heid, T., Jeong, S., Kunz, M., L., T. R., Luckman, A., Merryman Boncori, J., Moholdt, G., Muir, A., Neelmeijer, J., Rankl, M., VanLooy, J., and Van Niel, T.: The glaciers climate change initiative: Methods for creating glacier area, elevation change and velocity products, Remote Sensing of Environment, 162, 408–426, 2015.

Pettersson, R., Christoffersen, P., Dowdeswell, J., Pohjola, V., Hubbard, A., and Strozzi, T.: Ice thickness and basal conditions of Vestfonna Ice Cap, Eastern Svalbard, Geografiska Annaler: Series A, Physical Geography, 93, 311–322, , 2011.

Pinglot, J., Pourchet, M., Lefauconnier, B., Hagen, J., Isaksson, E., Vaikmae, R., and Kamiyama, K.: Accumulation in Svalbard glaciers deduced from ice cores with nuclear tests and Chernobyl reference layers, Polar Research, 18, 315–321, , 1999.

Pinglot, J., Hagen, J., Melvold, K., Eiken, T., and Vincent, C.: A mean net accumulation pattern derived from radioactive layers and radar soundings on Austfonna, Nordaustlandet, Svalbard, Journal of Glaciology, 47, 555–566, , 2001.

Pohjola, V., Christoffersen, P., Kolondra, L., Moore, J., Pettersson, R., Schäfer, M., Strozzi, T., and Reijmer, C.: Spatial distribution and change in the surface-velocity field of Vestfonna ice cap, Nordaustlandet, Svalbard, 1995-2010 using geodetic and satellite interferometry data, Geografiska Annaler: Series A, Physical Geography, 93, 323–335, , 2011.

Radi, V. and Hock, R.: Regionally differentiated contribution of mountain glaciers and ice caps to future sea-level rise, Nature Geoscience, 4, 91–94, , 2011.

Radi, V., Bliss, A., Beedlow, A., Hock, R., and Cogley, E. M. J.: Regional and global projections of twenty-first century glacier mass changes in response to climate scenarios from global climate models, Climate Dynamics, 42, 37–58, , 2014.

Rankl, M. and Braun, M.: Glacier elevation and mass changes over the central Karakoram region estimated from TanDEM-X and SRTM/X-SAR digital elevation models, Annals of Glaciology, 51, 273–281, , 2016.

Rankl, M., Kienholz, C., and Braun, M.: Glacier changes in the Karakoram region mapped by multimission satellite imagery, The Cryosphere, 8, 977–989, „ 2014.

Rignot, E. and Mouginot, J.: Ice flow in Greenland for the International Polar Year 2008-2009, Geophysical Research Letters, 39, 7 pp., , 2012.

Rignot, E., Mouginot, J., and Scheuchl, B.: Ice Flow of the Antarctic Ice Sheet, Science, 333, 1427–1430, , 2011.

Rosenau, R., Scheinert, M., and Dietrich, R.: A processing system to monitor Greenland outlet glacier velocity variations at decadal and seasonal time scales utilizing the Landsat imagery, Remote Sensing of Environment, 169, 1–19, , 2015.

Schäfer, M., Zwinger, T., Christoffersen, P., Gillet-Chaulet, F., Laakso, K., Pettersson, R., Pohjola, V., Strozzi, T., and Moore, J.: Sensitivity of basal conditions in an inverse model: Vestfonna ice cap, Nordaustlandet/Svalbard, The Cryosphere, 6, 771–783, „ 2012.

Schoof, C.: Ice sheet grounding line dynamics: Steady states, stability, and hysteresis, Journal of Geophysical Research, 112, 19 pp., , 2007.

Schoof, C.: Ice-sheet acceleration driven by melt supply variability, Nature, 468, 803–806, , 2010.

Schutz, B., Zwally, H., Shuman, C., Hancock, D., and DiMarzio, J.: Overview of the ICESat Mission, Geophysical Research Letters, 32, , 2005.

Schwaizer, G.: Performance assessment of the glacier ice velocity products for Greenland, and description of the evaluation methodology. In: Glaciers validation report, Issue 1.0, 2016.

Seehaus, T., Marinsek, S., Helm, V., Skvarca, P., and Braun, M.: Changes in ice dynamics, elevation and mass discharge of Dinsmoor-Bombardier-Edgew
glacier system, Antarctic Peninsula, Earth and Planetary Science Letters, 427, 125–135, 2015.

Seehaus, T., Marinsek, S., Skvarca, P., van Wessem, J., Reijmer, C., Seco, J., and Braun, M.: Dynamic Response of Sjögren Inlet Glaciers, Antarctic Peninsula, to Ice Shelf Breakup Derived from Multi-Mission Remote Sensing Time Series, Frontiers in Earth Science, 4, 66, , 2016.

Strozzi, T., Luckman, A., Murray, T., Wegmüller, U., and Werner, C. L.: Glacier motion estimation using SAR offset-tracking procedures, IEEE Transactions on Geoscience and Remote Sensing, 40, 2384–2391, , 2002.

Tachikawa, T., Hato, M., Kaku, M., and Iwasaki, A.: The characteristics of ASTER GDEM version 2, International Geoscience and Remote Sensing Symposium Proceedings, 2011.

van Pelt, W., Oerlemans, J., Reijmer, C., Pettersson, R., Pohjola, V., Isaksson, E., and D.Divine: An iterative inverse method to estimate basal topography and initialize ice flow models, The Cryosphere, 7, 987–1006, , 2013.

Vijay, S. and Braun, M.: Elevation Change Rates of Glaciers in the Lahaul-Spiti (Western Himalaya, India) during 2000-2012 and 2012-2013, Remote Sensing, 8, , 2016.

Zwally, H., Li, J., Robbins, J., Saba, J., Yi, D., and Brenner, A.: Mass gains of the Antarctic ice sheet exceed losses, Journal of Glaciology, 61, 1019–1036, , 2015.

Zwally, H., Li, J., Brenner, A., Beckley, M., Cornejo, H., Dimarzio, J., Giovinetto, M., Neumann, T., Robbins, J., Saba, J., Yi, D., and Wang, W.: Greenland ice sheet mass balance: distribution of increased mass loss with climate warming; 2003-07 versus 1992-2002, Journal of Glaciology, 57, 88–102, , 2011.

References

Aas, K., Dunse, T., Collier, E., Schuler, T., Berntsen, T., Kohler, J., and Luks, B.: The climatic mass balance of Svalbard glaciers: a 10-year simulation with a coupled atmosphere–glacier mass balance model, The Cryosphere, 10, 1089–1104, doi:10.5194/tc-10-1089-2016, 2016.

Atwood, D. K., Meyer, F., and Arendt, A.: Using L-band SAR coherence to delineate glacier extent, Canadian Journal of Remote Sensing, 36, S186–S195, doi:10.5589/m10-014, http://dx.doi.org/10.5589/m10-014, 2010.

Berthier, E., Cabot, V., Vincent, C., and Six, D.: Decadal Region-Wide and Glacier-Wide Mass Balances Derived from Multi-Temporal ASTER Satellite Digital Elevation Models. Validation over the Mont-Blanc Area, Frontiers in Earth Science, 4, 63, doi:10.3389/feart.2016.00063, http://journal.frontiersin.org/article/10.3389/feart.2016.00063, 2016.

Berthier, E., Schiefer, E., Clarke, G., and Menounos, B.: Contribution of Alaskan glaciers to sea-level rise derived from satellite imagery, Nature Geoscience, 3, 92–95, doi:10.1038/ngeo737, http://www.nature.com/ngeo/journal/v3/n2/suppinfo/ngeo737_S1.html, 2010.

Bishop, M., Olsenholler, J., Shroder, J., Barry, R., Raup, B., Bush, A., Copland, L., Dwyer, J., Fountain, A., Haeberli, W., Kääb, A., Paul, F., Hall, D., Kargel, J., Molnia, B., Trabant, D., and Wessels, R.: Global Land Ice Measurements from Space (GLIMS): Remote Sensing and GIS Investigations of the Earth's Cryosphere, Geocarto International, 19, 57–84, doi:10.1080/10106040408542307, http://dx.doi.org/10.1080/10106040408542307, 2004.

Błaszczyk, M., Jania, J., and Hagen, J.: Tidewater glaciers of Svalbard: Recent changes and estimates of calving fluxes, Polish Polar Research, 30, 85–142, 2009.

Błaszczyk, M., Jania, J., and Kolondra, L.: Fluctuations of tidewater glaciers in Hornsund Fjord (Southern Svalbard) since the beginning of the 20th century, Polish Polar Research, 34, 327–352, doi:10.2478/popore?2013?0024, 2013.

Braun, M., Pohjola, V., Pettersson, R., Möller, M., Finkelnburg, R., Falk, U., Scherer, D., and Schneider, C.: Changes of glacier frontal positions of Vestfonna (Nordaustlandet, Svalbard), Geografiska Annaler: Series A, Physical Geography, 93, 301–310, doi:10.1111/j.1468-0459.2011.00437.x, http://dx.doi.org/10.1111/j.1468-0459.2011.00437.x, 2011.

Brinkerhoff, D. and Johnson, J.: A stabilized finite element method for calculating balance velocities in ice sheets, Geoscientific Model Development, 8, 1275–1283, doi:10.5194/gmd-8-1275-2015, http://www.geosci-model-dev.net/8/1275/2015/, 2015.

Brinkerhoff, D. J., Aschwanden, A., and Truffer, M.: Bayesian Inference of Subglacial Topography Using Mass Conservation, Frontiers in Earth Science, 4, 8, doi:10.3389/feart.2016.00008, http://journal.frontiersin.org/article/10.3389/feart.2016.00008, 2016.

Brooks, A. and Hughes, T.: Streamline upwind/Petrov-Galerkin formulations for convection dominated flows with particular emphasis on the incompressible Navier-Stokes equations, Computer Methods in Applied Mechanics and Engineering", 32, 199 – 259, doi:http://dx.doi.org/10.1016/0045-7825(82)90071-8, http://www.sciencedirect.com/science/article/pii/0045782582900718, 1982.

Carrivick, J., Davies, B., James, W., Quincey, D., and Glasser, N.: Distributed ice thickness and glacier volume in southern South America, Global and Planetary Change, 146, 122–132, doi:http://dx.doi.org/10.1016/j.gloplacha.2016.09.010, http://www.sciencedirect.com/science/article/pii/S0921818116301515, 2016.

Clarke, G., Berthier, E., Schoof, C., and Jarosch, A.: Neural Networks Applied to Estimating Subglacial Topography and Glacier Volume, Journal of Climate, 22, 2146–2160, doi:10.1175/2008JCLI2572.1, http://dx.doi.org/10.1175/2008JCLI2572.1, 2009.

Clarke, G., Anslow, F., Jarosch, A., Radić, V., Menounos, B., Bolch, T., and Berthier, E.: Ice Volume and Subglacial Topography for Western Canadian Glaciers from Mass Balance Fields, Thinning Rates, and a Bed Stress Model, Journal of Climate, 26, 4282–4303, doi:10.1175/JCLI-D-12-00513.1, http://dx.doi.org/10.1175/JCLI-D-12-00513.1, 2013.

Cuffey, K. and Paterson, W.: The Physics of Glaciers, Butterworth-Heinemann publications, Elsevier, 2010.

Dowdeswell, J.: Drainage-basin characteristics of Nordaustlandet ice caps, Svalbard, Journal of Glaciology, 32, 31–38, 1986a.

Dowdeswell, J.: Remote sensing of ice cap outlet glacier fluctuations on Nordaustlandet, Svalbard, Polar Research, 4, 25–32, 1986b.

Dowdeswell, J.: On the nature of Svalbard icebergs, Journal of Glaciology, 35, 224–234, 1989.

Dowdeswell, J. and Collin, R.: Fast-flowing outlet glaciers on Svalbard ice caps, Geology, 18, 778–781, 1990.

Dowdeswell, J., Drewry, D., Cooper, A., and Gorman, M.: Digital mapping of the Nordaustlandet ice caps from airborne geophysical investigations, Annals of Glaciology, 8, 51–58, doi:10.1175/2010JCLI3656.1, 1986.

Fahnestock, M., Scambos, T., Moon, T., Gardner, A., Haran, T., and Klinger, M.: Rapid large-area mapping of ice flow using Landsat 8, Remote Sensing of Environment, 185, 84–94, doi:http://dx.doi.org/10.1016/j.rse.2015.11.023, http://www.sciencedirect.com/science/article/pii/S003442571530211X, 2016.

Fan, Q., Efrat, A., Koltun, V., Krishnan, S., and Venkatasubramanian, S.: Hardware-assisted Natural Neighbor Interpolation, In Proc. 7th Workshop on Algorithm Engineering and Experiments (ALENEX), 2005.

Farinotti, D., Huss, M., Bauder, A., and Funk, M.: An estimate of the glacier ice volume in the Swiss Alps, Global and Planetary Change, 68, 225–231, doi:10.1016/j.gloplacha.2009.05.004, 2009a.

Farinotti, D., Huss, M., Bauder, A., Funk, M., and Truffer, M.: A method to estimate the ice volume and ice-thickness distribution of alpine glaciers, Journal of Glaciology, 55, 422–430, doi:10.3189/002214309788816759, 2009b.

Farinotti, D., Brinkerhoff, D., Clarke, G., Fürst, J., Frey, H., Gantayat, P., Gillet-Chaulet, F., Girard, C., Huss, M., Leclercq, P., Linsbauer, A., Machguth, H., Martin, C., Maussion, F., Morlighem, M., Mosbeux, C., Pandit, A., Portmann, A., Rabatel, A., Ramsankaran, R., Reerink, T., Sanchez, O., Stentoft, P., Singh Kumari, S., van Pelt, W., Anderson, B., Benham, T., Binder, D., Dowdeswell, J., Fischer, A., Helfricht, K., Kutuzov, S., Lavrentiev, I., McNabb, R., Gudmundsson, G., Li, H., and Andreassen, L.: How accurate are estimates of glacier ice thickness? Results from ITMIX, the Ice Thickness Models Intercomparison eXperiment, The Cryosphere Discussions, 2016, 1–34, doi:10.5194/tc-2016-250, http://www.the-cryosphere-discuss.net/tc-2016-250/, 2016.

Farr, T., Rosen, P., Caro, E., Crippen, R., Duren, R., Hensley, S., Kobrick, M., Paller, M., Rodriguez, E., Roth, L., Seal, D., Shaffer, S., Shimada, J., Umland, J., Werner, M., Oskin, M., Burbank, D., and Alsdorf, D.: The Shuttle Radar Topography Mission, Reviews of Geophysics, 45, doi:10.1029/2005RG000183, http://dx.doi.org/10.1029/2005RG000183, 2007.

Favier, L., Durand, G., Cornford, S., Gudmundsson, G., Gagliardini, O., Gillet-Chaulet, F., Zwinger, T., Payne, J., and LeBrocq, A.: Retreat of Pine Island Glacier controlled by marine ice-sheet instability, Nature Climate Change, 4, 117–121, doi:10.1038/nclimate2094, http://dx.doi.org/10.1038/nclimate2094, 2014.

Franco, B., Fettweis, X., Lang, C., and Erpicum, M.: Impact of spatial resolution on the modelling of the Greenland ice sheet surface mass balance between 1990–2010, using the regional climate model MAR, The Cryosphere, 6, 695–711, doi:10.5194/tc-6-695-2012, 2012.

Frey, H., Machguth, H., Huss, M., Huggel, C., Bajracharya, S., Bolch, T., Kulkarni, A., Linsbauer, A., Salzmann, N., and Stoffel, M.: Estimating the volume of glaciers in the Himalayan-Karakoram region using different methods, The Cryosphere, 8, 2313–2333, doi:10.5194/tc-8-2313-2014, http://www.the-cryosphere.net/8/2313/2014/, 2014.

Fürst, J., Goelzer, H., and Huybrechts, P.: Effect of higher-order stress gradients on the centennial mass evolution of the Greenland ice sheet, The Cryosphere, 7, 183–199, doi:10.5194/tc-7-183-2013, 2013.

Fürst, J., Durand, G., Gillet-Chaulet, F., Tavard, L., Rankl, M., Braun, M., and Gagliardini, O.: The safety band of Antarctic ice shelves, Nature Climate Change, 6, 479–482, doi:10.1038/nclimate2912, 2016.

Gagliardini, O. and Zwinger, T.: The ISMIP-HOM benchmark experiments performed using the Finite-Element code Elmer, The Cryosphere, 2, 67–76, doi:10.5194/tc-2-67-2008, 2008.

Gagliardini, O., Zwinger, T., Gillet-Chaulet, F., Durand, G., Favier, L., de Fleurian, B., Greve, R., Malinen, M., Martín, C., Råback, P., Ruokolainen, J., Sacchettini, M., Schäfer, M., Seddik, H., and Thies, J.: Capabilities and performance of Elmer/Ice, a new-generation ice sheet model, Geophysical Model Development, 6, 1299–1318, doi:10.5194/gmd-6-1299-2013, 2013.

Gantayat, P., Kulkarni, A., and Srinivasan, J.: Estimation of ice thickness using surface velocities and slope: case study at Gangotri Glacier, India, Journal of Glaciology, 60, 277–282, doi:doi:10.3189/2014JoG13J078, http://www.ingentaconnect.com/content/igsoc/jog/2014/00000060/00000220/art00007, 2014.

Gardelle, J., Berthier, E., and Arnaud, Y.: Impact of resolution and radar penetration on glacier elevation changes computed from DEM differencing, Journal of Glaciology, 58, 419–422, doi:0.3189/2012JoG11J175, 2012.

Gardelle, J., Berthier, E., Arnaud, Y., and Kääb, A.: Region-wide glacier mass balances over the Pamir-Karakoram-Himalaya during 1999-2011, The Cryosphere, 7, 1263–1286, doi:10.5194/tc-7-1263-2013, http://www.the-cryosphere.net/7/1263/2013/, 2013.

Gärtner-Roer, I., Naegeli, K., Huss, M., Knecht, T., Machguth, H., and Zemp, M.: A database of worldwide glacier thickness observations, Global and Planetary Change, 122, 330 – 344, doi:10.1016/j.gloplacha.2014.09.003, http://www.sciencedirect.com/science/article/pii/S0921818114001878, 2014.

Gärtner-Roer, I., Andreassen, L., Bjerre, E., Farinotti, D., Fischer, A., Fischer, M., Helfricht, K., Huss, M., Knecht, T., Landmann, S. K. J., Li, I. L. H., Li, Z., Machguth, H., Naegeli, K., Navarro, F., Rabatel, A., Stentoft, P., and Zemp (eds.), M.: WGMS (2016): Glacier Thickness Database 2.0., World Glacier Monitoring Service, Zurich, Switzerland, doi:10.5904/wgms-glathida-2016-07, 2016.

Geuzaine, C. and Remacle, J.: Gmsh: a three-dimensional finite element mesh generator with built-in pre- and post-processing facilities, International Journal for Numerical Methods in Engineering, 79, 1309–1331, 2009.

Gilbert, J. and Lemaréchal, C.: Some numerical experiments with variable-storage quasi-Newton algorithms, Mathematical Programming, 45, 407–435, 1989.

Gillet-Chaulet, F., Gagliardini, O., Seddik, H., Nodet, M., Durand, G., Ritz, C., Zwinger, T., Greve, R., and Vaughan, D.: Greenland ice sheet contribution to sea-level rise from a new-generation ice-sheet model, The Cryosphere, 6, 1561–1576, doi:10.5194/tc-6-1561-2012, 2012.

Grabiec, M., Jania, J., Puczko, D., Kolondra, L., and Budzik, T.: Surface and bed morphology of Hansbreen, a tidewater glacier in Spitsbergen, Polish Polar Research, 33, 111–138, doi:10.2478/v10183-012-0010-7, 2012.

Hindmarsh, R.: The role of membrane-like stresses in determining the stability and sensitivity of the Antarctic ice sheets: back pressure and grounding line motion, Philosophical Transactions of the Royal Society A, 364, 1733–1767, doi:10.1098/rsta.2006.1797, 2006.

Huss, M. and Farinotti, D.: Distributed ice thickness and volume of all glaciers around the globe, Journal of Geophysical Research, 117, 10 pp., doi:10.1029/2012JF002523, 2012.

Huss, M. and Hock, R.: A new model for global glacier change and sea-level rise, Frontiers of Earth Science, 3, 1261–1273, doi:10.3389/feart.2015.00054, 2015.

Hutter, K.: Theoretical glaciology. Material science of ice and the mechanics of glaciers and ice sheets, Publishing Company/Tokyo, Terra Scientific Publishing Company, Dordrecht, Boston, Tokyo, Japan, and Hingham, 1983.

Ignatiuk, D., Piechota, A., Ciepły, M., and Luks, B.: Changes of altitudinal zones of Werenskioldbreen and Hansbreen in period 1990-2008, Svalbard, AIP Conference Proceedings, 1618, 275–280, doi:10.1063/1.4897727, 2014.

Jakobsson, M., Mayer, L., Coakley, B., Dowdeswell, J., Forbes, S., Fridman, B., Hodnesdal, H., Noormets, R., Pedersen, R., Rebesco, M., Schenke, H., Zarayskaya, Y., Accettella, D., Armstrong, A., Anderson, R., Bienhoff, P., Camerlenghi, A., Church, I., Edwards, M., Gardner, J., Hall, J., Hell, B., Hestvik, O., Kristoffersen, Y., Marcussen, C., Mohammad, R., Mosher, D., Nghiem, S., Pedrosa, M.,

Travaglini, P., and Weatherall, P.: The International Bathymetric Chart of the Arctic Ocean (IBCAO) Version 3.0, Geophysical Research Letters, 39, doi:10.1029/2012GL052219, http://dx.doi.org/10.1029/2012GL052219, l12609, 2012.

Jania, J., Mochnacki, D., and Gądek, B.: The thermal structure of Hansbreen, a tidewater glacier in southern Spitsbergen, Svalbard, Polar Research, 15, 53–66, 1996.

Joughin, I., Smith, B., Howat, I., Scambos, T., and Moon, T.: Greenland flow variability from ice-sheet-wide velocity mapping, Journal of Glaciology, 56, 415–430, doi:10.3189/002214310792447734, 2010.

Kamb, B. and Echelmeyer, K.: Stress-Gradient Coupling Glacier Flow. 1. Longitudinal Averaging of the Influence of Ice Thickness and Surface Slope, Journal of Glaciology, 32, 267–284, 1986.

Korona, J., Berthier, E., Bernard, M., Rémy, F., and Thouvenot, E.: SPIRIT. {SPOT} 5 stereoscopic survey of Polar Ice: Reference Images and Topographies during the fourth International Polar Year (2007-2009) , {ISPRS} Journal of Photogrammetry and Remote Sensing, 64, 204 – 212, doi:10.1016/j.isprsjprs.2008.10.005, 2009.

Krieger, G., Zink, M., Bachmann, M., Bräutigam, B., Schulze, D., Martone, M., Rizzoli, P., Steinbrecher, U., Walter Antony, J., De Zan, F., Hajnsek, I., Papathanassiou, K., Kugler, F., Rodriguez Cassola, M., Younis, M., Baumgartner, S., López-Dekker, P., Prats, P., and Moreira, A.: TanDEM-X: A radar interferometer with two formation-flying satellites, Acta Astronautica, 89, 83–89, doi:10.1016/j.actaastro.2013.03.008, 2013.

Lang, C., Fettweis, X., and Erpicum, M.: Future climate and surface mass balance of Svalbard glaciers in an RCP8.5 climate scenario: a study with the regional climate model MAR forced by MIROC5, The Cryosphere, 9, 945–956, doi:10.5194/tc-9-945-2015, 2015.

Lapazaran, J., Otero, J., Martín-Español, A., and Navarro, F.: On the errors involved in ice-thickness estimates I: ground-penetrating radar measurement errors, Journal of Glaciology, 62, 1008–1020, doi:10.1017/jog.2016.93, 2016.

Linsbauer, A., Paul, F., and Haeberli, W.: Modeling glacier thickness distribution and bed topography over entire mountain ranges with GlabTop: Application of a fast and robust approach, Journal of Geophysical Research, 117, n/a–n/a, doi:10.1029/2011JF002313, http://dx.doi.org/10.1029/2011JF002313, f03007, 2012.

Marzeion, B., Jarosch, A., and Hofer, M.: Past and future sea-level change from the surface mass balance of glaciers, The Cryosphere, 6, 1295–1322, doi:10.5194/tc-6-1295-2012, http://www.the-cryosphere.net/6/1295/2012/, 2012.

Marzeion, B., Cogley, J., Richter, K., and Parkes, D.: Attribution of global glacier mass loss to anthropogenic and natural causes, Science, 345, 919–921, doi:10.1126/science.1254702, http://science.sciencemag.org/content/345/6199/919, 2014.

McNabb, R., Hock, R., O'Neel, S., Rasmussen, L., Ahn, Y., Braun, M., Conway, H., Herreid, S., Joughin, I., Pfeffer, W., Smith, B., and Truffer, M.: Using surface velocities to calculate ice thickness and bed topography: a case study at Columbia Glacier, Alaska, USA, Journal of Glaciology, 58, 1151–1164, http://www.ingentaconnect.com/content/igsoc/jog/2012/00000058/00000212/art00011, 2012.

Moholdt, G., Nuth, C., Hagen, J., and Kohler, J.: Recent elevation changes of Svalbard glaciers derived from {ICESat} laser altimetry, Remote Sensing of Environment, 114, 2756–2767, doi:http://dx.doi.org/10.1016/j.rse.2010.06.008, http://www.sciencedirect.com/science/article/pii/S0034425710001987, 2010.

Möller, M., Obleitner, F., Reijmer, C., Pohjola, V., Głowacki, P., and Kohler, J.: Adjustment of regional climate model output for modeling the climatic mass balance of all glaciers on Svalbard, Journal of Geophysical Research: Atmospheres, 121, 5411–5429, doi:10.1002/2015JD024380, http://dx.doi.org/10.1002/2015JD024380, 2016.

Moran, M., Greenfield, R., Arcone, S., and Delaney, A.: Delineation of a complexly dipping temperate glacier bed using short-pulse radar arrays, Journal of Glaciology, 46, 274–286, doi:doi:10.3189/172756500781832882, http://www.ingentaconnect.com/content/igsoc/jog/2000/00000046/00000153/art00012, 2000.

Morland, L.: Unconfined ice-shelf flow, in: Dynamics of the West Antarctic ice sheet, Kluwer Academic Publishers, 1986.

Morlighem, M., Rignot, E., H. Seroussi, H., Larour, E., Ben Dhia, H., and Aubry, D.: A mass conservation approach for mapping glacier ice thickness, Geophysical Research Letters, 38, doi:10.1029/2011GL048659, http://dx.doi.org/10.1029/2011GL048659, 2011.

Morlighem, M., Rignot, E., Mouginot, J., Seroussi, H., and Larour, E.: Deeply incised submarine glacial valleys beneath the Greenland ice sheet, Nature Geoscience, 7, 418–422, doi:10.1038/ngeo2167, http://dx.doi.org/10.1038/ngeo2167, 2014.

Mosbeux, C., Gillet-Chaulet, F., and Gagliardini, O.: Comparison of adjoint and nudging methods to initialise ice sheet model basal conditions, Geoscientific Model Development, 9, 2549–2562, doi:10.5194/gmd-9-2549-2016, http://www.geosci-model-dev.net/9/2549/2016/, 2016.

Navarro, F., Martín-Español, A., Lapazaran, J., Grabiec, M., Otero, J., Vasilenko, E., and Puczko, D.: Ice Volume Estimates from Ground-Penetrating Radar Surveys, Wedel Jarlsberg Land Glaciers, Svalbard, Arctic, Antarctic, and Alpine Research, 46, 394–406, doi:10.1657/1938-4246-46.2.394, 2014.

Nuth, C. and Kääb, A.: Co-registration and bias corrections of satellite elevation data sets for quantifying glacier thickness change, The Cryosphere, 5, 271–290, doi:10.5194/tc-5-271-2011, 2011.

Nuth, C., Kohler, J., König, M., von Deschwanden, A., Hagen, J., Kääb, A., Moholdt, G., and Pettersson, R.: Decadal changes from a multi-temporal glacier inventory of Svalbard, The Cryosphere, 7, 1603–1621, doi:10.5194/tc-7-1603-2013, 2013.

Ottesen, D., Dowdeswell, J., Landvik, J., and Mienert, J.: Dynamics of the Late Weichselian ice sheet on Svalbard inferred from high?resolution sea-floor morphology, Boreas, 36, 286–306, doi:10.1111/j.1502-3885.2007.tb01251.x, http:https://dx.doi.org/10.1111/j.1502-3885.2007.tb01251.x, 2007.

Paolo, F., Fricker, H., and Padman, L.: Volume loss from Antarctic ice shelves is accelerating, Science, doi:10.1126/science.aaa0940, http://science.sciencemag.org/content/early/2015/03/25/science.aaa0940, 2015.

Paul, F., Bolch, T., Kääb, A., Nagler, T., Nuth, C., Scharrer, K., Shepherd, A., Strozzi, T., Ticconi, F., Bhambri, R., Berthier, E., Bevan, S., Gourmelen, N., Heid, T., Jeong, S., Kunz, M., L., T. R., Luckman, A., Merryman Boncori, J., Moholdt, G., Muir, A., Neelmeijer, J., Rankl, M., VanLooy, J., and Van Niel, T.: The glaciers climate change initiative: Methods for creating glacier area, elevation change and velocity products, Remote Sensing of Environment, 162, 408–426, doi:http://dx.doi.org/10.1016/j.rse.2013.07.043, http://www.sciencedirect.com/science/article/pii/S0034425713003532, 2015.

Pettersson, R., Christoffersen, P., Dowdeswell, J., Pohjola, V., Hubbard, A., and Strozzi, T.: Ice thickness and basal conditions of Vestfonna Ice Cap, Eastern Svalbard, Geografiska Annaler: Series A, Physical Geography, 93, 311–322, doi:10.1111/j.1468-0459.2011.00438.x, 2011.

Pinglot, J., Pourchet, M., Lefauconnier, B., Hagen, J., Isaksson, E., Vaikmae, R., and Kamiyama, K.: Accumulation in Svalbard glaciers deduced from ice cores with nuclear tests and Chernobyl reference layers, Polar Research, 18, 315–321, doi:10.1111/j.1751-8369.1999.tb00309.x, 1999.

Pinglot, J., Hagen, J., Melvold, K., Eiken, T., and Vincent, C.: A mean net accumulation pattern derived from radioactive layers and radar soundings on Austfonna, Nordaustlandet, Svalbard, Journal of Glaciology, 47, 555–566, doi:10.3189/172756501781831800, http://www.ingentaconnect.com/content/igsoc/jog/2001/00000047/00000159/art00004, 2001.

Pohjola, V., Christoffersen, P., Kolondra, L., Moore, J., Pettersson, R., Schäfer, M., Strozzi, T., and Reijmer, C.: Spatial distribution and change in the surface-velocity field of Vestfonna ice cap, Nordaustlandet, Svalbard, 1995-2010 using geodetic and satellite interferometry data, Geografiska Annaler: Series A, Physical Geography, 93, 323–335, doi:10.1111/j.1468-0459.2011.00441.x, http://dx.doi.org/10.1111/j.1468-0459.2011.00441.x, 2011.

Radić, V. and Hock, R.: Regionally differentiated contribution of mountain glaciers and ice caps to future sea-level rise, Nature Geoscience, 4, 91–94, doi:10.1038/ngeo1052, 2011.

Radić, V., Bliss, A., Beedlow, A., Hock, R., and Cogley, E. M. J.: Regional and global projections of twenty-first century glacier mass changes in response to climate scenarios from global climate models, Climate Dynamics, 42, 37–58, doi:10.1007/s00382-013-1719-7, http://dx.doi.org/10.1007/s00382-013-1719-7, 2014.

Rankl, M. and Braun, M.: Glacier elevation and mass changes over the central Karakoram region estimated from TanDEM-X and SRTM/X-SAR digital elevation models, Annals of Glaciology, 51, 273–281, doi:10.3189/2016AoG71A024, 2016.

Rankl, M., Kienholz, C., and Braun, M.: Glacier changes in the Karakoram region mapped by multimission satellite imagery, The Cryosphere, 8, 977–989, doi:10.5194/tc-8-977-2014, http://www.the-cryosphere.net/8/977/2014/, 2014.

Raup, B., Racoviteanu, A., Khalsa, S., Helm, C., Armstrong, R., and Arnaud, Y.: The GLIMS Geospatial Glacier Database: a New Tool for Studying Glacier Change, Global and Planetary Change, 56, 101–110, doi:10.1016/j.gloplacha.2006.07.018, 2007.

Rignot, E. and Mouginot, J.: Ice flow in Greenland for the International Polar Year 2008-2009, Geophysical Research Letters, 39, 7 pp., doi:10.1029/2012GL051634, 2012.

Rignot, E., Mouginot, J., and Scheuchl, B.: Ice Flow of the Antarctic Ice Sheet, Science, 333, 1427–1430, doi:10.1126/science.1208336, 2011.

Rosenau, R., Scheinert, M., and Dietrich, R.: A processing system to monitor Greenland outlet glacier velocity variations at decadal and seasonal time scales utilizing the Landsat imagery, Remote Sensing of Environment, 169, 1–19, doi:http://dx.doi.org/10.1016/j.rse.2015.07.012, http://www.sciencedirect.com/science/article/pii/S0034425715300742, 2015.

Schäfer, M., Zwinger, T., Christoffersen, P., Gillet-Chaulet, F., Laakso, K., Pettersson, R., Pohjola, V., Strozzi, T., and Moore, J.: Sensitivity of basal conditions in an inverse model: Vestfonna ice cap, Nordaustlandet/Svalbard, The Cryosphere, 6, 771–783, doi:10.5194/tc-6-771-2012, http://www.the-cryosphere.net/6/771/2012/, 2012.

Schoof, C.: Ice sheet grounding line dynamics: Steady states, stability, and hysteresis, Journal of Geophysical Research, 112, 19 pp., doi:10.1029/2006JF000664, 2007.

Schoof, C.: Ice-sheet acceleration driven by melt supply variability, Nature, 468, 803–806, doi:10.1038/nature09618, 2010.

Schutz, B., Zwally, H., Shuman, C., Hancock, D., and DiMarzio, J.: Overview of the ICESat Mission, Geophysical Research Letters, 32, doi:10.1029/2005GL024009, 2005.

Schwaizer, G.: Performance assessment of the glacier ice velocity products for Greenland, and description of the evaluation methodology. In: Glaciers validation report, Issue 1.0, http://sen3app.fmi.fi/index.php?page=Deliverables_&style=main&p=2, 2016.

Seehaus, T., Marinsek, S., Helm, V., Skvarca, P., and Braun, M.: Changes in ice dynamics, elevation and mass discharge of Dinsmoor-Bombardier-Edgeworth glacier system, Antarctic Peninsula, Earth and Planetary Science Letters, 427, 125–135, doi:10.1016/j.epsl.2015.06.047, http://www.sciencedirect.com/science/article/pii/S0012821X15004100, 2015.

Seehaus, T., Marinsek, S., Skvarca, P., van Wessem, J., Reijmer, C., Seco, J., and Braun, M.: Dynamic Response of Sjögren Inlet Glaciers, Antarctic Peninsula, to Ice Shelf Breakup Derived from Multi-Mission Remote Sensing Time Series, Frontiers in Earth Science, 4, 66, doi:10.3389/feart.2016.00066, http://journal.frontiersin.org/article/10.3389/feart.2016.00066, 2016.

Strozzi, T., Luckman, A., Murray, T., Wegmüller, U., and Werner, C. L.: Glacier motion estimation using SAR offset-tracking procedures, IEEE Transactions on Geoscience and Remote Sensing, 40, 2384–2391, doi:10.1109/TGRS.2002.805079, 2002.

Tachikawa, T., Hato, M., Kaku, M., and Iwasaki, A.: The characteristics of ASTER GDEM version 2, International Geoscience and Remote Sensing Symposium Proceedings, 2011.

van Pelt, W., Oerlemans, J., Reijmer, C., Pettersson, R., Pohjola, V., Isaksson, E., and D.Divine: An iterative inverse method to estimate basal topography and initialize ice flow models, The Cryosphere, 7, 987–1006, doi:10.5194/tc-7-987-2013, http://www.the-cryosphere.net/7/987/2013/, 2013.

Vijay, S. and Braun, M.: Elevation Change Rates of Glaciers in the Lahaul-Spiti (Western Himalaya, India) during 2000-2012 and 2012-2013, Remote Sensing, 8, doi:10.3390/rs8121038, http://www.mdpi.com/2072-4292/8/12/1038, 2016.

Zwally, H., Li, J., Robbins, J., Saba, J., Yi, D., and Brenner, A.: Mass gains of the Antarctic ice sheet exceed losses, Journal of Glaciology, 61, 1019–1036, doi:10.3189/2015JoG15J071, http://www.ingentaconnect.com/content/igsoc/jog/2015/00000061/00000230/art00001, 2015.

Zwally, H., Li, J., Brenner, A., Beckley, M., Cornejo, H., Dimarzio, J., Giovinetto, M., Neumann, T., Robbins, J., Saba, J., Yi, D., and Wang, W.: Greenland ice sheet mass balance: distribution of increased mass loss with climate warming; 2003-07 versus 1992-2002, Journal of Glaciology, 57, 88–102, doi:10.3189/002214311795306682, 2011.

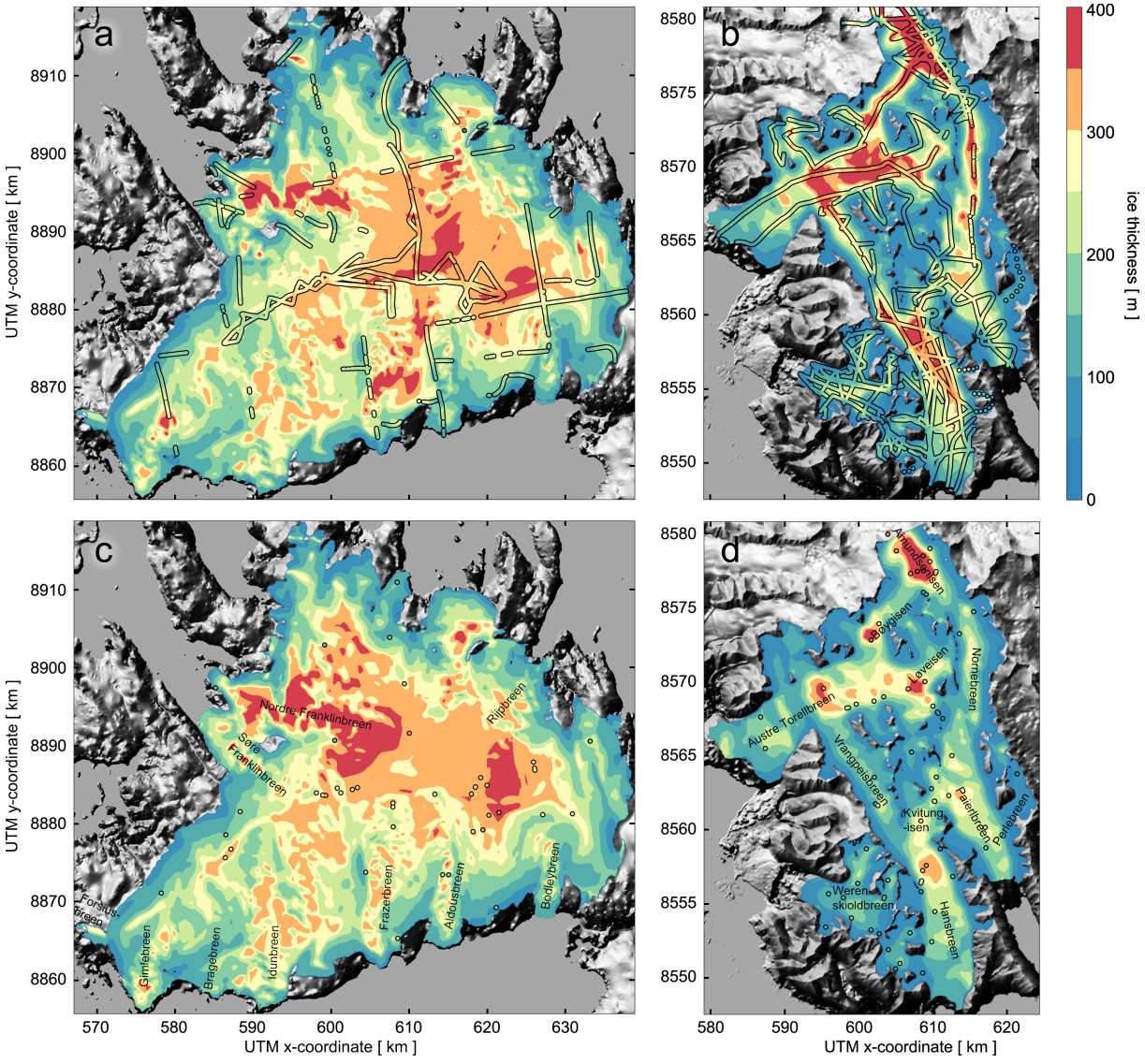

Figure 4. Ice thickness map for VIC (a,c) and THPB/WSB (b,d) as suggested by the first-step reconstruction approach. Thickness values for marine ice fronts are non-zero and a natural outcome of the underlying mass budget calculation. For VIC, thickness measurements (coloured dots) were collected with airborne radio-echo sounding instruments (Dowdeswell et al., 1986) as well as with ground-based pulsed radar systems (Pettersson et al., 2011; Navarro et al., 2014). For THPB/WSB, measurements were collected during several GPR campaigns between 2004-2012 (Navarro et al., 2014). The upper (a,b) and lower (c, d) panels show the respective thickness fields when all or only 1% of all thickness measurements were used in the first-step reconstruction, respectively. For the ice cap, mean thickness values are not very sensitive to the data availability, whereas the not well constrained reconstruction for THPB and WSB produces low biased estimates. Background: grey-scale hill-shaded topography based on a NPI ~~50m~~ 50 m DEM.

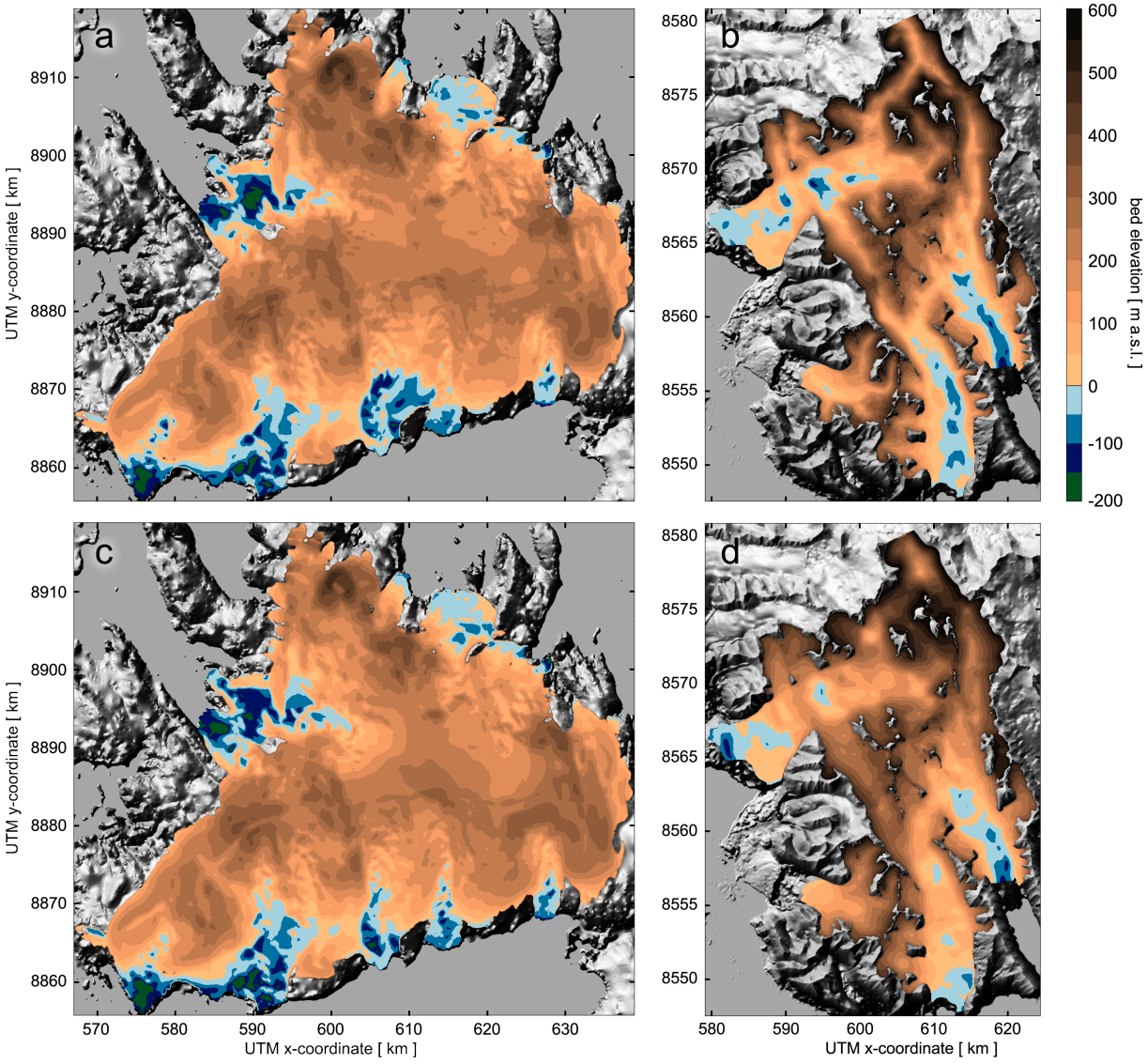

Figure 5. Bedrock topography associated to the thickness field in Fig. 4 for VIC (a,c) and THPB/WSB (b,d). In absence of direct measurements, negative values over larger areas were not anticipated for Gimlebreen and Idunbreen based from a direct interpolation of thickness data (Pettersson et al., 2011) . Upper and lower panels reflect the respective amount of considered thickness measurements as in Fig. 4. Ice-free background: grey-scale hill-shaded topography based on a NPI ~~50m~~ 50 m DEM. Ice-covered background: grey-scale hill-shaded bedrock topography.

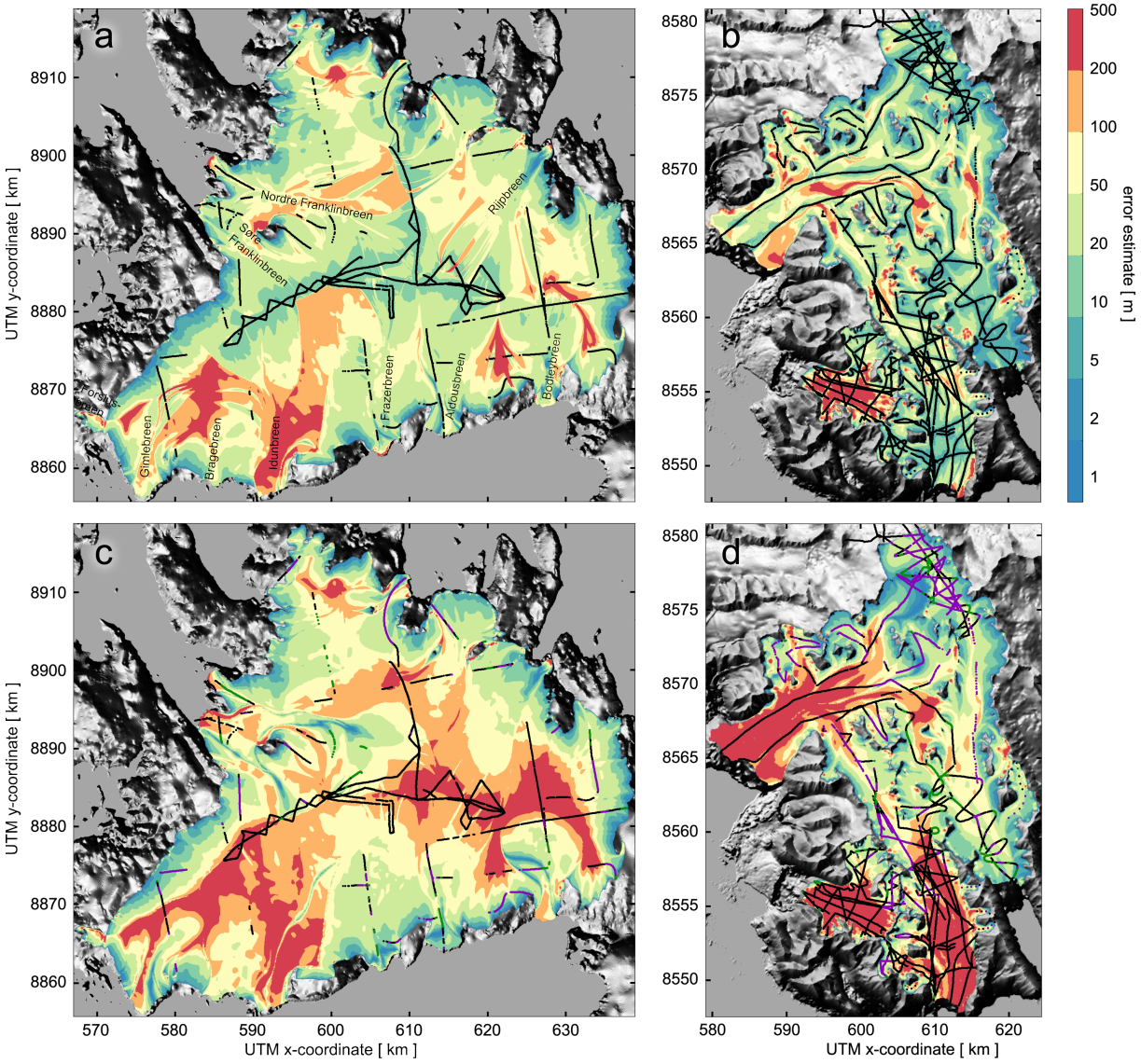

Figure 6. Error-estimate map based on the error propagation presented in Sect. (2.0.4) for VIC (a,c) and THPB/WSB (b,d). Values are most elevated in the vicinity of unconstrained ice divides and ridges as well as in other stagnant areas. Error estimates are equal to the ~~5m~~ measurement uncertainty where observations were collected. Upper and lower panels reflect the amount of considered thickness measurements as in Fig. 4. For panels (c,d), the withheld measurements (dots) are put into three categories. The first category (black dots) comprises all locations where the difference between observed and reconstructed thickness values are within the error bounds. For the other two categories, the difference exceeds these bounds and measured thickness values are either overestimated (green dots) or underestimated (purple dots) by the reconstruction. Background: grey-scale hill-shaded topography based on a NPI ~~50m~~ 50 m DEM.

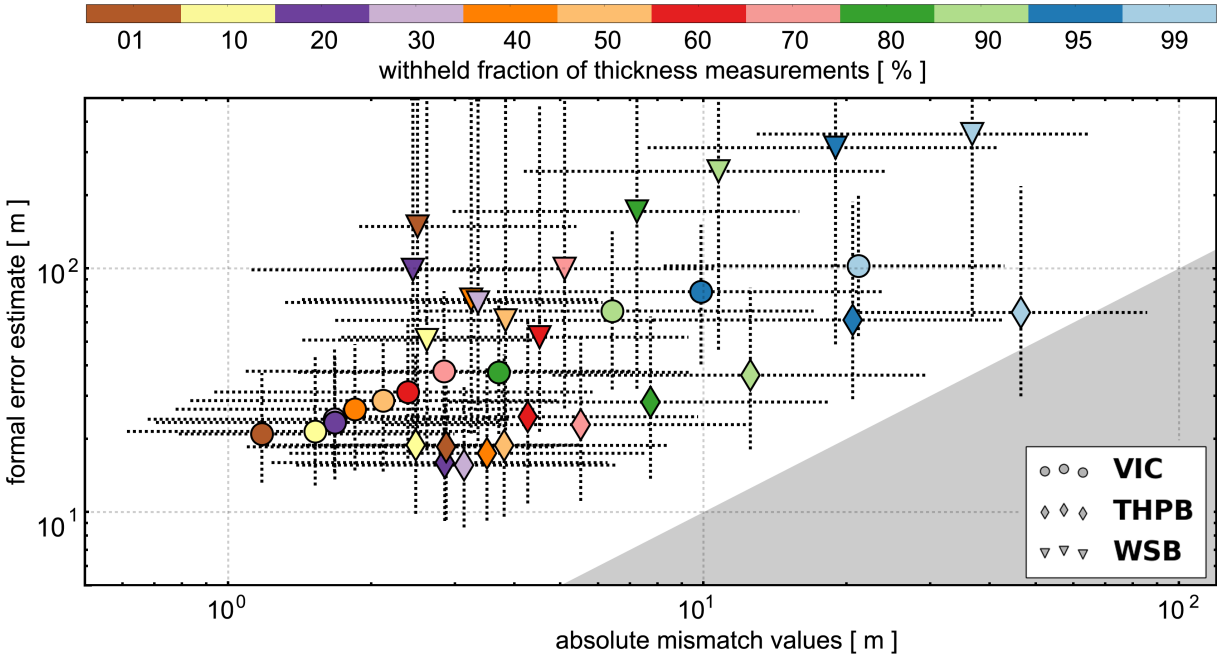

Figure 7. ~~Normalised median~~ Median values for the absolute thickness mismatches and the error estimates at measurement locations not included during the reconstruction. ~~Medians are normalised to the average thickness value of the withheld measurements.~~ Marker colours indicate the respective fraction of all measurements withheld from the reconstruction. Dashed crosses span the interquartile range of all mismatch values (horizontal) and all formal error estimates (vertical). For orientation, the grey background shading was added to highlight the identity line.

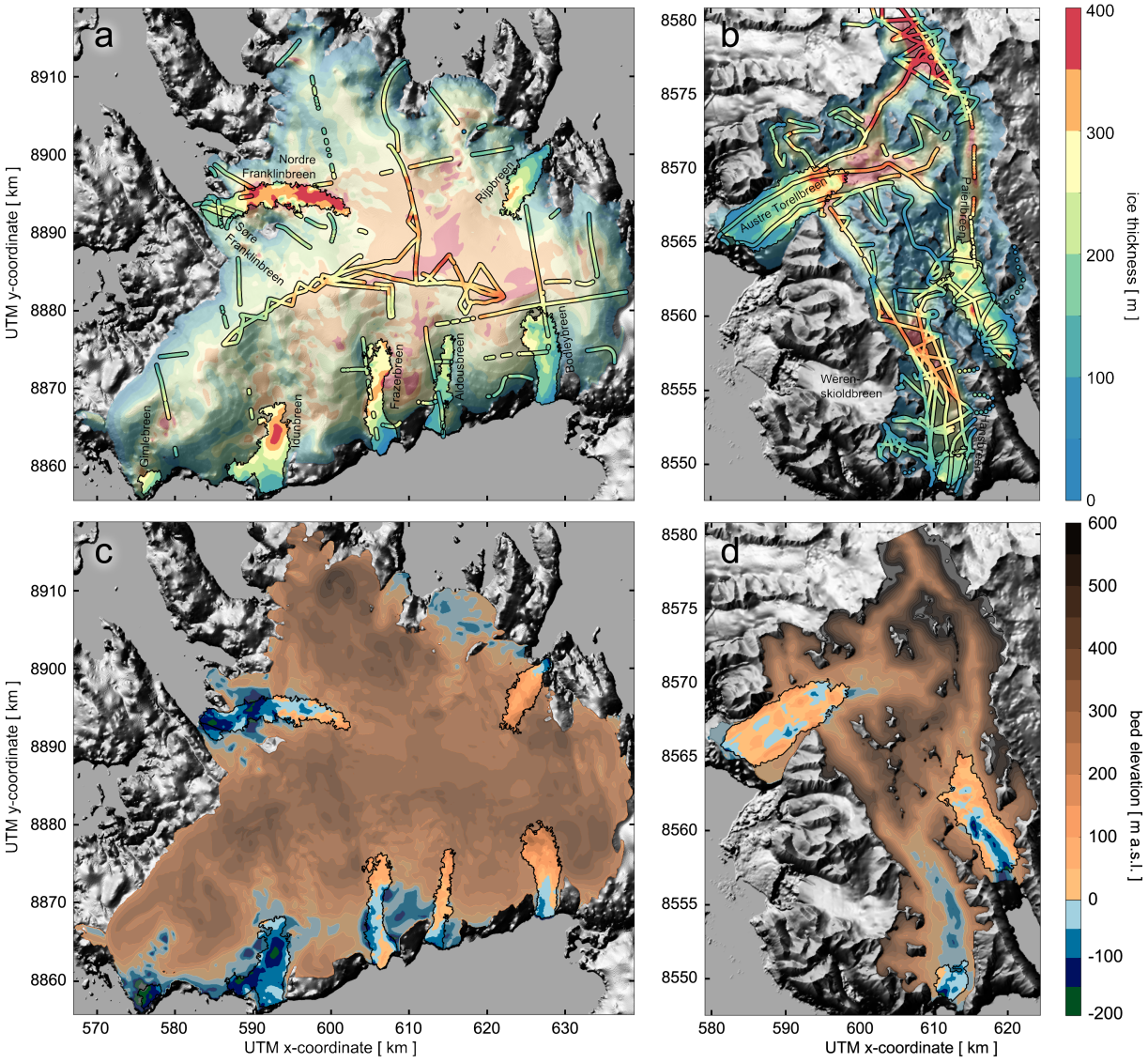

Figure 8. Ice thickness (a,b) as in Fig. 4 and associated bedrock topography (c,d) as in Fig. 5 for VIC (a,c) and THPB (b,d). Along the outlet glaciers (non-transparent lurid colours), the two fields were updated in the second-step accounting for velocity observations in the mass conservation. Partially transparent areas in these maps (unsaturated colours) stem from the first-step reconstruction, for which values are inferred from the ~~apparent~~ flux solution.~~Along the outlet glaciers (non-transparent lurid colours), the two fields were updated accounting for velocity observations in the mass conservation.~~

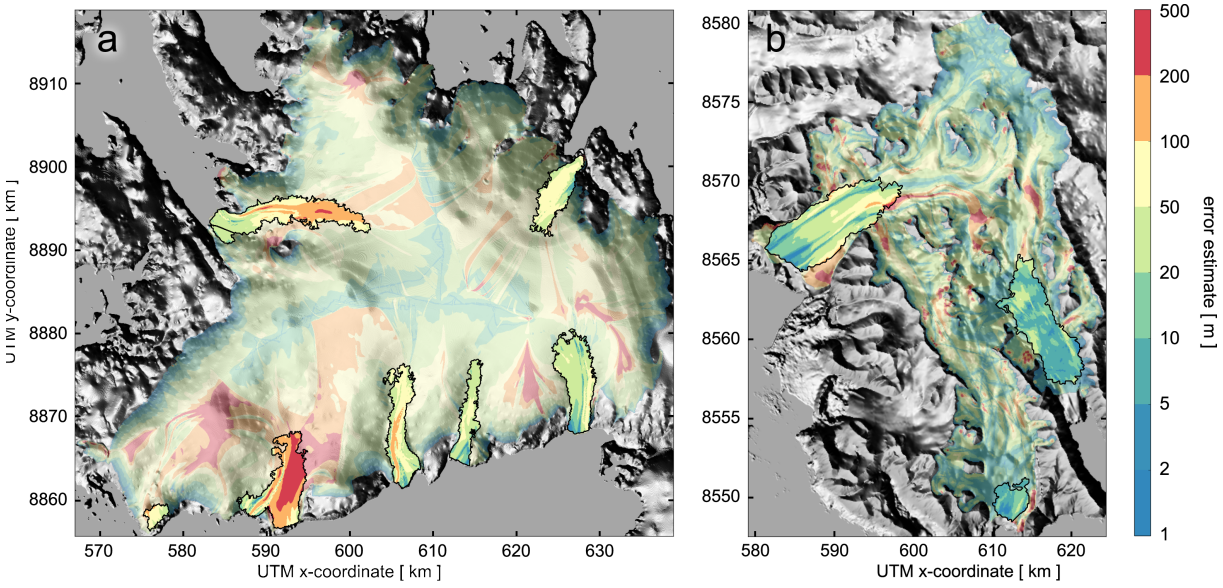

Figure 9. Error estimate map as in Fig. ~~7~~ 6 for VIC (a) and THPB (b). Partially transparent areas in the thickness maps (unsaturated colours) stem from the first-step reconstruction, for which ice ~~thicknesses are~~ thickness is inferred from the ~~apparent flux~~ ice-flux solution. Along the outlet glaciers (non-transparent lurid colours), error estimates are updated relying on velocity observations (Fig. 2c, d).

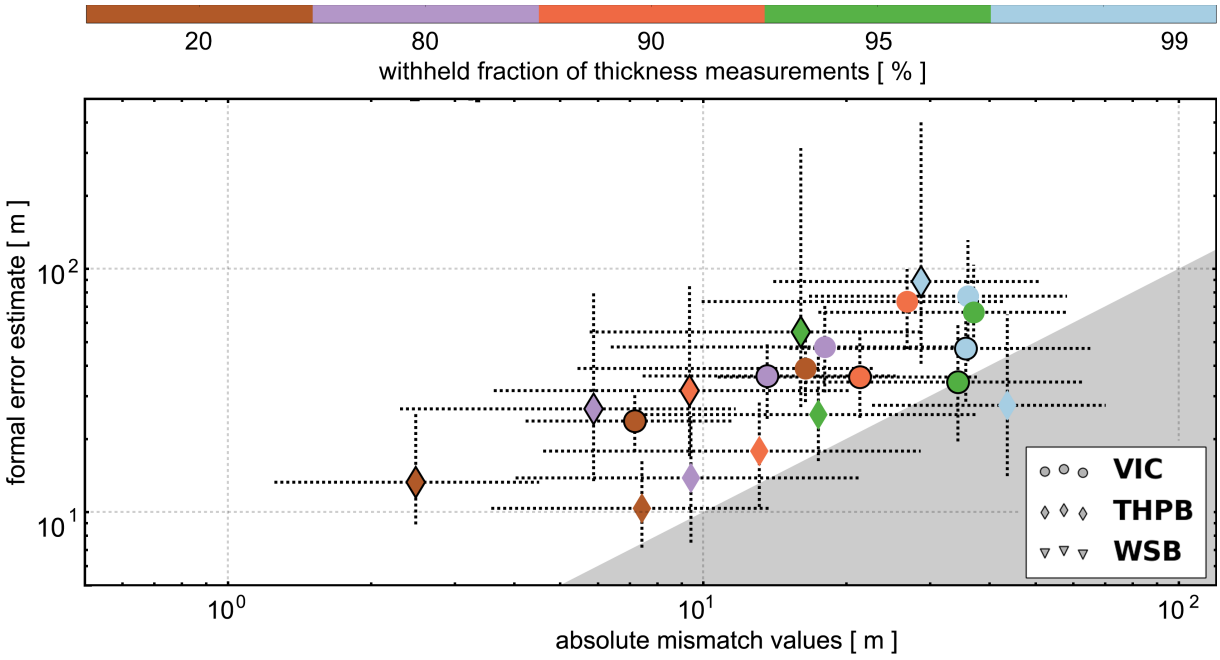

Figure 10. Median values for the absolute thickness mismatches and the error estimates as in Fig. (7). Values are only calculated within the sub-domains. Symbols with black edges represent the results from the first step. Symbols without edge line indicates the second-step results.

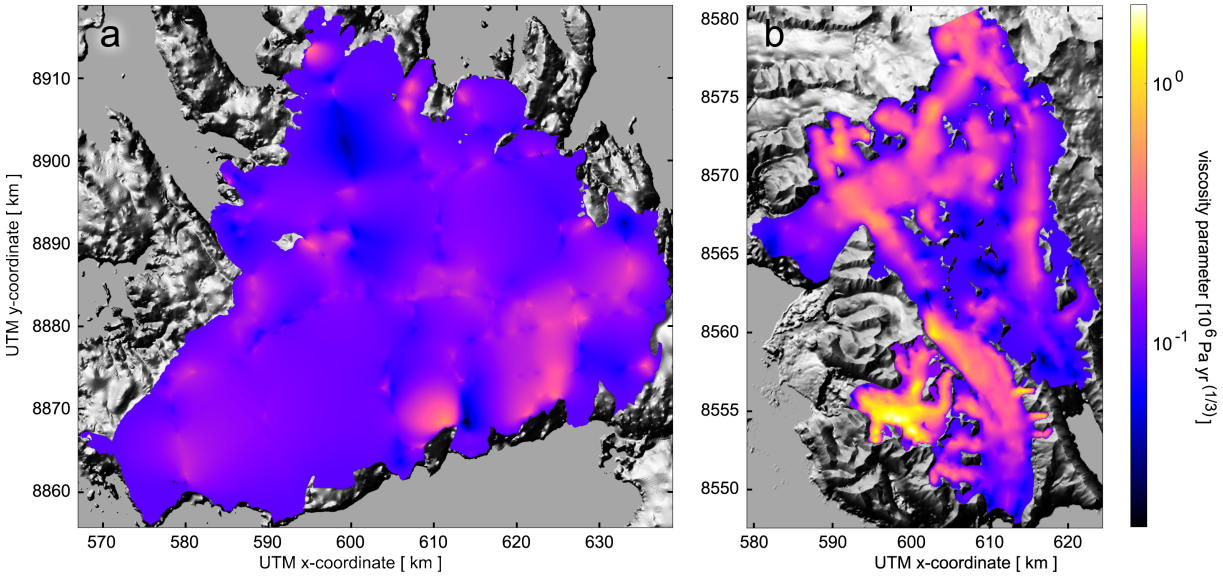

Figure A1. The ice-viscosity parameter B for VIC (a) and THPB/WSB (b) is inferred during the first-step of the reconstruction as explained in Sect. 2.0.3. This parameter is used to match observed and reconstructed thickness values. An interpretation in terms of material property is delicate because the parameter compensates for input uncertainties and inconsistencies as well as for assumptions in the first-step reconstruction. Background: grey-scale hill-shaded topography based on a NPI ~~50m~~ 50 m DEM.

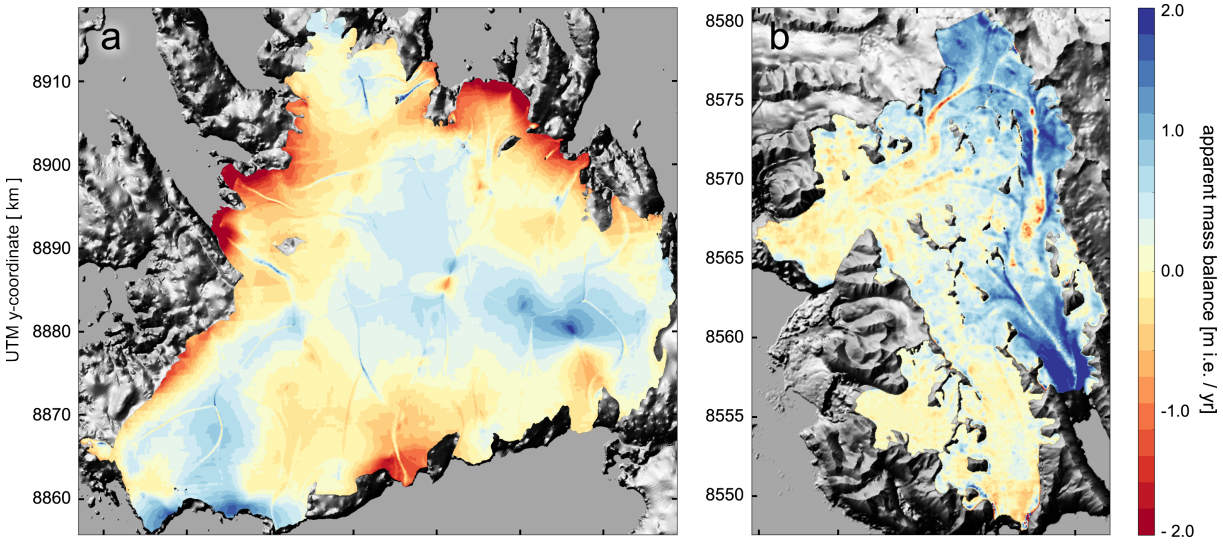

Figure A2. Apparent mass balance ȧ for VIC (a,c) and THPB/WSB (b,d). Panels (a,b) give the initial input as given by the SMB and the measured surface elevation changes. Panels (c,d) show the final field after adaptation of ȧ during the optimisation in accordance with the cost function. Background: grey-scale hill-shaded topography based on a NPI 50 m DEM.

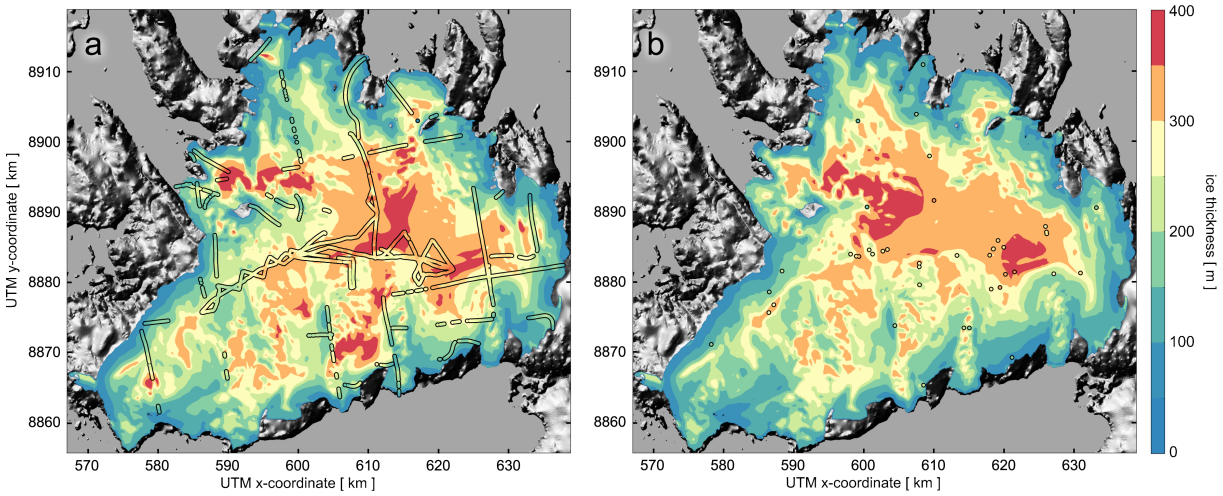

Figure A3. Ice thickness map for VIC as in Fig. 4 based on the 2003-2013 WRF-SMB field using all (a) or only 1% (b) of the thickness measurements.

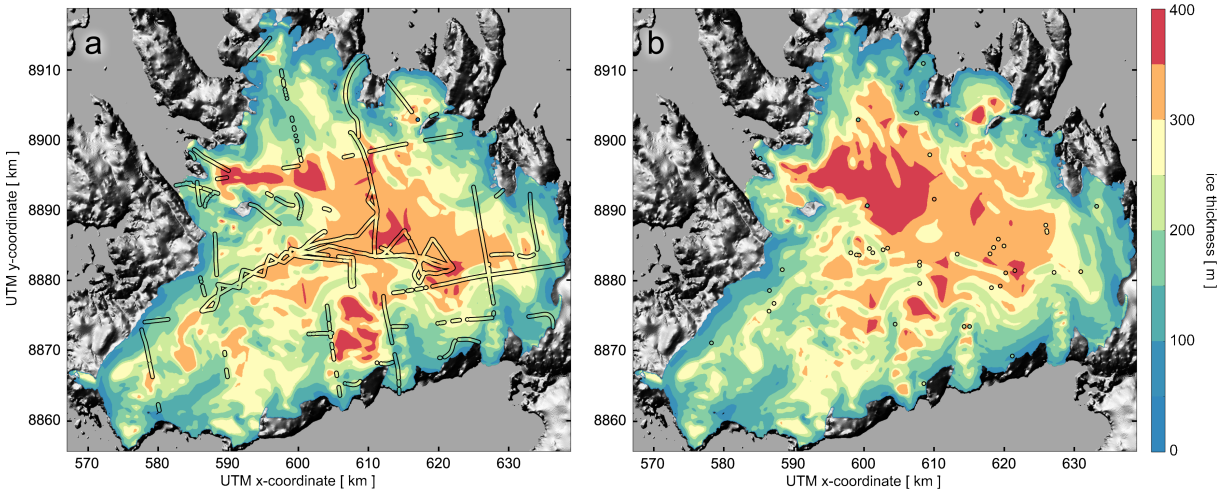

Figure A4. Ice thickness map for VIC as in Fig. 4. Here, the reconstruction is conducted with the NPI ~~50m~~ 50 m DEM as surface topography using either all (a) or only 1% (b) of the thickness measurements.

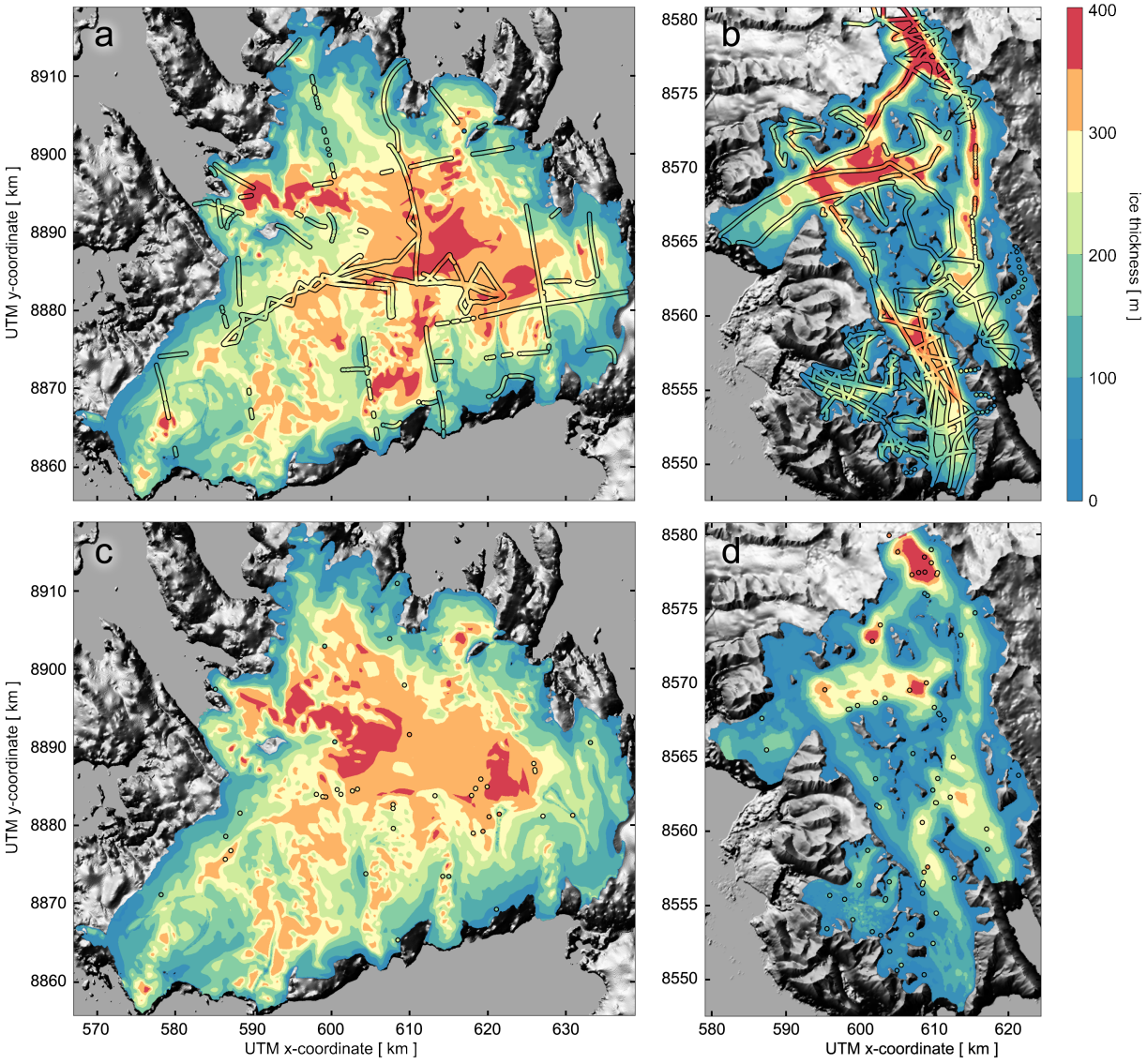

Figure A5. Ice thickness for VIC (a,c) and THPB/WSB (b,d) as in Fig. 4. Here, the first-step flux solution is not corrected to avoid negative flux values in the SIA-equation used to infer the ice thickness (Sect. 2.0.3). For WSB, you see that many patches appear with very small thickness values. These bogus variations are a consequence of zero transitions in the flux field. For VIC and THPB such bogus variations are limited to some few small areas.